Photochemical and Photophysical Studies of Excited State Intramolecular Proton Transfer (ESIPT) in Biphenyl Compounds

by

Niloufar Behin Aein
B.Sc., Carleton University, 2005

A Dissertation Submitted in Partial Fulfilment of the
Requirements for the Degree of

MASTER OF SCIENCE
in the Department of Chemistry

Photochemical and Photophysical Studies of Excited State Intramolecular Proton Transfer (ESIPT) in Biphenyl Compounds

by

Niloufar Behin Aein
B.Sc., Carleton University, 2005

Supervisory Committee

Dr. P. Wan, (Department of Chemistry)
Supervisor

Dr. D. J. Berg, (Department of Chemistry)
Departmental Member

Dr. F. Hof, (Department of Chemistry)
Departmental Member

Supervisory Committee

Dr. P. Wan, (Department of Chemistry)
Supervisor

Dr. D. J. Berg, (Department of Chemistry)
Departmental Member

Dr. F. Hof, (Department of Chemistry)
Departmental Member

Abstract

This Thesis aims to examine the effects of substituents on the adjacent proton accepting phenyl ring with respect to a new type of excited state intramolecular proton transfer (ESIPT) process discovered by Wan and co-workers. Therefore, a number of 2-phenylphenols **23-28** were synthesized with electron-donor and electron-acceptor substituents such as methyl, methoxy, and ketone moieties on the adjacent proton accepting phenyl ring.

The results obtained from examination of photochemical deuterium exchange showed that all derivatives except for ketone **27** underwent deuterium exchange (Φ_{ex} = 0.019 - 0.079), primarily at the 2'-position on photolysis in D_2O-CH_3CN. In general, compounds with methoxy moiety (ies) on the adjacent proton accepting ring showed higher deuterium exchange yields.

Diol **28** has the potential to undergo photosolvolysis as well as ESIPT process since it has both a benzyl alcohol and a phenol chromophore on the same molecule. Irradiation

of **28** in 1:1 H_2O-CH_3OH gave the corresponding methyl ether product in high yield. Photolysis of **28** in 1:1 D_2O-CH_3OH also showed that ESIPT competes very well with photosolvolysis. Thus, this work has established that ESIPT can compete efficiently with photosolvolysis.

Semi-empirical AM1 (examination of HOMOs and LUMOs) calculations show a large degree of charge transfer in the electronic excited state (except **27**), from the phenol ring to the attached phenyl ring of the studied compounds. The AM1 calculation for ketone **27** showed that the carbonyl oxygen is more basic than the carbon atoms of the benzene ring, which explains the lack of deuterium exchange observed for **27**.

Table of Contents

Supervisory Committee ii

Abstract iii

Table of Contents v

Abbreviations viii

List of Structures ix

List of Figures xi

List of Schemes xiv

List of Tables xv

Acknowledgments xvi

Chapter 1 1

Introduction 1

1.1 Ground State Proton Transfer 1

1.2 Excited State Proton Transfer (ESPT) 1

1.2.1 Excited State Intermolecular Proton Transfer ($ESI_{er}PT$) 3

1.2.2 Excited State Intramolecular Proton Transfer (ESIPT) 4

1.2.2.1 Direct ESIPT 4

1.2.2.2 Requirements of Direct ESIPT Process 8

1.2.2.3 Water-Mediated ESPT (*formal* ESIPT) 10

1.2.2.4 ESIPT in Hydroxyaromatic Compounds 11

1.3 Photosolvolysis 13

1.4 Proposed Research 14

Chapter 2 Results and Discussion 16

2.1 Synthesis 16
2.2 Geometries of Substrates in the Ground State 17
2.3 Photochemical Product Studies 21
2.3.1 Photochemical Deuterium Exchange 21
2.3.2 Photosolvolysis versus ESIPT of **28** 33
2.3.3 Quantum Yields of Exchange for **23-26** and **28** 37
2.4 Fluorescence Measurements 39
2.5 Mechanisms of Photochemical Reactions 45
2.5.1 Direct ESIPT 45
2.5.2 Water-Mediated ESPT 49
2.5.3 Photosolvolysis 50
2.6 Conclusions 53
Chapter 3 Experimental 55
3.1 General 55
3.2 Materials 55
3.2.1 Synthesis 55
3.2.1.1 2’-Methylbiphenyl-2-ol (**23**) 56
3.2.1.2 4’-Methoxybiphenyl-2-ol (**25**) 56
3.2.1.3 3’, 5’-Dimethoxybiphenyl-2-ol (**26**) 57
3.2.1.4 4’-Acetylbiphenyl-2-ol (**27**) 57
3.2.1.5 2’-Methoxybiphenyl-2-ol (**24**) 57
3.2.1.6 4’-(1’’-Hydroxyethyl) biphenyl-2-ol (**28**) 58
3.3 Photolysis 59

3.3.1 General Procedure for Photochemical Exchange of **23-26** in D_2O-CH_3CN…. 59

3.3.1.1 Photolysis of **23** in 1:9 D_2O-CH_3CN. 60

3.3.1.2 Photolysis of **24** in 1:1 D_2O-CH_3CN 60

3.3.1.3 Photolysis of **25** in 1:1 in D_2O-CH_3CN 61

3.3.1.4 Photolysis of **26** in 1:3 in D_2O-CH_3CN 61

3.3.1.5 Photolysis of **28** in 1:3 D_2O-CH_3CN 62

3.3.1.6 Photosolvolysis of **28** in H_2O-CH_3OH 62

3.3.1.7 Photolysis of **28** in 1:1 in D_2O-CH_3OH 62

3.4 Quantum Yields 63

3.5 General Procedure for Steady-State and Time-Resolved Fluorescence Measurements 63

Appendix 65

NMR Spectra of Synthesized Compounds 65

References 78

Abbreviations

ACN (CH_3CN)	Acetonitrile
EDG	Electron Donating Group
EWG	Electron Withdrawing Group
ESPT	Excited State Proton Transfer
ESIPT ($ESI_{ra}PT$)	Excited State Intramolecular Proton Transfer
$ESI_{er}PT$	Excited State Intermolecular Proton Transfer
HOMO	Highest Occupied Molecular Orbital
LUMO	Lowest Unoccupied Molecular Orbital
LFP	Laser Flash Photolysis
MO	Molecular Orbital
MS	Mass Spectrum
NMR	Nuclear Magnetic Resonance
QM	Quinone Methide
TLC	Thin Layer Chromatography

List of Structures

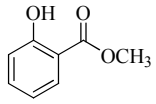

1

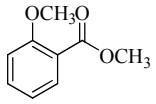

2

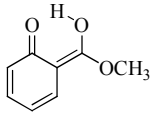

3

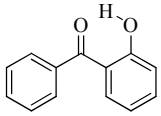

4

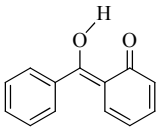

5

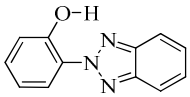

6

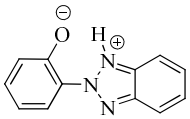

7

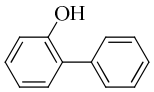

8

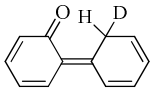

9

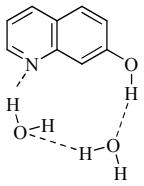

10

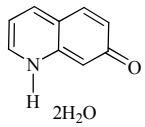

11

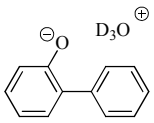

12

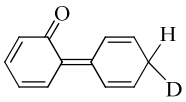

13

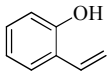

14

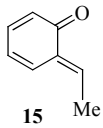

15

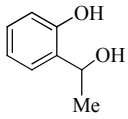

16

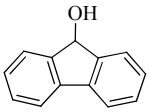

17

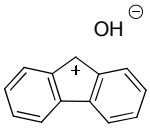

18

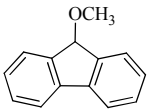

19

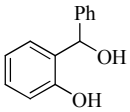

20

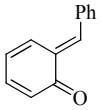

21

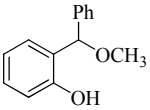

22

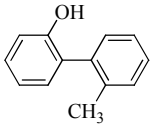

23

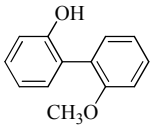

24

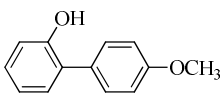

25

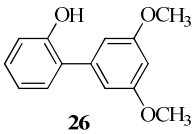

26

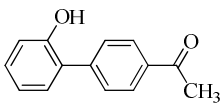

27

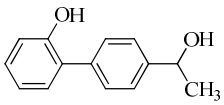

28

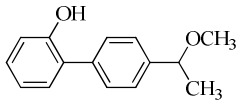

29

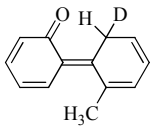

30

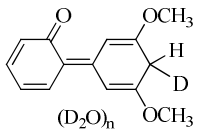

31

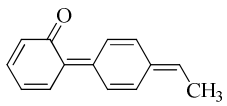

32

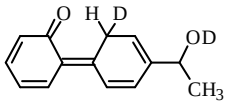

33

List of Figures

Figure 1.1 Jablonski diagram. 2

Figure 1.2 Optimized geometry (Chem 3D, AM1/MOPAC) in the ground state of **8** (dihedral angle ~54^{o})..... 9

Figure 2.1 Heat of formation associated with rotation about the biaryl bond of **25** (▲), **26** (×), and **27** (*), as predicted by AM1 calculation. 18

Figure 2.2 Optimized geometries (Chem 3D, AM1/MOPAC) in the ground state for **23** (69.2°, top), **26** (52.7^{o}, middle), and **28** (52.0^{o}, bottom). 20

Figure 2.3 ^{1}H NMR (500 MHz, $(CD_3)_2CO$) showing the expanded aromatic region of **23** before (bottom) and after (top) 1 h irradiation in 1:9 (v/v) D_2O-CH_3CN. NMR integration indicates 33% and 14% deuteration at the H_a and H_c positions respevtively..... 22

Figure 2.4 ^{1}H NMR (500 MHz, $(CD_3)_2CO$) showing the expanded aromatic region of **24** before (bottom), after photolysis (middle 0.005M D_2O in CH_3CN, 254 nm, 16 lamps) and (top, 0.25 M D_2O in CH_3CN, 254 nm, 16 lamps) respectively, in 5 minutes. ^{1}H NMR integration indicates 20% and 37% deuteration at the H_a position. 25

Figure 2.5 Plot of % deuterium exchange at the 2'-position of **24** as a function of D_2O content in CH_3CN as measured by ^{1}H NMR (Photolysis time 5 min). 27

Figure 2.6 ^{1}H NMR (300 MHz , $(CD_3)_2CO$) showing the expanded aromatic region of **26** before (bottom), after photolysis (254 nm, 16 lamps) time 30 min (middle) and 2 h (top), respectively, in 1:3 (v/v) D_2O-CH_3CN. NMR

integration indicates 71%, 7% and 99%, 22% deuteration at H_a ,and H_b positions. 31

Figure 2.7 Plot of % Deuterium Exchange at the 2'(●) and 4'(▲)-positions of **26** versus photolysis time in 1:3 (v/v) D_2O-CH_3CN, as measured by ^{1}H-NMR. 32

Figure 2.8 ^{1}H NMR (300 MHz, CD_3CN) of **28** before (bottom) photolysis. ^{1}H NMR (300 MHz, CD_3CN) after photolysis (254 nm, 16 lamps, and 10 min) in 1:1 H_2O-CH_3OH indicates the formation of mixture (middle) and pure **29** (top). 34

Figure 2.9 ^{1}H NMR (300 MHz, CD_3CN) showing the expanded aromatic region of **28** before (bottom), and after photolysis (254 nm, 16 lamps, and 10 min; top) in 1:1 (v/v) D_2O-CH_3OH. ^{1}H NMR integration indicates 26% deuteration at the H_a position. 36

Figure 2.10 ^{1}H NMR (300 MHz, CD_3CN) showing the expanded aromatic region of **29** as pure compound (bottom), and after photolysis (254 nm, 16 lamps, and10 min; top) in 1:1 (v/v) D_2O-CH_3OH. ^{1}H NMR integration indicates 31% deuteration at H_a position. 37

Figure 2.11 Fluorescence emission spectrum for **24** in neat CH_3CN (♦). Fluorescence emission spectra for **24** in 1:9 (v/v) CH_3CN -H_2O (▲), and (●) pH = 12 (100% H_2O). The emission at 420 nm is assigned to the phenolate. 41

Figure 2.12 Fluorescence emission spectrum for **26** in neat CH_3CN (♦). Fluorescence emission spectra for **26** in various solvents, (▲) 4:6 (v/v) CH_3CN- H_2O,

(■) 2:8 (v/v) CH_3CN- H_2O, and (●) pH = 12 (100% H_2O). The emission at 420 nm is assigned to the phenolate. 43

Figure 2.13 Fluorescence emission spectrum for **25** in neat CH_3CN (♦). Fluorescence emission spectra for **25** in various solvents, (▲) 3:7 (v/v) CH_3CN- H_2O, (●) 1:9 (v/v) CH_3CN- H_2O, and (■) pH = 12 (100% H_2O). The emission at 400 nm observed at pH12 is assigned to the phenolate. 44

Figure 2.14 Calculated (AM1, Chem 3D/MOPAC) HOMO (left) and LUMO (right) for **23**. 46

Figure 2.15 Calculated (AM1, Chem 3D/MOPAC) HOMO (left) and LUMO (right) for ketone **27**. 48

Figure 2.16 Calculated (AM1, Chem 3D/MOPAC) HOMO (left) and LUMO (right) for diol **28**. 50

List of Schemes

Scheme 1.1 ESIPT for Methyl Salicylate (**1**)..... 5

Scheme 1.2 Direct ESIPT Mechanism of **8** in D_2O. 8

Scheme 1.3 Direct ESIPT Process in **8**. 9

Scheme 1.4 Water-mediated ESPT (*formal* ESIPT) mechanism of **10**. 10

Scheme 1.5 Water-mediated ESPT (*formal* ESIPT) mechanism of **8**. 11

Scheme 1.6 ESIPT process in **14**. 12

Scheme 1.7 Photosolvolysis of **17** in H_2O-CH_3OH. 13

Scheme 1.8 Photosolvolysis of **20** in H_2O-CH_3OH. 14

Scheme 2.1 Water-mediated ESPT for **24**. 42

Scheme 2.2 Proposed mechanism of direct ESIPT for **23**. 47

Scheme 2.3 Proposed mechanism of water-mediated ESPT for **26**..... 49

Scheme 2.4 Proposed mechanism of photosolvolysis for **28**..... 51

Scheme 2.5 Proposed mechanism of direct ESIPT and photosolvolysis for **28**. 52

List of Tables

Table 2.1 Calculated Structural Parameters for Hydroxybiaryls in the Ground State..... 19

Table 2.2 Deuterium Exchange Data for **24-26** and **28** using 'H NMR Analysis. 29

Table 2.3 Deuterium Exchange Data for **24**, **25** and **26** using MS Analysis. 29

Table 2.4 Product Quantum Yields for **23-26** and **28**. 38

Table 2.5 Fluorescence Parameters for **23-26** and **28**. 40

Acknowledgments

I would like to express my deepest appreciation and most sincere thanks to a number of people for their contribution in making this Thesis possible. Above all, I am most thankful to my supervisor Dr. Peter Wan for allowing me the opportunity to complete my Master project, with his guidance, support, and patience throughout this Thesis.

There are a number of people whom I would like to acknowledge for their helpful discussion, input and friendship. They are Yunyan Hou, Alfredo Franco-Cea, Dr. Nikola Basaric, Jonathan Chui, Dr. Cornelia Bohne and her students, and Chris Greenwood.

Finally, I would like to thank my family. They have been supportive of many endeavours throughout my life. Utmost thanks to my mother for all her emotional support, and encouragement. Thanks to my sister and her children, and my brothers who were always there for me. I would like to dedicate this work to the memory of my father, who did not have a chance to see me graduate. He will always be a very special person to me.

Chapter 1

Introduction

1.1 Ground State Proton Transfer

Studies of hydrogen transfer have been of great significance for the understanding of a wide variety of elementary reactions. For example, proton transfer reactions are one of the simplest and most essential processes in chemistry. A ground state proton transfer reaction, which is normally known as acid-base reaction, is one of the most fundamental and important types of reaction in chemical[1] and biological[2] systems. According to the Brønsted-Lowry acid-base theory, an acid, which is known as "proton donor", is the substance that can donate H^+ ions to a base, known as "proton acceptor". The reaction between acid and base is a proton transfer, and the measure of acidity is expressed by K_a and pK_a.[3]

1.2 Excited State Proton Transfer (ESPT)

Excited state proton transfer (ESPT) reactions, which have received considerable attention in recent years, are not as common as those occurring in the ground state. The acid-base properties of organic compounds in the electronic excited state are considerably different from those in the ground state. Compared to the ground state, many acid dissociation constants in the electronic excited state (pK_a^*) increase by 5-10 orders of magnitude.[3] This is not surprising since pK_a values are related to the electronic structure, which changes on excitation. The various processes that can occur upon excitation of a molecule are shown in the following Jablonski diagram (Figure 1.1). As in the diagram

shown, the molecule may be in a singlet or a triplet state. The ground state is assigned as S_o, which is the lowest energy singlet state, and the first excited singlet state is assigned as S_1. The triplet excited states are given as T_n (e.g, T_1 or T_2). The non-radiative deactivational pathways include internal conversion (IC) and intersystem crossing (ISC), and the radiative deactivational pathways include fluorescence and phosphorescence emission. Radiative transitions are indicated with straight arrows (⟶), while nonradiative transitions are generally indicated with wavy arrows (⇝).

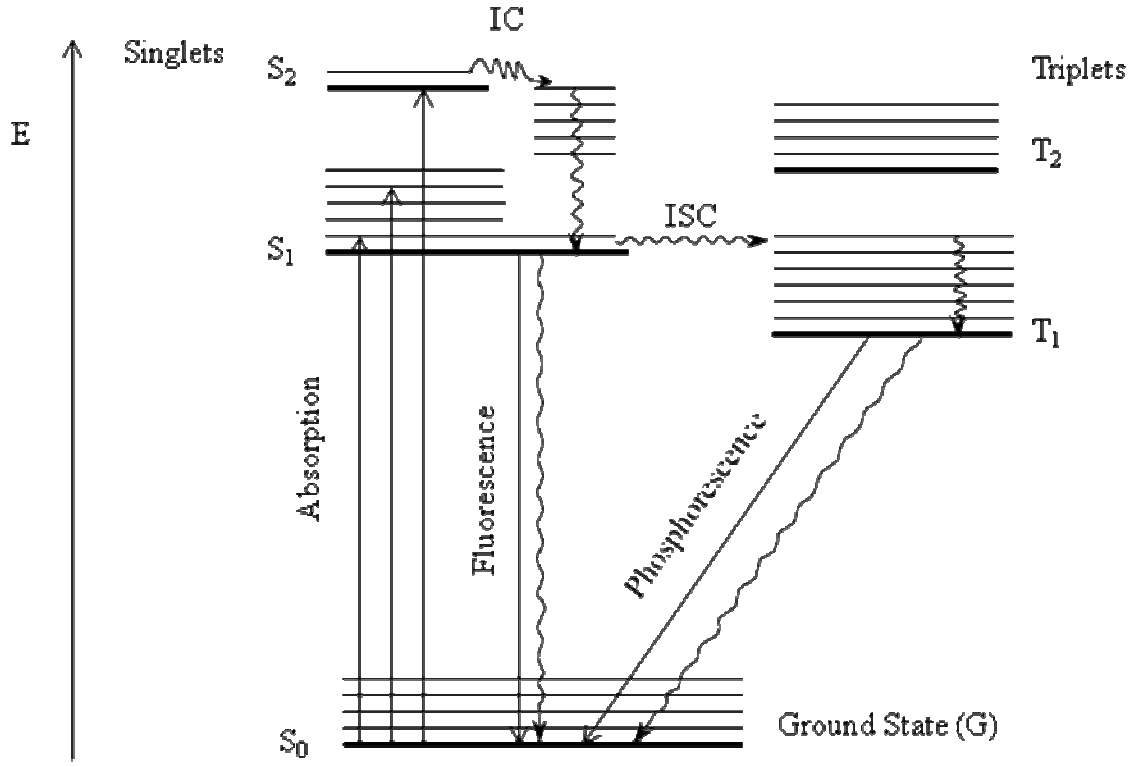

Figure 1.1 Jablonski diagram (Adapted from D. N. Sathyanarayana's "Electronic absorption spectroscopy and related techniques", Page 384).[4]

Quantum yields[5] are defined as the number of distinct events occurring per photon absorbed by the system. Mathematically, the quantum yield of a process is defined as follows (Eq. [1.1]);

$$\Phi = \frac{\text{number of molecules reacting or formed}}{\text{number of quanta absorbed}} \qquad [1.1]$$

The number of quanta absorbed can be measured by an actinometer, which is a reaction system for which the quantum yield is known. The quantum yield of photochemical reactions, referring specially to the primary process, is always ≤ 1. The primary process is here defined as starting with absorption of a photon and ending with the disappearance of the molecule or its deactivation to a nonradiative state.

1.2.1 Excited State Intermolecular Proton Transfer ($ESI_{er}PT$)

In the $ESI_{er}PT$ process, the proton is transferred from one molecule (proton donor) to another molecule (proton acceptor). The investigation of this process was begun by Weber[6,7] and Förster[7,8] in 1931 and 1949, respectively. Weber reported the shift of acid-base equilibrium of series of aromatic compounds in the excited state.[7] Förster provided the correct explanation for Weber's observation and initiated the field of excited state intermolecular proton transfers ($ESI_{er}PT$). He proposed a valuable method to estimate the pK_a of a molecule in an excited state (pK_a^*), based on its pK_a in the ground state, and the absorption and/or emission spectra of the molecule. The method is now known as the Förster cycle.[7] Based on this theory, it is predicted that the acidity of photoacids (such as hydroxyaryls and aromatic amines) and basicity of photobases (such as nitrogen heteroaromatics) increase upon electronic excitation.[9]

1.2.2 Excited State Intramolecular Proton Transfer (ESIPT)

ESIPT occurs between heteroatoms, like oxygen or nitrogen, which are part of an aromatic or polycyclic aromatic system. In the electronic excited state, the electron density of the lone pair of these atoms is altered. This alteration results in changes to the acidity and basicity of the molecule; therefore, the atom(s) to which electron density is transferred become more basic. The majority of ESIPT reactions involve the transfer of a proton from an oxygen donor to an oxygen or nitrogen acceptor. A few cases are known where a nitrogen atom can function as a donor and a carbon atom as an acceptor.[10] In case of hydroxybiphenyls, the phenolic OH functions as an acid site and the basic site is a heteroatom, such as an oxygen, or heterocylic nitrogen atom. The detailed mechanism for ESIPT is related to the distance between proton donor and proton acceptor in molecule. Therefore, the ESIPT process is further subdivided into direct ESIPT and solvent-mediated ESPT (*formal* ESIPT).

1.2.2.1 Direct ESIPT

The pioneering studies on direct (intrinsic) ESIPT were begun in 1955 by Weller.[7,11] He reported an unusually large Stokes shift in fluorescence emission observed for methyl salicylate (**1**) in methylcyclohexane at room temperature. When the acidic proton of **1** was methylated to give **2**, the fluorescence emission observed became the common mirror image of the absorption, and with no Stokes shift. He proposed that the Stokes fluorescence emission corresponded to an excited state isomer which was formed *via* excited state intramolecular proton transfer (ESIPT).

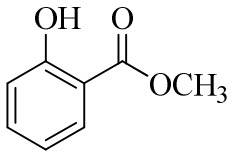

1

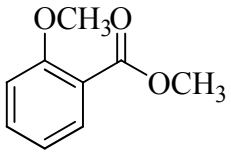

2

For illustration, the large Stokes shift of **1** can be explained by Scheme 1.1. In the ground state, **1** adopts an enol form **E** (based on the phenol) which is stabilized by intramolecular hydrogen bonding. The photoexcited keto form **3*****(K)** is produced by rapid proton transfer from the photoexcited enol form **1*****(E)**, which ultimately gives the ground state keto form **3**, which subsequently regenerates the original enol form **1** (**E**). It is proposed that the observed large Stokes-shifted band for **1** is due to the fluorescence emission of **3*****(K)**, which deactivates it to give **3**(**K**).

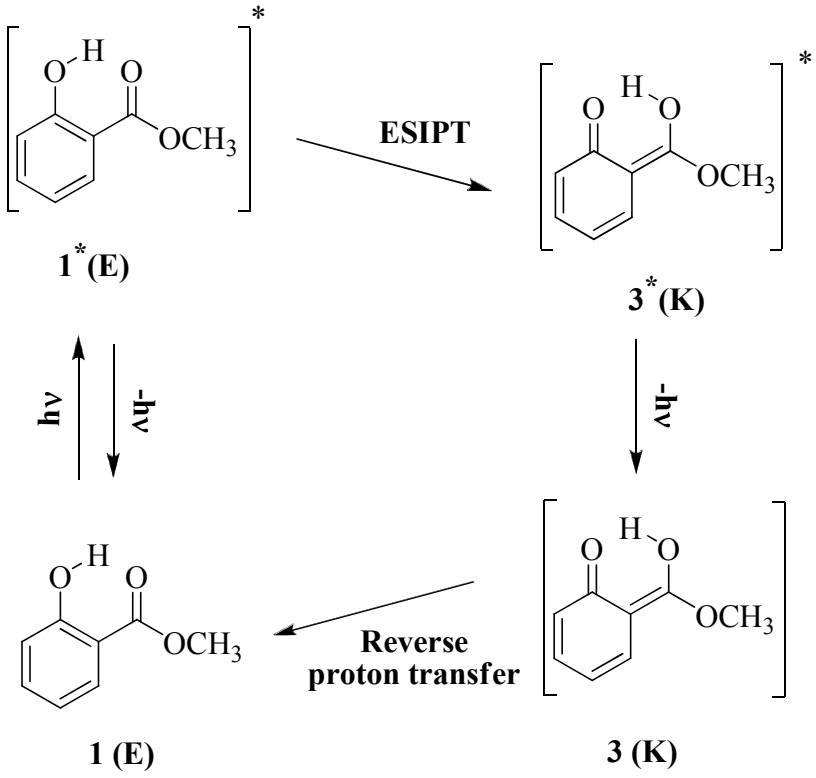

Scheme 1.1 ESIPT for Methyl Salicylate (**1**).

The direct ESIPT process has been applied to many industrial applications such as photostabilizers in polymers to reduce the harmful effects of UV irradiation on the material. For instance, Allen *et al.*[12] reported that 2-hydroxybenzophenone (**4**) undergoes very efficient ESIPT to give the corresponding excited state photo-tautomer **5**, which on relaxation rapidly returns to the starting material *via* deactivation to the corresponding ground state and reverse proton transfer (Eq. [1.2]).

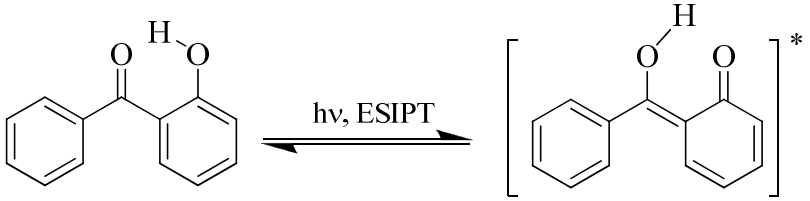

[1.2]

Keto form **4** Enol form **5**

The 2-hydroxyphenylbenzotriazole (**6**) also undergoes very efficient ESIPT to give the corresponding excited state photo-tautomer **7**, which on relaxation rapidly returns to starting material (Eq. [1.3]).

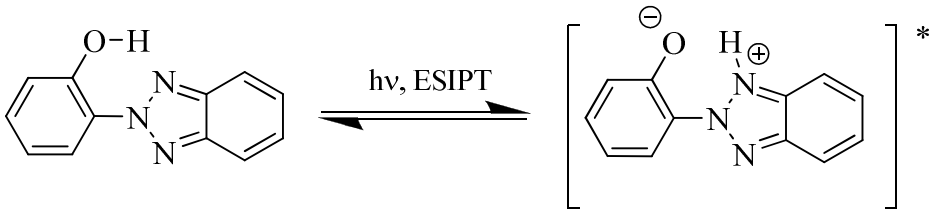

[1.3]

Enol form **6** Keto form **7**

New examples of the direct ESIPT process have been reported by Wan and co-workers.[13,14] They showed that 2-phenylphenol (**8**) undergoes deuterium exchange at the 2'-position when photolysed in deuterated protic solvents (e.g. D_2O, CH_3OD). The

exchange reaction was interpreted as arising when **8**-*OD** undergoes ESIPT to the 2'-position of the adjacent benzene ring, to give an *o*-quinone methide intermediate **9** (Scheme 1.2). This intermediate can lose either hydrogen or deuterium from the site of the deuteration. Loss of hydrogen (which should be kinetically preferred) generates deuterated 2-phenylphenol (**8**-*2'D*). The direct ESIPT mechanism of **8**-*OD* was confirmed by photolysis of **8**-*OD* at low concentrations of D_2O in CH_3CN, and also in the solid state.

Photolysis of **8** was carried out in low D_2O concentrations, which did not affect the efficiency of deuterium exchange at the 2'-position except at very low D_2O content. The observed sharp rise in exchange efficiency at these low D_2O concentrations was observed and interpreted as due to the exchange of **8**-*OH* to generate **8**-*OD*. Thus, when the substrate is **8**-*OD*, the efficiency of deuterium exchange at 2'-position becomes independent of D_2O content. Additionally, irradiation of powdered crystals of **8**-*OD* also showed deuterium exchange at the 2'-position.[14]

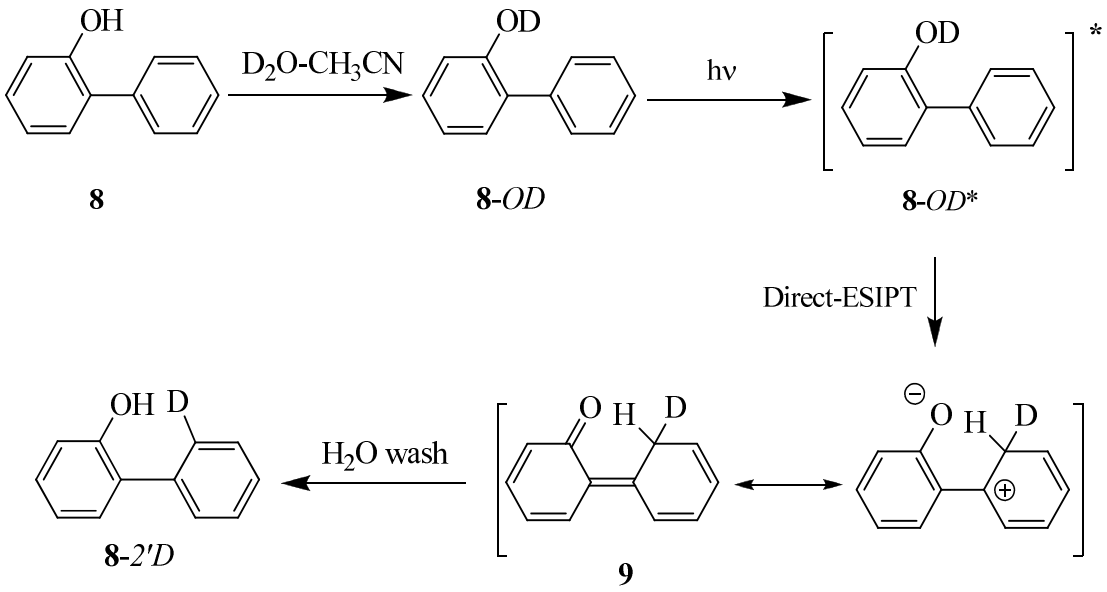

Scheme 1.2 Direct ESIPT Mechanism of **8** in D_2O.

1.2.2.2 Requirements of Direct ESIPT Process

Direct ESIPT is a complex process which occurs in subpicosecond timescales. Due to the kinetic limitation in ESIPT reactions and short diffusion time in the excited state, the molecule must have the proper structural orientation before ESIPT can occur. Two of the most important requirements of the ESIPT process is the presence of the desired reactive conformation and the possibility of intramolecular hydrogen bonding between the acidic and the basic moieties of the molecule in the ground state. Both of these must be satisfied if excitation will ultimately lead to intramolecular proton transfer.

Upon excitation of a molecule to the first excited singlet state, the charge densities of the molecule change. Semi-empirical AM1 calculations can be used to predict the structural and electronic properties of molecules undergoing possible ESIPT. For instance, AM1 calculations for **8** show that the compound exists in a twisted form in the ground state, with a dihedral angle between the two rings of about ~54^o (Figure 1.2).

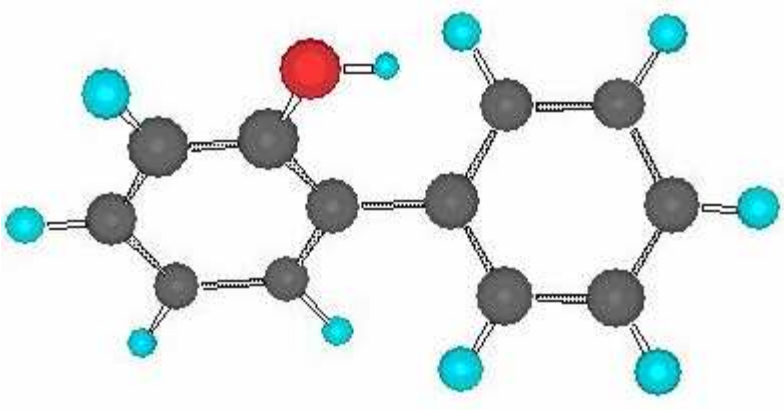

Figure 1.2 Optimized geometry (Chem 3D, AM1/MOPAC) in the ground state of **8** (dihedral angle ~54^{o}).

This twisted ground state structure allows some overlap between the s-orbital of the hydroxyl group with the accepting π-system of the adjacent benzene ring. The twisted geometry of the molecule and overlap of the hydroxyl group with the accepting π-system are essential requirements for efficient proton transfer between donor and acceptor upon electronic excitation (Scheme 1.3).[13, 14]

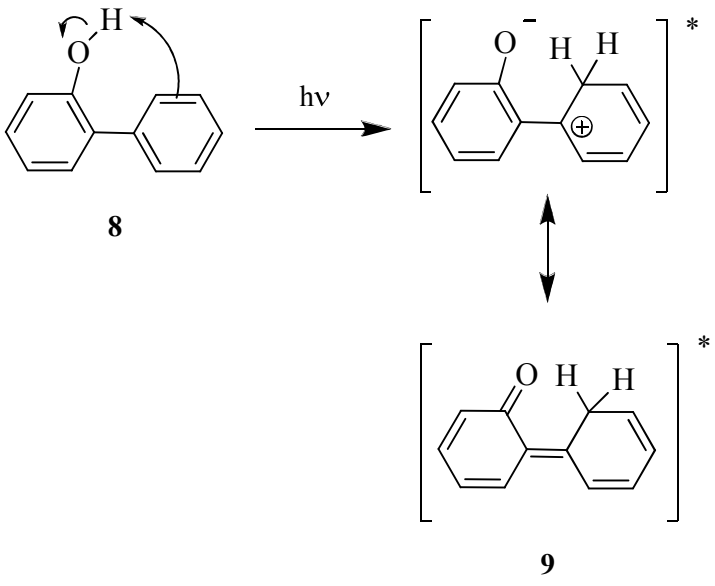

8 **9**

Scheme 1.3 Direct ESIPT Process in **8**.

1.2.2.3 Water-Mediated ESPT (*formal* ESIPT)

Water-mediated ESPT occurs when the donor and acceptor groups are sufficiently far apart that intrinsic proton transfer is not possible. In this case, the proton transfer may be facilitated by protic solvent molecules. This process has been widely studied. For example, the water-mediated ESPT of 7-hydroxyquinoline (**10**)[15] has been studied by Tokumura *et al.* and for **8** by Wan and co-workers.[13, 14] A hydrogen bonded solute-solvent complex is usually already present in the ground state and when the molecule is excited, a proton transfer between the donor and acceptor groups takes place *via* a proton shuttle or relay. Intermolecular proton transfer reactions typically involve a double proton transfer: one proton is exchanged between the donor and solvent molecule and another between the solvent molecule and the acceptor group (Schemes 1.4 and 1.5).

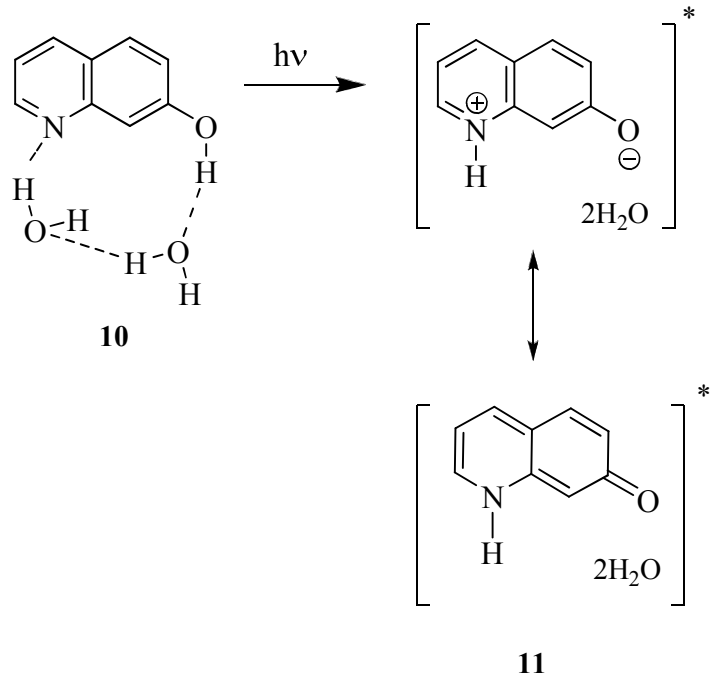

Scheme 1.4 Water-mediated ESPT (*formal* ESIPT) mechanism of **10**.

Phenol **8** also undergoes photoinduced deuterium exchange at the 4'-position of the ring (that does not possess the OH group), *via* a water-mediated ESPT mechanism (Scheme 1.5). The experimental results support this mechanism since the efficiency of this process is highly dependent on the water content of the solvent system.

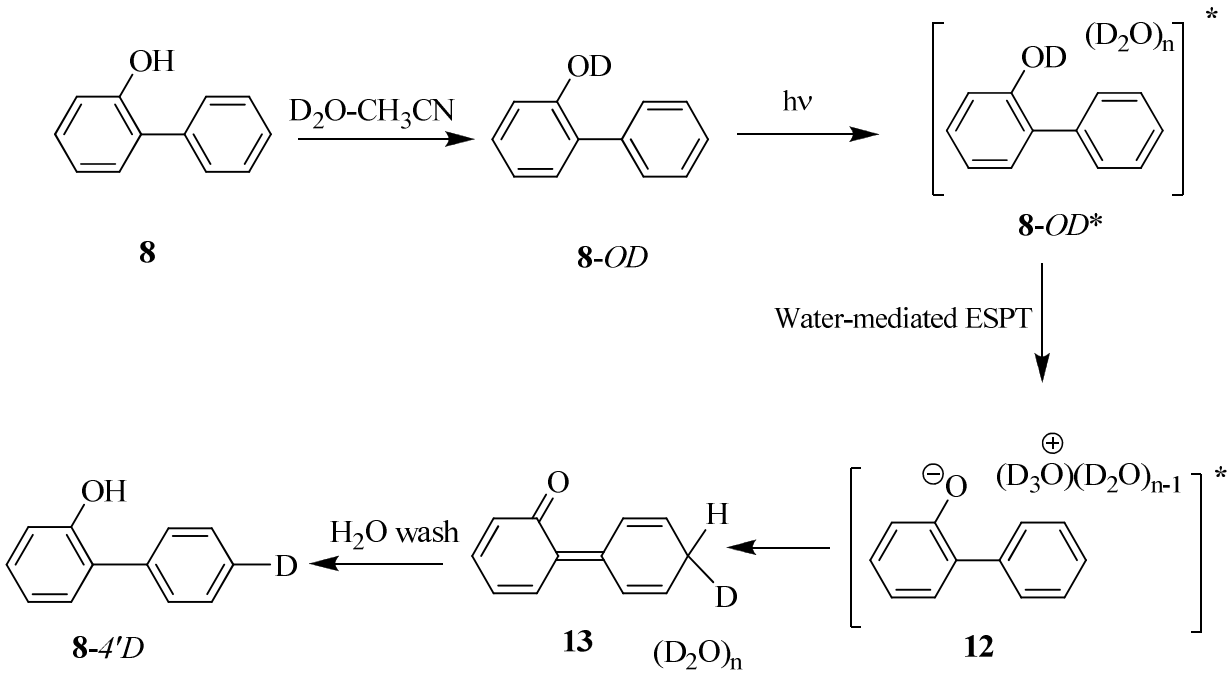

Scheme 1.5 Water-mediated ESPT (*formal* ESIPT) mechanism of **8**.

The fluorescence emission band of the phenolate **12** is clearly observable upon addition of significant amounts of H_2O, and further supports the formation of **12** in the water-mediated ESPT (*formal* ESIPT) mechanism.

1.2.2.4 ESIPT in Hydroxyaromatic Compounds

A number of studies concerning the ESIPT process in hydroxyaromatic compounds such as phenols and naphthols have been reported.[16] Phenolic compounds

play an important role in many chemical and biological processes[17] and their behaviour in the electronic excited state is of significant research interest.[18]

Proton transfer to an aromatic compound is a class of electrophilic reaction that has been known for many years. It requires harsh conditions such as concentrated acids, or use of the dangerous and environmentally harmful chemical reagents. Discovery of an efficient ESIPT process in phenolic compounds under mild conditions might lead to a more preferable route. The first example of ESIPT to carbon (from phenol) was reported by Yates *et al.*[19], while studying the photohydration reaction of *o*-hydroxystyrene (**14**) (Scheme 1.6). Photolysis of **14** in aqueous CH_3CN gave the hydration product **16** in high yield. Proton transfer from phenol OH to the β-carbon is believed to be the primary photochemical step (ESIPT) in S_1, forming **15**. The intermediate quinone methide **15** is trapped by water to give photohydration product **16**.[20]

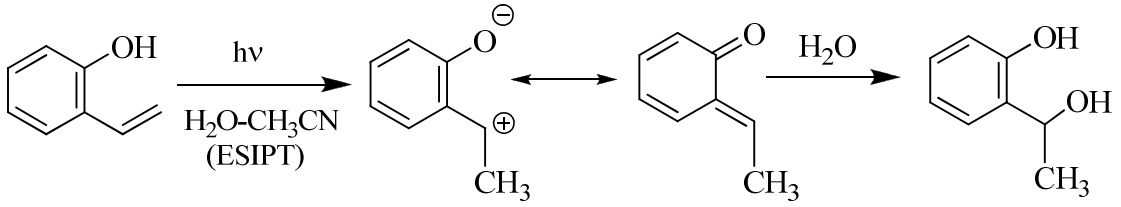

14 **15** **16**

Scheme 1.6 ESIPT process in **14**.

Wan and co-workers[13, 14] have presented results for the photochemical deuterium exchange in **8** and related compounds that is entirely consistent with a direct ESIPT from the phenol moiety to the ring which does not possess the OH group (2'-position). This is the first explicit direct ESIPT to a carbon atom that is part of an aromatic ring. A number of other related hydroxyaromatic systems have been studied[21] , all of which have been shown to undergo direct or solvent-mediated ESIPT.

1.3 Photosolvolysis

Photosolvolysis has the potential to become a useful reaction in synthetic organic chemistry since mild reaction conditions are required. Mechanistic insight into the photosolvolysis pathways showed that these reactions generate ion pairs, which are much less common intermediates than radicals or radical pairs in organic photochemistry.

A considerable amount of work on photosolvolysis reaction has been carried out by Wan and co-workers.[22] For example, it has been reported the photolysis of 9-fluorenol (**17**) in aqueous methanol gave the corresponding methyl ether product **19.** The formally anti-aromatic 9-fluorenyl cation **18** was generated from the corresponding **17,** by way of a photo-dehydroxylation pathway (Scheme 1.7).

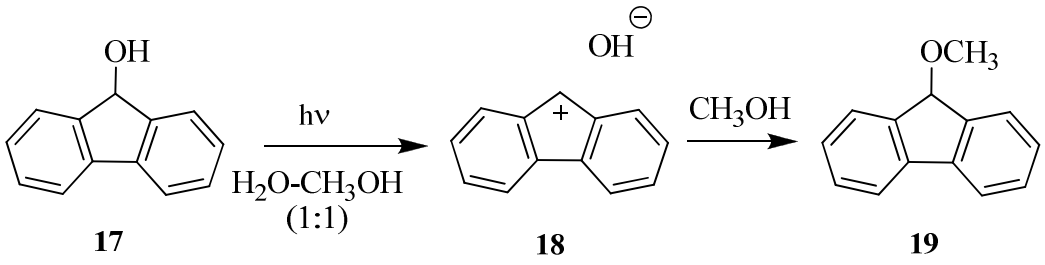

Scheme 1.7 Photosolvolysis of **17** in H_2O-CH_3OH.

It has also been reported that photolysis of hydroxybenzyl alcohol derivatives **20** give rise to quinone methide **21** in aqueous solutions.[23] In MeOH-water, the corresponding methyl ether product **22** was formed (Scheme 1.8). In this reaction, a formal loss of H_2O from photoexcited **20** occurs, presumably driven by the enhanced acidity of the phenolic OH in S_1.

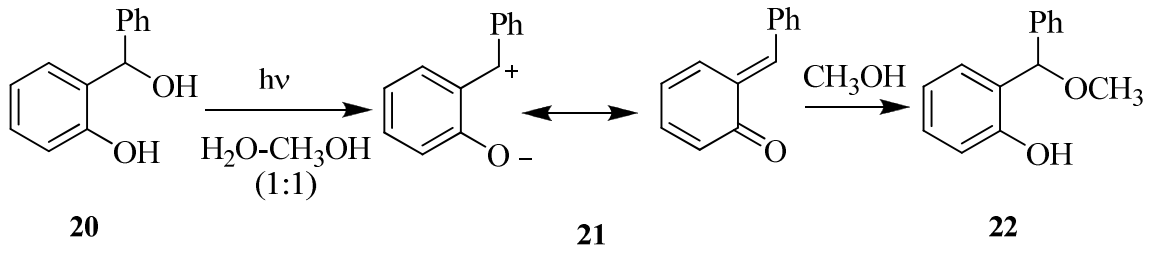

Scheme 1.8 Photosolvolysis of **20** in H_2O-CH_3OH.

1.4 Proposed Research

ESIPT between a phenol OH and a carbon atom that is a part of an aromatic ring adjacent to the phenol has now been observed by Wan and co-workers[13,14] for a variety of related substrates. The proton accepting ring includes biphenyl, fluorene, pyridine, naphthalene, and anthracene.[24] However, information regarding substituent effects on the proton accepting ring is lacking. Therefore, 2-phenylphenols **23-28** were synthesized with electron-donor and electron-acceptor groups to study substituent effects on the ESIPT process anticipated for these compounds.

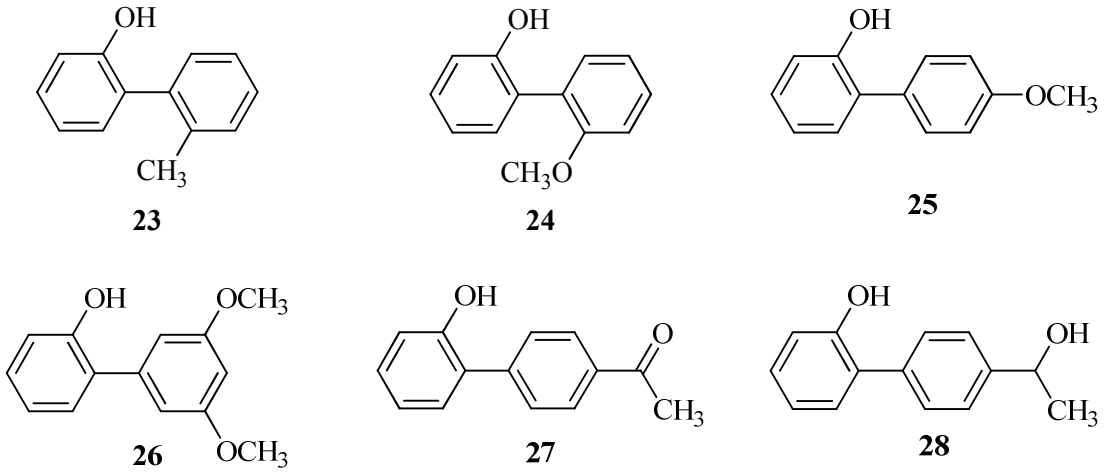

A number of reasons led us to choose the above compounds. The main reason was to investigate the effect of substituents on the ESIPT process and the second reason was the possibility of a competing photosolvolysis reaction in **28** due to the presence of the benzyl alcohol moiety. It would be natural to expect that all of **23-28** to undergo ESIPT based on the result obtained for **8**.

The addition of a simple alkyl group at the *ortho* position might have a huge effect on dihedral angle of these biaryls in the electronic excited state. Therefore, compound **23** is a very suitable candidate to investigate this effect on the ESIPT process.

The quantum yield for deuterium exchange for **8** (i.e. formation of **8**-*2'D*) was modest (0.041 in 1:3 D_2O-CH_3CN). The presence of an electron donating group on the adjacent proton accepting ring should stabilize the cationic intermediates, which could change the quantum yield of ESIPT substantially. Therefore, compounds **24, 25**, and **26** were chosen for study.

The effect of an acetyl substituent in **27** could provide additional insights for the ESIPT pathway. Furthermore, reduction of biphenyl ketone **27** readily gives **28**, which has the potential to undergo photosolvolysis as well as ESIPT. The simplicity of these six compounds and their relatively straightforward synthesis are final reasons for choosing this set of biphenyls for study in this Thesis.

Chapter 2

Results and Discussion

2.1 Synthesis

The general procedure for the synthesis of **23** and **25**-**27** employed the well-known Suzuki coupling reaction, adapted from the work of Nam *et al.*[25] All the starting materials were purchased from Aldrich and used as received. The required boronic acids were coupled with 2-bromophenol to form the biaryl bond. All derivatives **23** and **25**-**27** were successfully synthesized in yields varying from 38 to 71% (Eq. [2.1]).

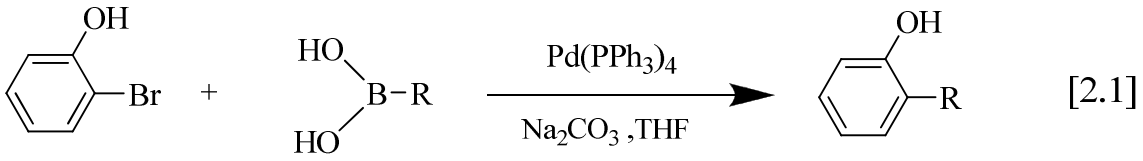

[2.1]

23 R = 2-methylphenyl
25 R = 4-methoxyphenyl
26 R = 3,5-dimethoxyphenyl
27 R = 4-acetylphenyl

Phenol **24** was prepared based on a published report,[26] modified by the addition of polyethylene glycol (PEG) as solvent. Initially, the reaction mixture was dissolved in acetone as reported in the original paper. The reaction was monitored by TLC but no new spot was detected after four hours. Addition of PEG resulted in formation of the expected product after three hours. On stirring at room temperature for 24 hours, **24** was synthesized in 85% yield (Eq. [2.2]).

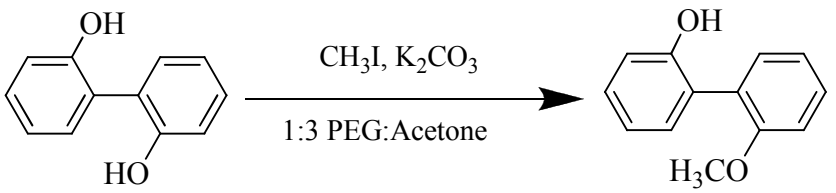

[2.2]

24

Alcohol **28** was made *via* standard reduction of ketone **27** in CH_3OH using $NaBH_4$ (91%) (Eq. [2.3]).

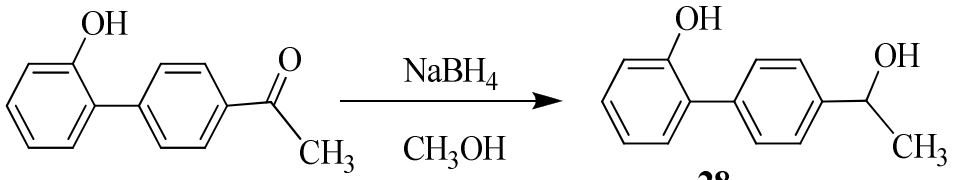

[2.3]

27 **28**

2.2 Geometries of Substrates in the Ground State

The structural and electronic features provided by semi-empirical AM1 calculations can help in the understanding of the mechanism of ESIPT reactions. It was mentioned in Section 1.2.2.2 that suitable ground state molecular structures (as exemplified by dihedral angles (DA, φ) and bond lengths) are considered to be important for ESIPT processes. Therefore, the molecular geometry in the ground state was obtained for each molecule using semi-empirical AM1 calculations.

Using AM1, the relative energies associated with rotation about the aryl-aryl bond for **25**, **26**, and **27** are shown in Figure 2.1. Optimized geometries were obtained by fixing the biaryl angle and allowing all other coordinates to reach a minimum energy conformation. The process was repeated for twisting about the aryl-aryl bond at 10^o increments.

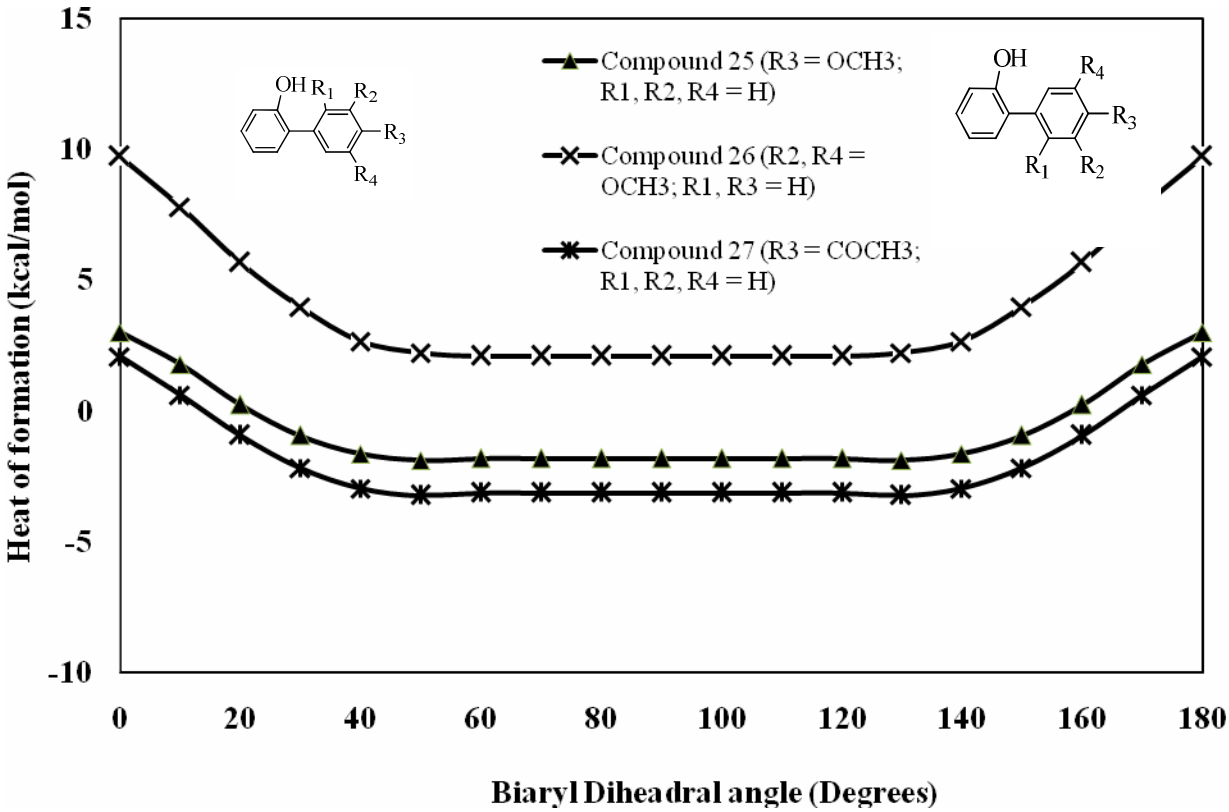

Figure 2.1 Heat of formation associated with rotation about the biaryl bond of **25** (▲), **26** (×), and **27** (*), as predicted by AM1 calculation.

All of these compounds show a wide shallow energy minimum ranging between twist angles of 50° and 140° indicating that biaryl bond is rotationally flexible. The dihedral angles (DA, φ) and bond lengths for the lowest energy structure of each molecule using semi-empirical AM1calculations are presented in Table 2.1 and shown in Figure 2.2. The data show that the lowest energy ground state geometries are twisted with the dihedral angle between the benzene rings being 69.2°, 57.6°, 50.0°, 52.7° and 52.0° for **23**, **24**, **25**, **26**, and **28**, respectively (Table 2.1). The data are consistent with an earlier result reported for **8** (~54°),[14] with the exception of **23** (69.2°), for which the dihedral angle is considerably larger. Among these phenylphenols, **23** may be expected to least likely undergo efficient ESIPT.

Table 2.1 Calculated Structural Parameters for Hydroxybiaryls in the Ground State.

Compound	Dihedral Angle [a]	OH-C(2') Distance[b]
23	69.2°	4.69 Å
24	57.6°	3.44 Å
25	50.0°	3.92 Å (4.96 Å)
26	52.7°	2.29 Å (3.29 Å)
28	52.0°	2.28Å (3.29 Å)

[a]Dihedral angle between the two aryl rings as predicted by semi-empirical AM1 geometry optimization in the ground state. [b]Distance between the OH proton and the carbon atom at the 2'-position of the other aryl ring, as predicted by AM1 geometry optimization in the ground state.

Semi-empirical AM1 calculations in the ground state for **23** show that the dihedral angle between the two aromatic rings as well as the critical OH-C (2') distance are larger than for the other biphenyls. This is expected to reduce the degree of charge transfer or interaction between two rings in the excited state. These informative calculations indicate that the larger dihedral angles cause the hydroxyl proton to lie farther away from the 2'-carbon atom which might affect the efficiency of ESIPT. The dihedral angle for **23** and the critical OH-C (2') are larger than for the other molecules which might cause a lower deuterium exchange quantum yield.

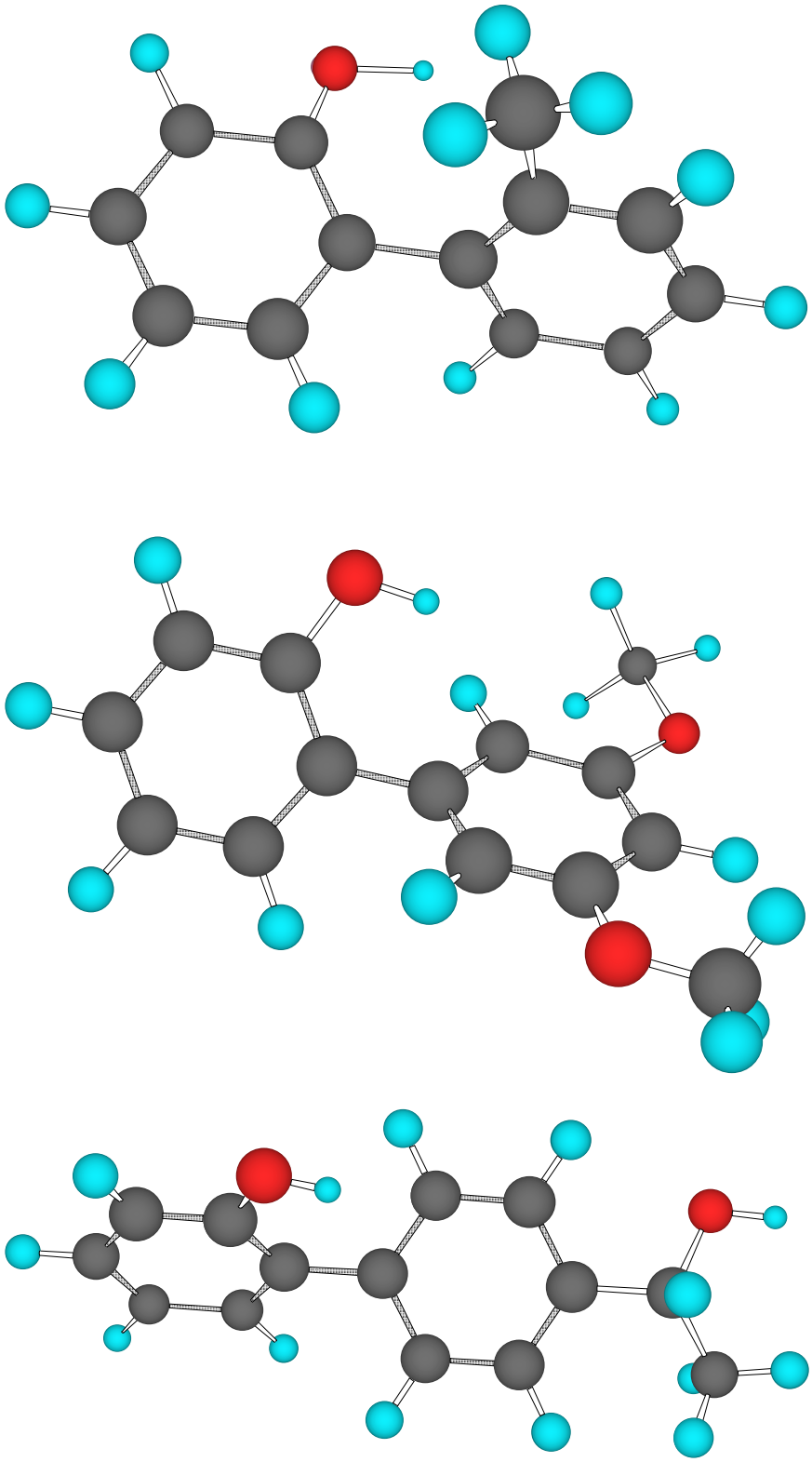

Figure 2.2 Optimized geometries (Chem 3D, AM1/MOPAC) in the ground state for **23** (69.2°, top), **26** (52.7°, middle), and **28** (52.0°, bottom).

2.3 Photochemical Product Studies

2.3.1 Photochemical Deuterium Exchange

Product studies of **23**-**28** were carried out with irradiation at 254 nm in different solutions. Initially, photolysis of **23**-**28** was carried out in 1:1 (v/v) H_2O-CH_3CN (10^{-3} M, 254 nm, 16 lamps, and 5-120 min) which resulted in complete recovery of substrate. These results are consistent with ESIPT being the only photochemical pathway for compounds **23**-**28**.

ESIPT would be discernable only on photolysis in deuterated protic solvents (e.g. D_2O or CH_3OD). Thus, photoreactions were subsequently carried out in D_2O-CH_3CN (10^{-3} M, and 16 lamps) at various photolysis times. The results show that all of **23**-**26** and **28** undergo deuterium exchange at the 2'-position (labelled as proton H_a in all of these compounds) of the ring which does not possess the OH group, followed by a much less efficient exchange at the 4'-position (H_c for **23** and **24**; H_b for **26**).

The exchange is readily observable by 'H NMR; however the NMR analysis cannot distinguish the amount of di-deuterated from mono-deuterated compounds (since there are two equivalent *ortho* positions for **25**, **26**, and **28**). Relative amount of mono-, di-, and higher deuterated products would be discernable only by MS analysis. One would expect to observe greater mono-deuterated compound at lower conversion, and increase of the di-deuterated product (at the *ortho* positions) at higher conversion.

Photolysis of **23** in 1:9 (v/v) D_2O-CH_3CN (10^{-3} M, 254 nm, 16 lamps, and 1 h) gave the corresponding deuterated compounds at 2'and 4'-positions (Eq. [2.4]).

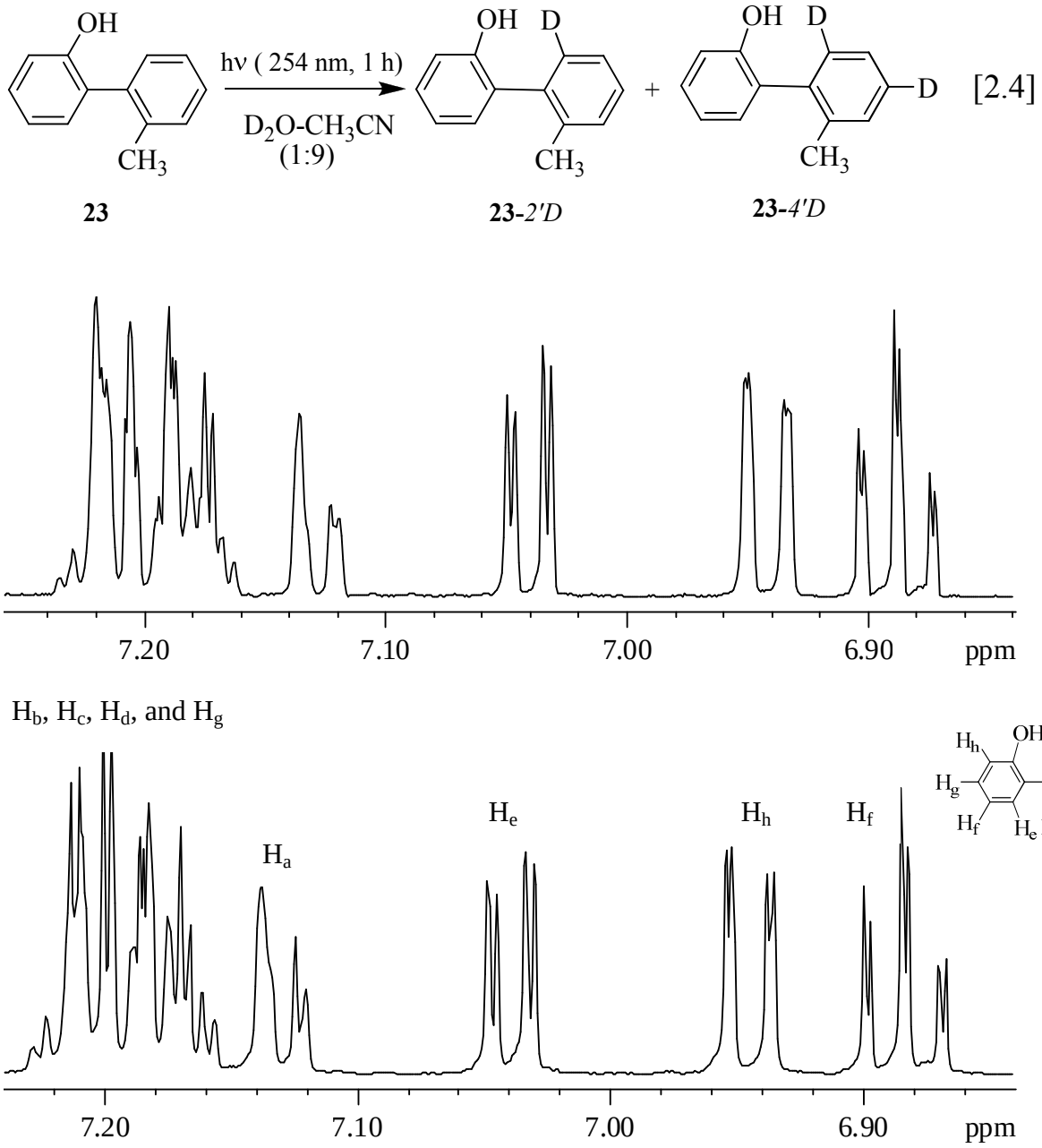

Figure 2.3 ^{1}H NMR (500 MHz, $(CD_3)_2CO$) showing the expanded aromatic region of **23** before (bottom) and after (top) 1 h irradiation in 1:9 (v/v) D_2O-CH_3CN. NMR integration indicates 33% and 14% deuteration at the H_a and H_c positions respectively. The estimated error for the percentage deuterium exchange calculation for the 2'-position is ±9% and for the 4'-position is ±6%.

The efficiency for the exchange at the 2'-position is higher than that of the exchange at the 4'-position. After 1 hour of irradiation in 1:9 (v/v) D_2O-CH_3CN, the efficiency for deuterium exchange at 2'-position and the 4'-position are 33% and 14%, respectively. The exchange at the 2'-position is readily observable by 'H NMR (500 MHz) and the aromatic region of **23** prior to and after 1 hour irradiation is presented in Figure 2.3.

After 1 hour of irradiation (254 nm, 16 lamps, and 1:9 (v/v) D_2O-CH_3CN), deuterium exchange at the 2'-position is obvious from the reduction of the area of the peak assigned to H_a (δ 7.15 ppm, d). The peaks corresponding to the protons H_b, H_c, H_d, and H_g overlap and are not resolvable, even when run on 500 MHz instrument. The deuterium exchange at the 4'-position (H_c) was roughly estimated by measuring the intensity of the combined peak areas of H_b, H_c, H_d, and H_g before photolysis and subtracting the intensity of their combined peak areas after photolysis. The possible deuterium exchange at H_g can be excluded because the splitting pattern of the adjacent protons (H_f and H_h) was unchanged after photolysis. A similar argument can be made to exclude exchange at H_b, namely, the splitting pattern of the peak assigned to the adjacent proton H_a was unchanged after photolysis. Based on previous work the exchange at H_d would seem unlikely.[14]

Since **24**, **25**, and **26** all have methoxy substituent(s) on the adjacent benzene ring, it would be natural to expect that the photochemical behaviour of **24**, **25**, and **26** would be similar. However, it was not clear whether methoxy substituted at the *ortho*, *meta*, or *para* position(s) would enhance deuterium exchange in the excited state. Indeed, the photolysis of **24**, **25** and, **26** in 1:3 (v/v) D_2O-CH_3CN (10^{-3} M, 254 nm, and 16 lamps) at

various times gave the corresponding deuterated compounds of **24** and **26** at the 2'and 4'-positions and the deuterated compounds of **25** at the 2'-position.

The photochemical deuteration of **24** at the 2'-position was obvious. The reduction of the area of the peak assigned to this proton (δ 7.23 ppm, dd, H_a) upon irradiation at 254 nm (16 lamps and 5 min) in 0.005 M D_2O (in CH_3CN) and in 0.25 M D_2O (in CH_3CN) (Eq. [2.5]) was observed.

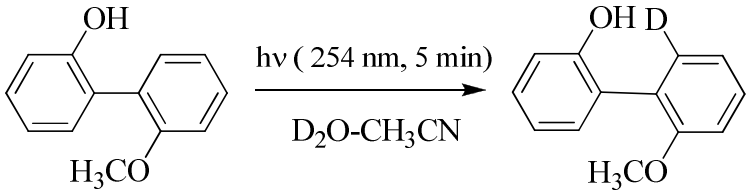

24 **24-*2'D***

[2.5]

The reduction of the area of the peak (deuterium exchange) at H_a was measured to be 20% and 37% in 0.005 M and 0.25 M D_2O, respectively (Figure 2.4). The deuterium incorporation at H_a was also confirmed by the growth of a broad doublet at H_b (δ 6.99 ppm) on top of the original doublet of doublets of doublets (ddd) splitting pattern (but with no net increase in integration), due to the unresolvable coupling with a deuterium (I = 1) now present at the 2'-position. Unresolvable coupling to deuterium was also observed for the proton at H_c (δ 7.34 ppm). As more deuterium is incorporated into the 2'-position, the splitting pattern for the H_b proton resembles more of a doublet of doublets than a ddd pattern. Due to the low conversion of these experiments, the exchange at H_c was not observable. No significant changes in coupling were observed for H_d, which is consistent with the distal nature of this proton to the exchange site.[27]

MS analysis also indicated that after 5 min irradiation (254 nm and 16 lamps) in 0.005 M D_2O (in CH_3CN), the compound was 69% non-deuterated and 31% mono-

deuterated (Table 2.3). This result is in agreement with the expectation that, at low conversion, a greater proportion of deuteration at one of the *ortho* positions would prevail.

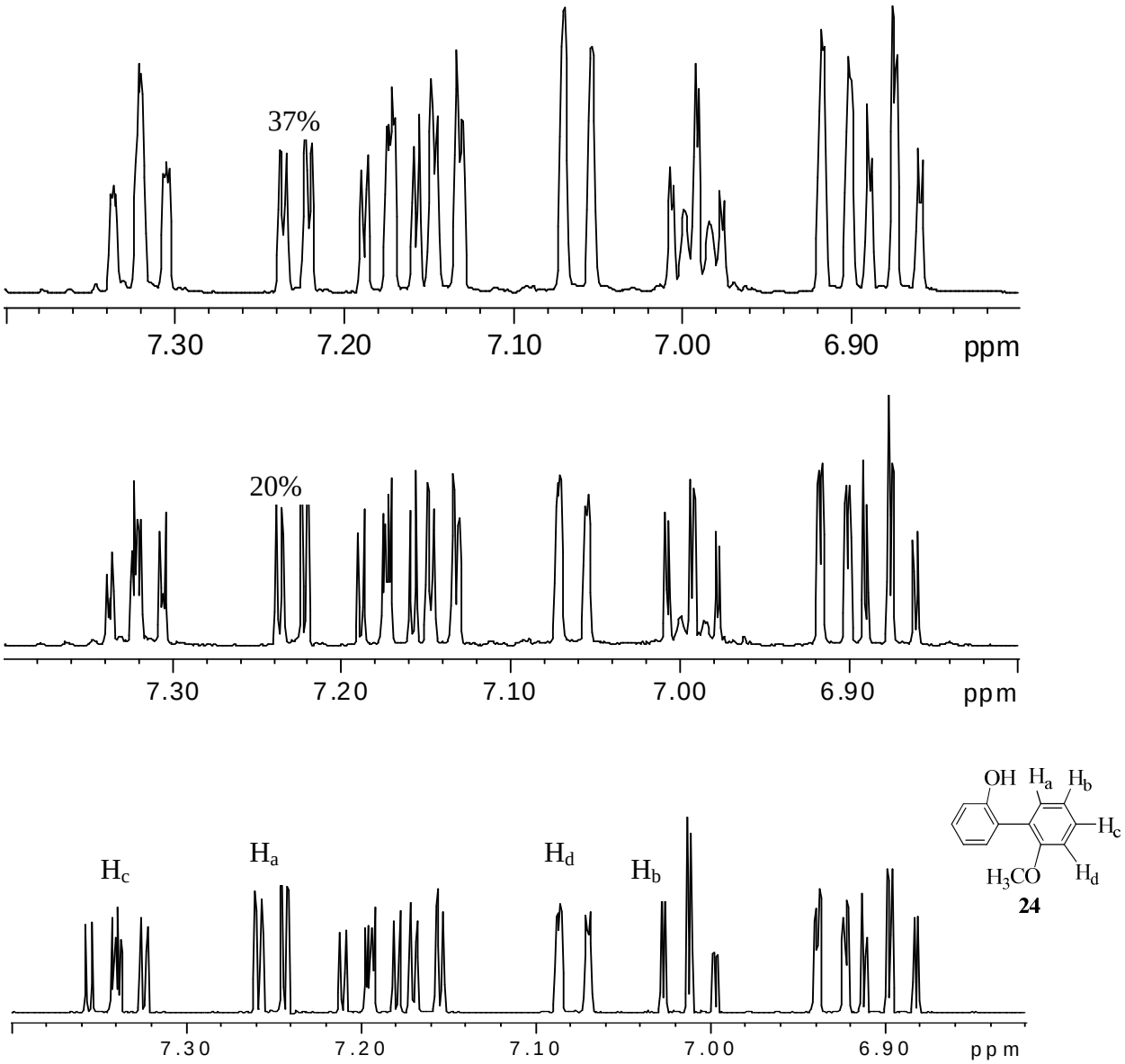

Figure 2.4 ^{1}H NMR (500 MHz, $(CD_3)_2CO$) showing the expanded aromatic region of **24** before (bottom), after photolysis (middle 0.005M D_2O in CH_3CN, 254 nm, 16 lamps) and (top, 0.25 M D_2O in CH_3CN, 254 nm, 16 lamps) respectively, in 5 minutes. ^{1}H NMR integration indicates 20% and 37% deuteration at the H_a position. The estimated error for the percentage deuterium exchange calculation for the 2'-position is ±10% and for the 4'-position is ±5%.

The deuterium exchange at the 4'-position for **24** is not obvious in Figure 2.4 but upon irradiation at 254 nm in 1:1 (v/v) D_2O-CH_3CN (10^{-3} M, 254 nm, 16 lamps, and 2 hours) both deuterium incorporation at the 2' and 4'-positions are evident from the reduction of the area of the peak assigned to the two protons (Eq. [2.6]). The deuterium exchange at the 2' and 4'-positions were measured to be 96% and 71%, respectively, by 'H NMR (500 MHz).

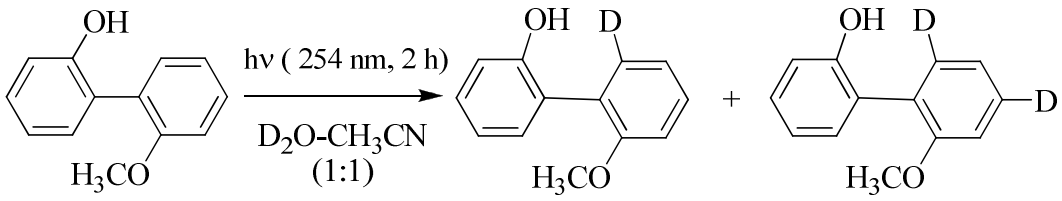

[2.6]

24 **24-*2'D*** **24-*4'D***

The study of the effect of water concentration on ESIPT efficiency in previously reported papers led to the conclusion that the observed ESIPT for **8** was intrinsic.[14] Therefore, the effect of water concentration on the photochemical exchange was also examined in this work, by photolysis of **24** at different concentrations of D_2O (in CH_3CN) at a fixed photolysis time (16 lamps, 5 min). The formation of **24**-*2'D* was analyzed by ^1H NMR, and the results from these runs appear in Figure 2.5.

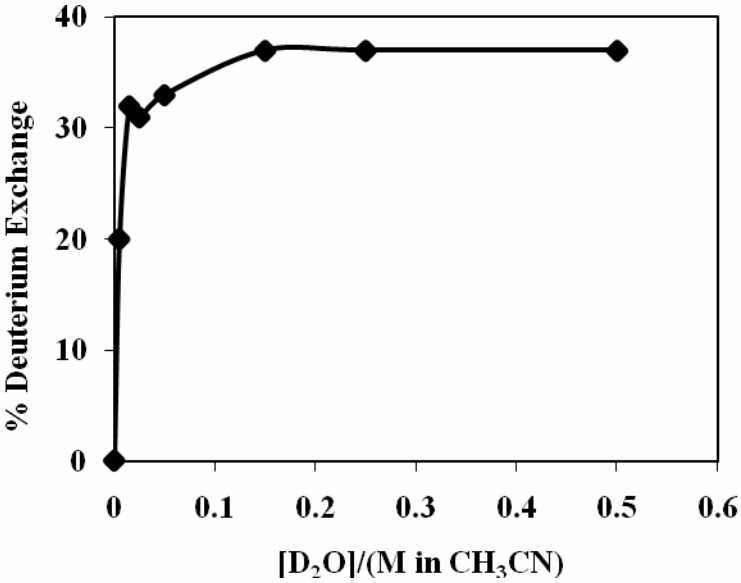

Figure 2.5 Plot of % deuterium exchange at the 2'-position of **24** as a function of D_2O content in CH_3CN as measured by ^1H NMR (Photolysis time 5 min).

As shown in Figure 2.5 for **24**, there is a sharp rise between 0 and 0.05 M D_2O (in CH_3CN) in deuterium exchange efficiency at the 2'-position. The sharp rise observed at low D_2O concentrations is due to the conversion of **24**-*OH* to **24**-*OD*. There is no dependence on D_2O content for exchange yield once all of **24**-*OH* has been fully converted to **24**-*OD*. This is consistent with an exchange mechanism arising from direct proton transfer from the phenol OH (OD) to the 2'-carbon atom of the adjacent phenyl ring in the excited state.

Photolysis of **25** in 1:1 (v/v) D_2O-CH_3CN (10^{-3} M, 254 nm, 16 lamps, and 2 h) also gave deuterated starting material at the H_a position (**25**-*2'D*) (Eq. [2.7]).

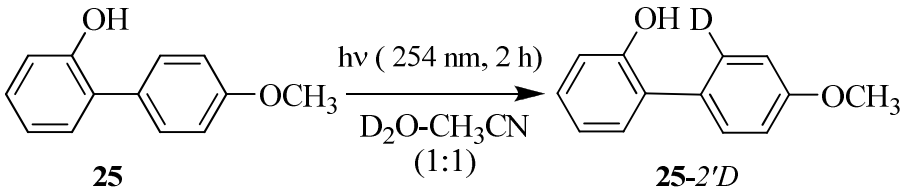

25 **25**-*2'D* [2.7]

After 2 h photolysis, **25**-*2'D* was formed (100% exchanged based on NMR integration) (Table 2.2). It should be noted that NMR analysis cannot distinguish the amount of dideuterated (since there are two equivalent *ortho* positions) from monodeuterated material. At low conversions, one would expect a greater proportion of deuteration at one of the *ortho* positions. At higher conversions, the extent of the dideuterated product (at both *ortho* positions) is expected to increase and this was confirmed by MS analysis. The MS analysis indicated extensive deuteration with significant M+1, M+2, and M+3 peaks which are 5% non-deuterated, 25% mono-deuterated, 62% di-deuterated, and 8% tri-deuterated (Table 2.3). The ^{1}H NMR spectrum of **25** after 2h irradiation shows a decrease in intensity of the OH peak which indicates that not all the initial OD has been fully converted to OH after the washing with H_2O. Therefore, the MS analysis showed greater amounts of deuterium content than what is present due to exchange on the benzene ring positions.

Photolysis of **26** in 1:3 (v/v) D_2O-CH_3CN (2 h) also yielded deuterated starting material **26**-*2'D* and **26**-*4'D*. The deuterium exchange was readily observed by ^{1}H NMR (500 MHz). The extent of deuterium exchange at the 2' and 4'-positions were measured to be 99% and 22%, respectively (Table 2.2). The deuterium incorporation in **26** was also confirmed by MS which showed the significant M+1, M+2, and M+3 peaks after 2 hours of photolysis and gave 3.8% none-deuterated, 8.5% mono-deuterated, 52% di-deuterated, and 35.7% tri-deuterated (Table 2.3).

Table 2.2 Deuterium Exchange Data for **24-26** and **28** using ^{1}H NMR Analysis.

Compound	Photolysis conditions	^{1}H NMR Analysis[a]	
		%D-2’	%D-4’
23	1:1 D_2O-CH_3CN (2h)	33	14
24	0.5:99.5 D_2O-CH_3CN (5 min)	37	0
24	1:1 D_2O-CH_3CN (2h)	96	71
25	1:1 D_2O-CH_3CN (2h)	100	0
26	1:3 D_2O-CH_3CN (2h)	99	22
26	1:3 D_2O-CH_3CN (30 min)	71	7
28	1:1 D_2O-CH_3CN (10 min)	14	0

[a]Percentage deuterium exchange at the 2’-(%D-2’) and 4’-(%D-4’) positions as measured by 'H NMR (500 MHz).

Table 2.3 Deuterium Exchange Data for **24**, **25** and **26** using MS Analysis.

Compound	Photolysis conditions	MS Analysis[a]			
		%0-D	%1-D	%2-D	%3-D
24	0.5:99.5 D_2O-CH_3CN (5 min)	69	31	0	0
25	1:1 D_2O-CH_3CN (2h)	5	25	62	8
26	1:3 D_2O-CH_3CN (2h)	4	9	52	36

[a] Percentages of non-deuterated (% 0-D), mono-deuterated (% 1-D), di-deuterated (% 2-D), and tri-deuterated (% 3-D) of **24**, **25** and **26** as measured by MS.

To gain further insights into the ESIPT process, the photolysis of **26** in 1:3 (v/v) D_2O-CH_3CN as a function of time appears in Figures 2.6 and 2.7. The results are llustrate the relative efficiency of exchange (by ^{1}H NMR) of the 2’ versus 4’-positions in **26** (as well as in **23** and **24).**

As shown in Figure 2.6, photolysis of **26** in 1:3 (v/v) D_2O-CH_3CN resulted in the quick disappearance of the signal due to the 2'-protons (δ 6.73 ppm, d, H_a) (Eq. [2.8]). Indeed, after 2 hours of photolysis, this proton had completely exchanged and the signal due to the 4'-proton (δ 6.47, t, H_b) broadened with deuterium incorporation at H_a since coupling with deuterium is not resolvable. Deuterium incorporation at the 4'-position is also evident from the reduction of the area of the peak assigned to the H_b at this position (δ 6.47, t). After 30 min of irradiation time in 1:3 (v/v) D_2O-CH_3CN, the 2'-positions and 4'-position are 71% and 7% exchanged with deuterium. The yield of **26**-*2'D* increased significantly from 71% to 99% after 2h irradiation in the same solvent system, while the yield of **26**-*4'D* increased from 7% to 22%. The results from Figure 2.6 clearly show that the efficiency for exchange at the 2'-positions is much higher than that for the exchange at the 4'-position at all photolysis times. All other peaks remain unchanged, consistent with the absence of deuterium exchange at these positions on photolysis.

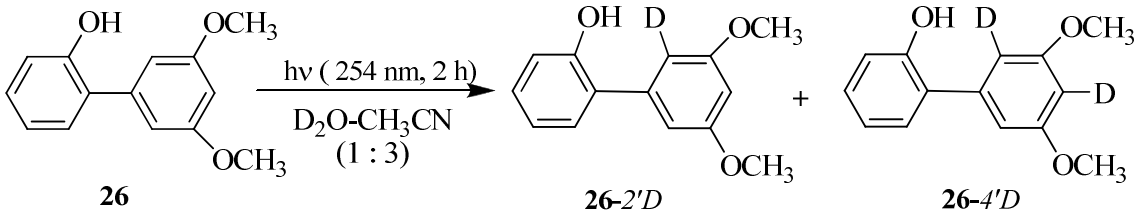

26 **26**-*2'D* **26**-*4'D* [2.8]

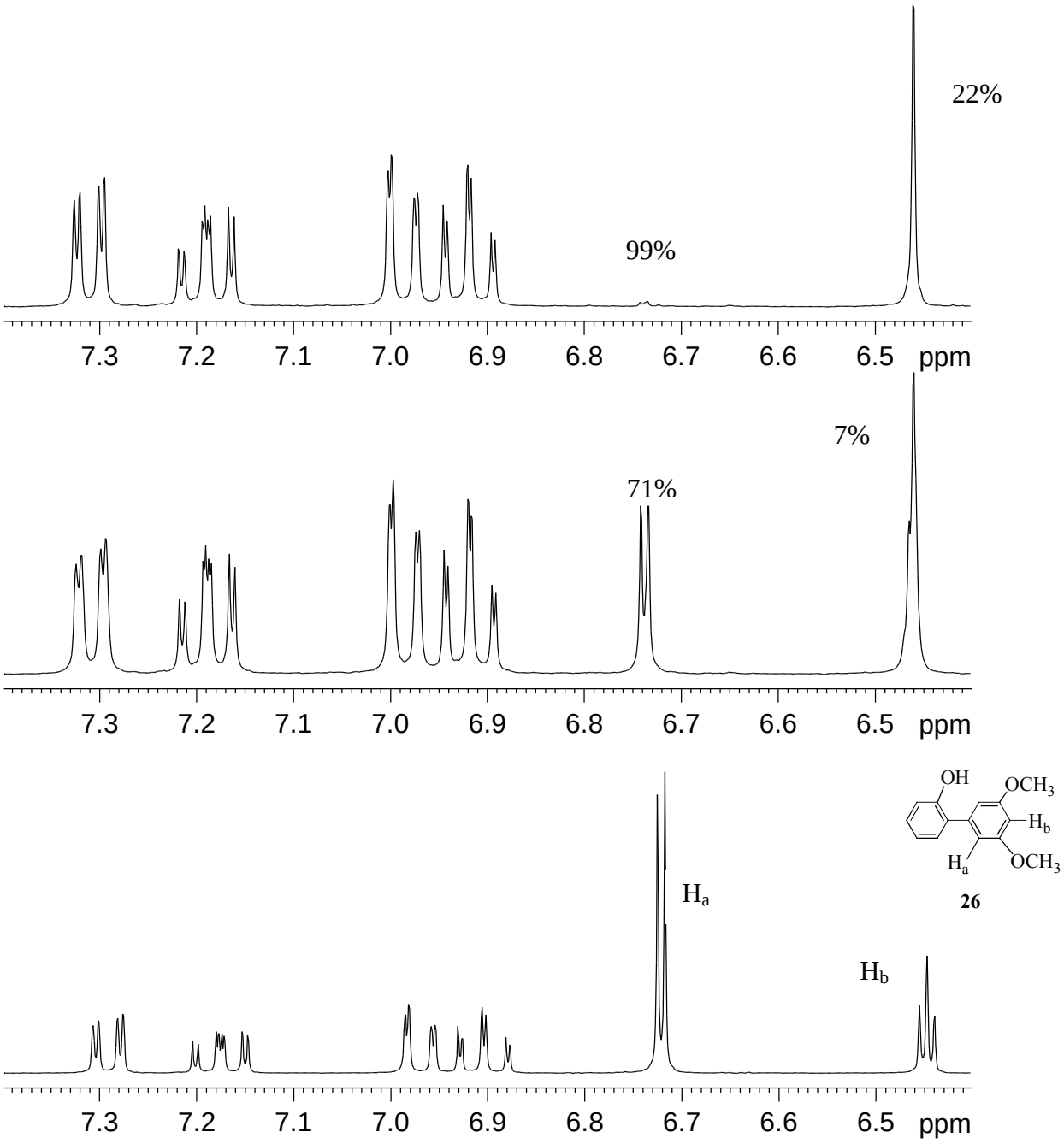

Figure 2.6 ^{1}H NMR (300 MHz , $(CD_3)_2CO$) showing the expanded aromatic region of **26** before (bottom), after photolysis (254 nm, 16 lamps) time 30 min (middle) and 2 h (top), respectively, in 1:3 (v/v) D_2O-CH_3CN. NMR integration indicates 71%, 7% and 99%, 22% deuteration at H_a, and H_b positions. The estimated error for the percentage deuterium exchange calculation for the 2'-position is ±8% and for the 4'-position is ±6%.

The yields of **26**-*2'D* and **26**-*4'D* generated in these runs were quantified by ^{1}H NMR and results are presented in Figure 2.7. The ^{1}H NMR data were normalized since there are two H_a protons for every one of H_b. The plot shows that deuterium exchange at the 2'-positions is significantly more efficient (≈ 9 times higher) than at the 4'-position. Therefore, we can assume that when deuterium is incorporated at H_b, a significant fraction of these molecules will also be deuterated at H_a.

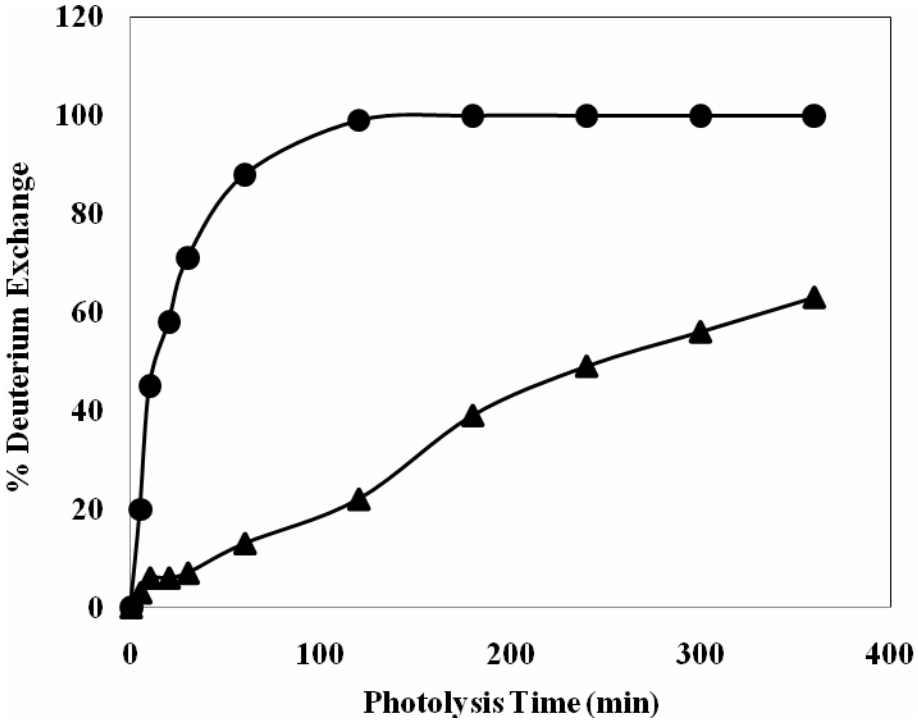

Figure 2.7 Plot of % Deuterium Exchange at the 2'(●) and 4'(▲)-positions of **26** versus photolysis time in 1:3 (v/v) D_2O-CH_3CN, as measured by ^{1}H-NMR**.**

Photolysis of **27** in D_2O-CH_3CN for up to 2 hours resulted in complete recovery of starting material with no evidence for deuterium incorporation into the benzene ring positions. This is the only compound studied with an electron withdrawing group on the

phenyl ring adjacent to the phenol.[27] An aromatic ketone also alters the photophysical characteristics of the biphenyl substantially.

2.3.2 Photosolvolysis versus ESIPT of 28

Since no evidence of reaction was observed upon photolysis of **27** in D_2O-CH_3CN for up to 2 hours, it was decided to investigate the photochemical properties of the closely related biphenyl alcohol **28**. Reduction of biphenyl ketone **27** with $NaBH_4$ in CH_3OH gave biphenyl alcohol **28**, which has the potential to undergo efficient photosolvolysis as well as ESIPT due to the presence of both benzyl alcohol and a phenol chromphore on the same molecule. As a result, our first investigation was photosolvolysis: the photolysis of **28** in 1:1 H_2O-CH_3OH (10^{-3} M, 254 nm, and 10 min) which afforded the methyl ether product **29** in 67% yield (Eq. [2.9]).

The reaction mixture showed the presence of a sharp singlet at δ 3.2 ppm in the ^1H NMR spectrum which was assigned to the methyl ether protons. The methyl ether product was isolated and characterized by ^1H NMR and MS. The ^1H NMR spectra of the photolysis appears in Figure 2.8.

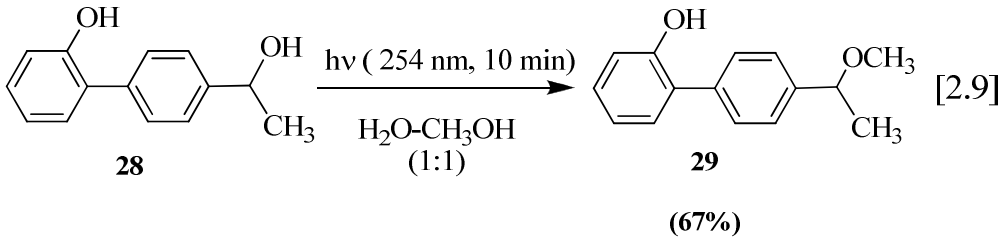

28 **29**

(67%)

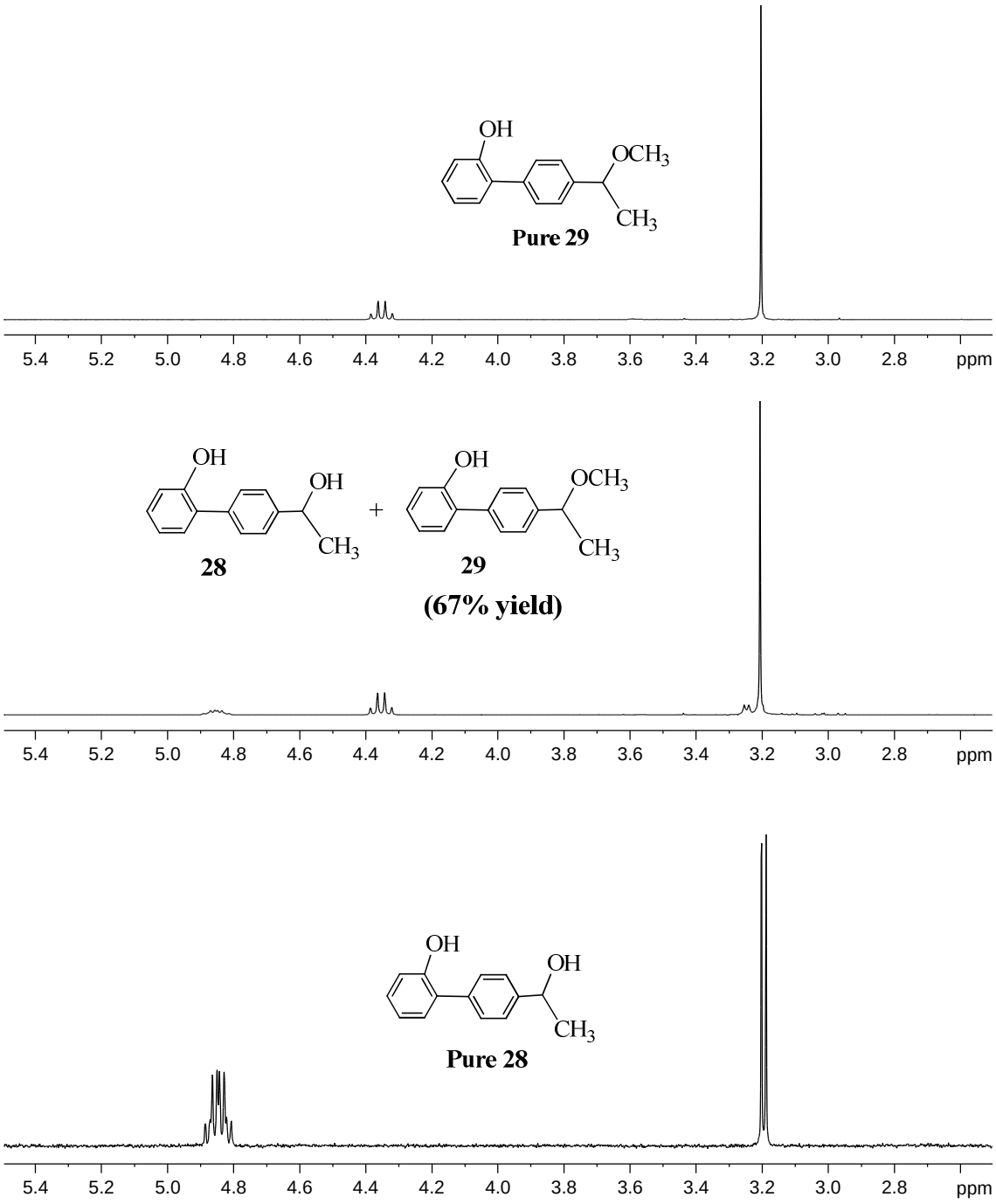

Figure 2.8 ^{1}H NMR (300 MHz, CD_3CN) of **28** before (bottom) photolysis. ^{1}H NMR (300 MHz, CD_3CN) after photolysis (254 nm, 16 lamps, and 10 min) in 1:1 H_2O-CH_3OH indicates the formation of mixture (middle) and pure **29** (top). The photosolvolysis reaction was carried out only once, therefore no error was estimated.

Photolysis of **28** was also examined in 1:1 (v/v) D_2O-CH_3OH (10^{-3} M, 254 nm, and 10 min) and the product mixture analyzed by 'H NMR (300 MHz), initially as a mixture, and then after their separation.

The aromatic region of the ^1H NMR (300 MHz) of separated **28** prior to and following irradiation in 1:1 (v/v) D_2O-CH_3OH (10^{-3} M, 254 nm, and 10 min) are presented in Figures 2.10 and 2.11. These spectra show that **28** was 26% deuterated at the 2'-position (**28**-*2'D*) after photolysis. This was readily evident by examination of the expanded aromatic region of the ^1H NMR of **28** after photolysis. The area of the peak assigned to H_a (δ 7.50 ppm, d) decreased with irradiation. A broad peak is observed on top of the doublet at δ 7.40 ppm assigned to H_b, but with no net increase in integration, which is consistent with deuterium incorporation at the adjacent sites (H_a, δ 7.50 ppm).

Photolysis of **28** under the above conditions also yielded the corresponding methyl ether **29** as a predominant product (60%), of which 31% was deuterated at the 2'-position (**29**-*2'D*). The deuterium exchange was readily observed by ^1H NMR (300 MHz) (Figure 2.10) and the reduction in the area of the ^1H NMR signal was assigned to the H_a (δ 7.50 ppm, d), which corresponds to the protons at the 2'-position. The formation of a broad peak on top of the doublet assigned to the H_b proton (δ 7.40 ppm, d), with no reduction in the peak area, is due to the coupling to deuterium that is now incorporated at the 2′-position. All other peaks remained unchanged, which is consistent with the absence of deuterium exchange at these positions upon photolysis.

The results obtained from the above run shows clearly that the ESIPT is a major photochemical pathway and competes very well with the photosolvolysis in the studied

solvent even when the exchangeable deuterium content was limited due to the use of CH_3OH (and not CH_3OD).

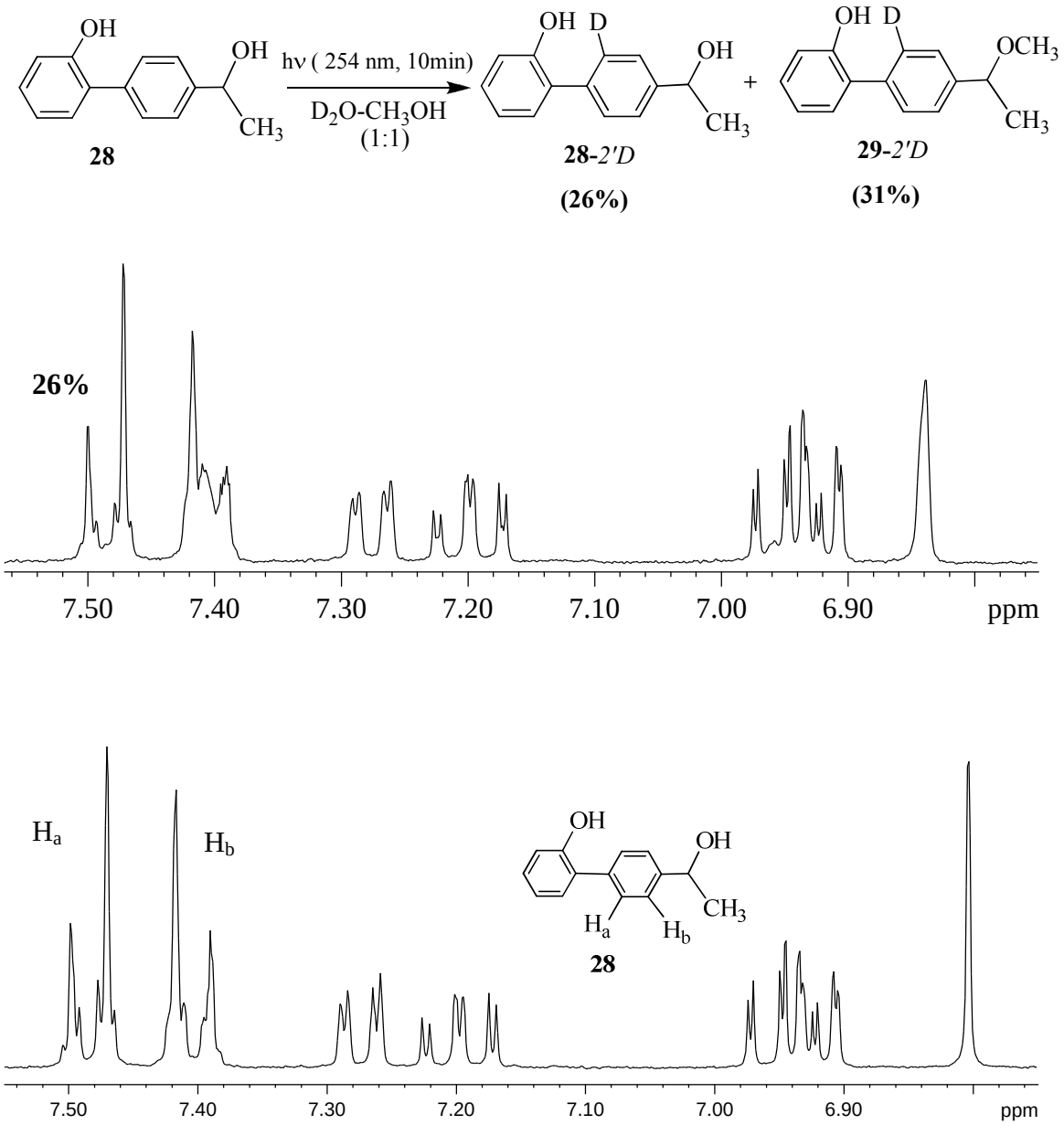

[2.10]

Figure 2.9 ^{1}H NMR (300 MHz, CD_3CN) showing the expanded aromatic region of **28** before (bottom), and after photolysis (254 nm, 16 lamps, and 10 min; top) in 1:1 (v/v) D_2O-CH_3OH. ^{1}H NMR integration indicates 26% deuteration at the H_a position. The photosolvolysis reaction was carried out only once, therefore no error was estimated.

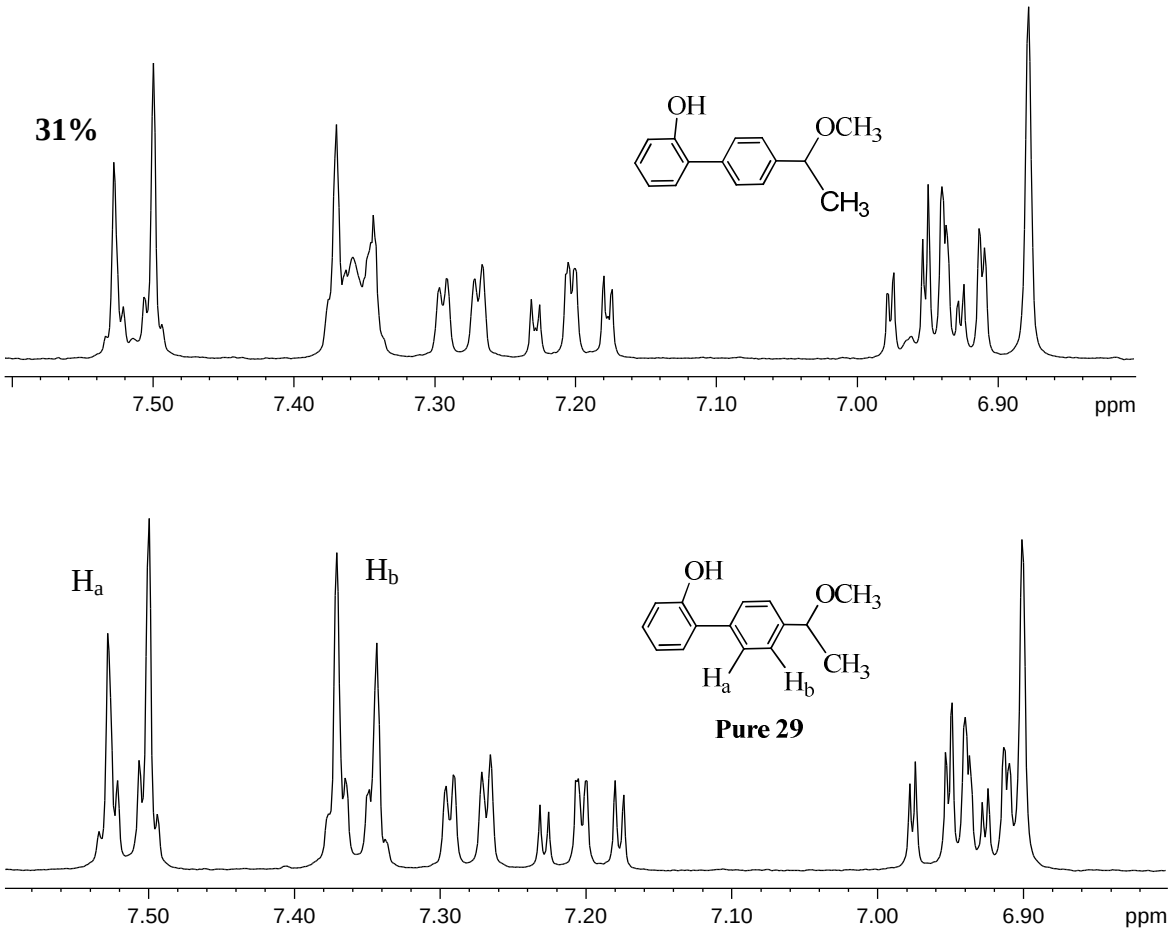

Figure 2.10 ^{1}H NMR (300 MHz, CD_3CN) showing the expanded aromatic region of **29** as pure compound (bottom), and after photolysis (254 nm, 16 lamps, and10 min; top) in 1:1 (v/v) D_2O-CH_3OH. ^{1}H NMR integration indicates 31% deuteration at H_a position. The photosolvolysis reaction was carried out only once, therefore no error was estimated.

2.3.3 Quantum Yields of Exchange for 23-26 and 28

Quantum yields for deuterium exchange (Φ_{ex}) for **23-26**, and **28** were measured using the deuterium exchange reaction of 2,2'-biphenol (Φ_{ex} = 0.034 ± 10%) as a reference standard.[14] The results are shown in Table 2.4.

Table 2.4 Product Quantum Yields for **23-26** and **28**.

Compound	Φ_{ex}[a] ±0.004
23	0.019
24	0.057
25	0.064
26	0.079
28	0.029

[a] Quantum yield of formation of **23**-*2'D*, **24**-*2'D*, **25**-*2'D*, **26**-*2'D*, and **28**-*2'D*, respectively in 1:3 (v/v) D_2O-CH_3CN. Estimated error is ±10% of the final value, which are relative to the quantum yield for deuterium incorporation reported for 2,2'-biphenol (0.034±10%).[14]

The quantum yields for formation of **23**-*2'D*, **24**-*2'D*, **25**-*2'D*, **26**-*2'D*, and **28**-*2'D*, in 1:3 (v/v) D_2O-CH_3CN (10^{-3} M, 254 nm, 16 lamps, and 10 min) are 0.019, 0.057, 0.064, 0.079, and 0.029 ± 0.004, respectively (Table 2.4).

The results in Table 2.4 show that the quantum yield for the deuterium exchange at the 2'-position is the lowest for **23**. The AM1 calculations for **23** show that the larger dihedral angle between two rings causes the hydroxyl proton to lie farther away from the 2'-carbon atom (Figure 2.2), which might affect the efficiency of intrinsic ESIPT to the *ortho* position and lower the quantum yield.

Quantum yields for the deuterium exchange of methoxy-substituted compounds (**24**, **25**, and **26**) clearly show a dramatic increase in the ESIPT efficiency as compared to **23** and **28.** The strong electron-donating methoxy groups on the accepting phenyl ring

stabilize the cationic intermediate generated upon the ESIPT process. Diol **28** has the lowest quantum yield which is consistent with a competing photosolvolysis reaction at the benzylic position.[27]

2.4 Fluorescence Measurements

Fluorescence studies are essential for the characterization of molecules that react upon excitation to S_1. The results provide direct and indirect information about the mechanistic behaviour of molecules in the singlet excited sate (S_1). A large Stokes shift which comes from an extended excited state relaxation process is obvious when observed in a fluorescence measurement. In particular, addition of water to the organic solvent may lead to the quenching of fluorescence thus providing data supporting photoprotropic events such as ESIPT occurring *via* S_1. Therefore, steady-state and time-resolved fluorescence parameters were measured for **23-26** and **28** and given in Table 2.5. Biphenyl ketone **27** was non-fluorescent, consistent with a very fast intersystem crossing to the triplet state for this compound.

Fluorescence quantum yields were measured for the phenylphenols **23-26** and **28** in CH_3CN (relative to the reported fluorescence quantum yield of fluorene in CH_3CN (Φ_f = 0.68)) [28] and were found to be 0.47, 0.39, 0.47, 0.14, and 0.39, respectively. Fluorescence lifetimes were also measured for the phenylphenols **23-26** and **28** in CH_3CN and were found to be 1.5, 1.7, 1.9, 0.8 and 1.8 ns, respectively (Table 2.5).

Table 2.5 Fluorescence Parameters for **23-26** and **28**.

Compound	λ_{max}^{ab} (nm)	$\lambda_{max}^{fl(em)}$ (nm)	Φ_f [a] ± 0.05	τ (ns) [b] ± 0.2
23	273	316	0.47	1.5
24	279	341	0.39	1.7
25	283	334	0.47	1.9
26	285	345	0.14	0.8
28	285	328	0.39	1.8

[a] Fluorescence quantum yields in neat CH_3CN, which are measured relative to the reported fluorescence quantum yield of fluorene in CH_3CN ($\Phi_f = 0.68$).[28] [b] Fluorescence lifetime in neat CH_3CN measured by single photon counting.

Measurements of fluorescence quantum yields showed high fluorescence efficiencies (up to 0.47) in organic solvents for all the biphenyls (Table 2.5). The results show that compound **26** has the lowest value of fluorescence quantum yield (Φ_f =0.14 ± 0.05) and lifetime (τ = 0.8 ± 0.2 ns) (Table 2.5). This is expected since **26** undergoes an intrinsic ESIPT in neat CH_3CN more efficiently than the other compounds (recall the results in Table 2.4 show that **26** has the highest deuterium exchange quantum yield).

Fluorescence emission spectra of reactive derivatives were measured in CH_3CN and aqueous CH_3CN. These spectra clearly show a strong emission band at longer wavelengths upon addition of significant amounts of water (> 5 M) for **23, 24**, **26**, and **28** (400-420 nm). This long wavelength emission band was assigned to the corresponding phenolate anion formed by a water-mediated ESPT mechanism (Scheme 2.1). This was

confirmed by comparison to the fluorescence emission spectrum observed in basic solution with the longer wavelength emission band formed upon addition of water. Both peaks are superimposibl after normalization of their intensities.

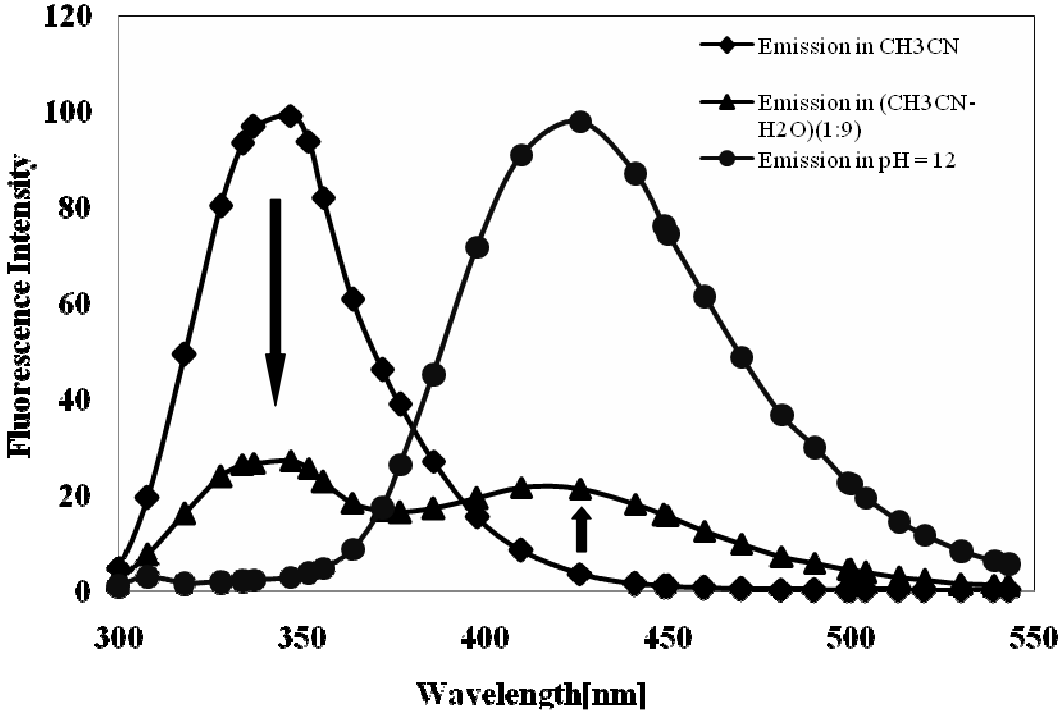

Figure 2.11 Fluorescence emission spectrum for **24** in neat CH_3CN (♦). Fluorescence emission spectra for **24** in 1:9 (v/v) CH_3CN -H_2O (▲), and (●) pH = 12 (100% H_2O).The emission at 420 nm is assigned to the phenolate.

For illustration, the fluorescence emission of **24** in neat CH_3CN gives a strong peak at λ_{max}= 341 nm (Figure 2.11) assignable to emission from the phenol. Addition of a significant amount of water (CH_3CN-H_2O (1:9)) resulted in quenching of the 341 nm band and formation of a red-shifted band at 420 nm. The intensity of the fluorescence at 420 nm increases upon addition of water, while the fluorescence intensity of the original 341 nm emission decreases. Emission of $\mathbf{24}^-$ (phenolate) formed by dissolving **24** in basic solution (H_2O: pH 12) also shows a strong peak at λ_{max}= 420 nm. The position of the longer wavelength emission band observed for **24** in CH_3CN-H_2O (1:9) is essentially

identical to the emission band of **24**$^-$. This evidence indicates that the longer wavelength emission in aqueous CH_3CN of **24** is due to the excited phenolate ion. Scheme 2.1 shows the mechanism for water-mediated ESPT from the OH proton of **24** to the solvent (water) in the excited state, to form the corresponding excited state phenolate ion **24**$^-$, which is consistent with previous work.[13, 14]

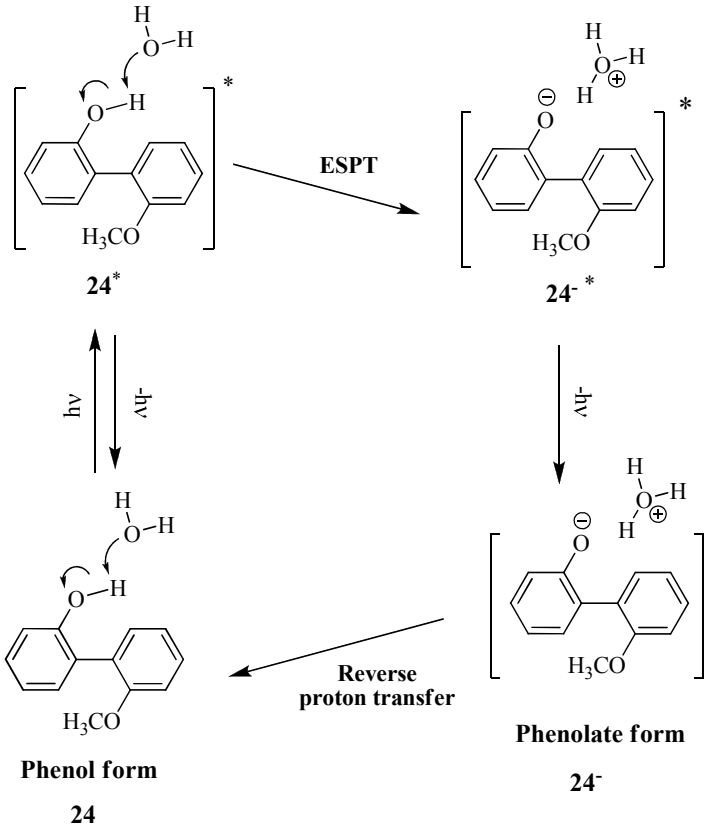

Scheme 2.1 Water-mediated ESPT for **24**.

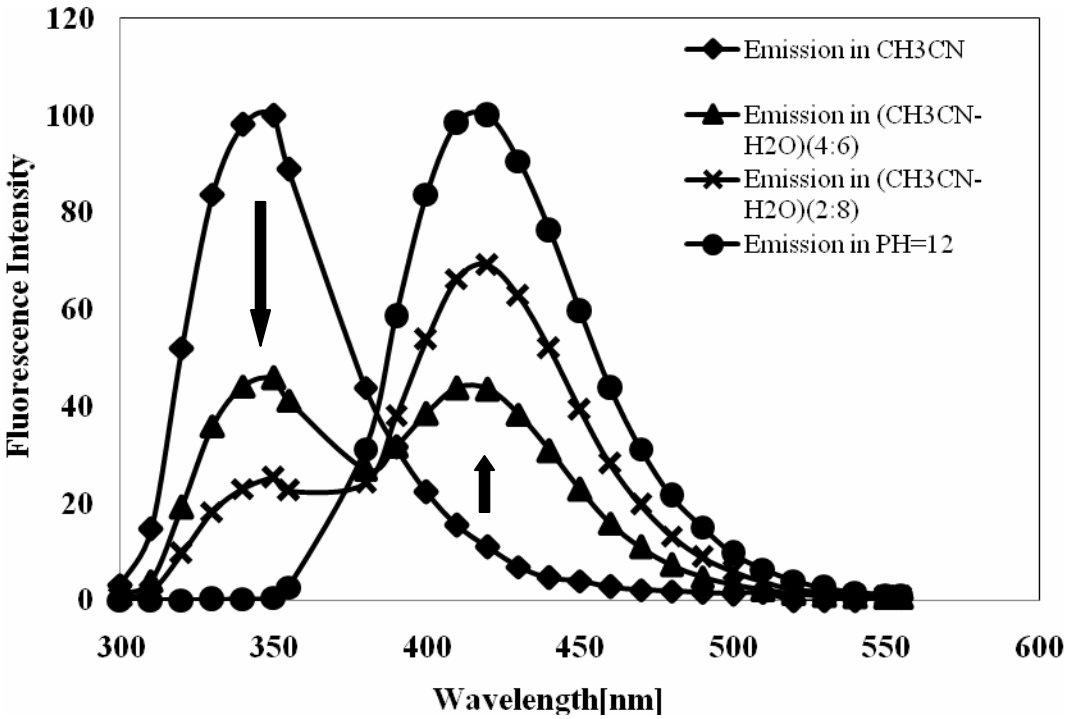

Figure 2.12 Fluorescence emission spectrum for **26** in neat CH_3CN (♦). Fluorescence emission spectra for **26** in various solvents, (▲) 4:6 (v/v) CH_3CN-H_2O, (■) 2:8 (v/v) CH_3CN- H_2O, and (●) pH = 12 (100% H_2O). The emission at 420 nm is assigned to the phenolate.

The fluorescence emission of **26** (Figure 2.12) shows similar behaviour to that observed for **24**. The fluorescence emission of **26** in neat CH_3CN gave a strong peak at λ_{max}= 350nm (Figure 2.12). Addition of significant amounts of water (CH_3CN-H_2O (4:6) or CH_3CN-H_2O (2:8)) caused quenching of emission at 350nm and formation of a new band at 420nm. The intensity of the new 420nm band increases upon addition of water.

Relatively large amounts of water were required for the efficient formation of **26**$^-$, just like that observed for exchange of **26** to give **26**-*4'D*. In Section 2.3.1, the plot of the percentage of deuterium exchange at the 2'-position of **24** was expressed as a function of D_2O content (Figure 2.5). These results indicated that the deuterium exchange at the 2'-position for **24** was independent of water content (occurring *via* direct ESIPT) while the

exchange at the 4'-position required the presence of significant amounts of water. These observations suggest that deuterium exchange at the more distal 4'-position occurs *via* water-mediated ESPT. That is, the excited state phenolate ion is reactive in this protonation pathway, whereas the phenol itself is reactive in a direct-ESIPT mechanism for exchange at the 2'-position.

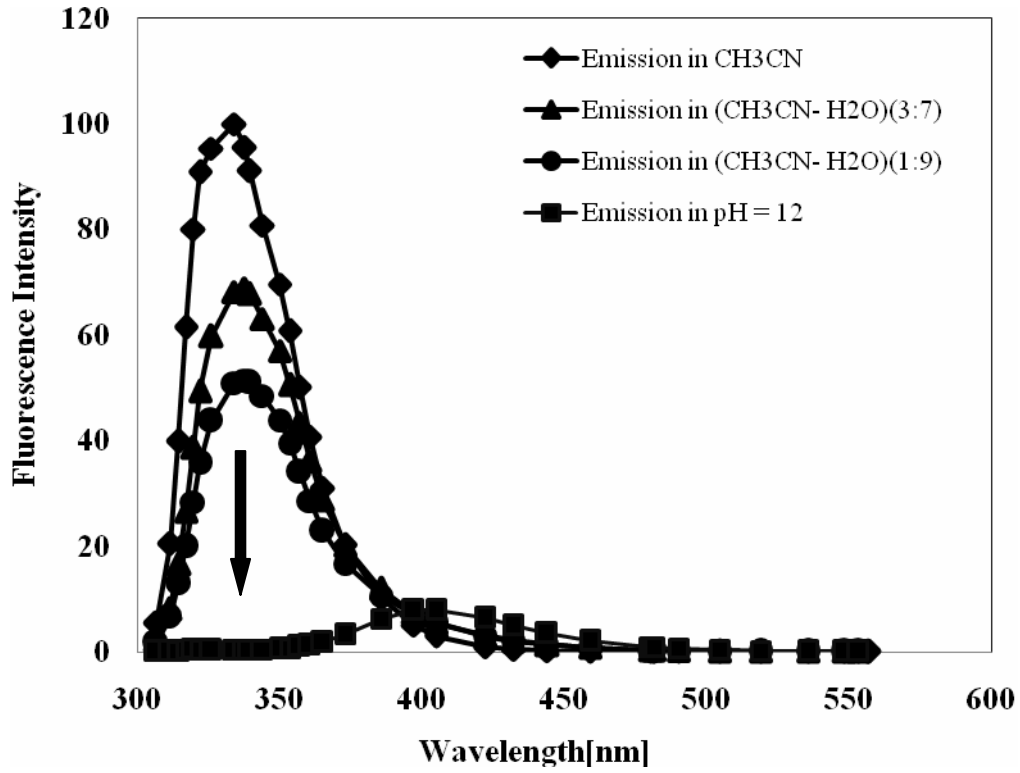

Figure 2.13 Fluorescence emission spectrum for **25** in neat CH_3CN (♦). Fluorescence emission spectra for **25** in various solvents, (▲) 3:7 (v/v) CH_3CN-H_2O, (●) 1:9 (v/v) CH_3CN- H_2O, and (■) pH = 12 (100% H_2O). The emission at 400 nm observed at pH12 is assigned to the phenolate.

As exemplified for **24** and **26**, the fluorescence emission of all the fluorescence bands for the biphenyl compounds was quenched upon the addition of water with simultaneous formation of a phenolate emission band at longer wavelength. The only

exception was **25**, which did not give observable phenolate emission upon addition of water (Figure 2.13), although in all other respects it behaved like the other compounds with respect to fluorescence quenching and deuterium incorporation *via* ESIPT at the 2'-position. In addition **25** also gave a very weak phenolate emission in basic aqueous solution compared to the other biphenyls, indicating that other unidentified non-radiative pathways are present for the phenolate excited state of **25**.

2.5 Mechanisms of Photochemical Reactions

2.5.1 Direct ESIPT

Direct proton transfer (ESIPT) from the phenolic OH to the 2'-position of all compounds (except for **27**) was observed in deuterated solvent (D_2O). In case of the direct-ESIPT pathway, the 3'and 4'-positions would be too far away for overlap with the OH proton. Proton transfer to the 4'-position was eventually observed upon the addition of more water, but not to the 3'-position. It seems clear that protonation at the 3'-position would generate a high energy non-Kekulé quinone methide intermediate and would explain why this pathway has never been observed.

In recent years, computer simulations have provided new insights into ESIPT. In particular, the enhanced acidity of hydroxyarenes in the excited state may be quantitatively predicted through simple HOMO and LUMO calculations. Therefore, HOMOs and LUMOs (Chem 3D, AM1/MOPAC) were calculated for all compounds in this study and some results are discussed in the following section to illustrate the utility of these calculations.

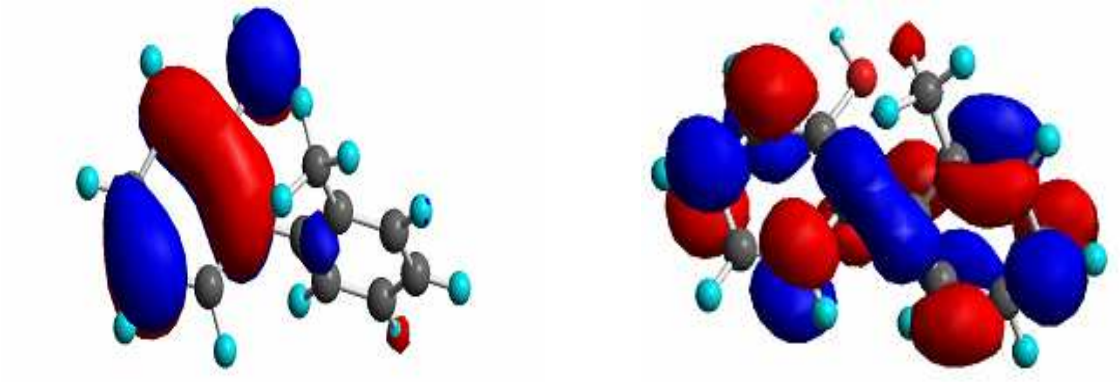

Figure 2.14 Calculated (AM1, Chem 3D/MOPAC) HOMO (left) and LUMO (right) for **23**.

The calculated HOMO for compound **23** (Figure 2.14) shows a large electron density on the oxygen atom, whereas the corresponding electron density in the LUMO is localized not on the oxygen, but is diffused into the benzene ring including the adjacent phenyl ring. It is clear in the above figure that transfer of electron density is taking place upon going from the HOMO to the LUMO. Thus, photoexcitation of these hydroxylbiphenyls should result in the transfer of electron density from hydroxyphenyl moiety to the adjacent phenyl ring resulting in a decrease in the basicity of the oxygen atom and increase in basicity of the adjacent phenyl ring. The drastic increase in acidity of phenol and basicity of carbons in the adjacent phenyl ring upon electronic excitation should be sufficient for ESIPT. Indeed, this is what was observed.

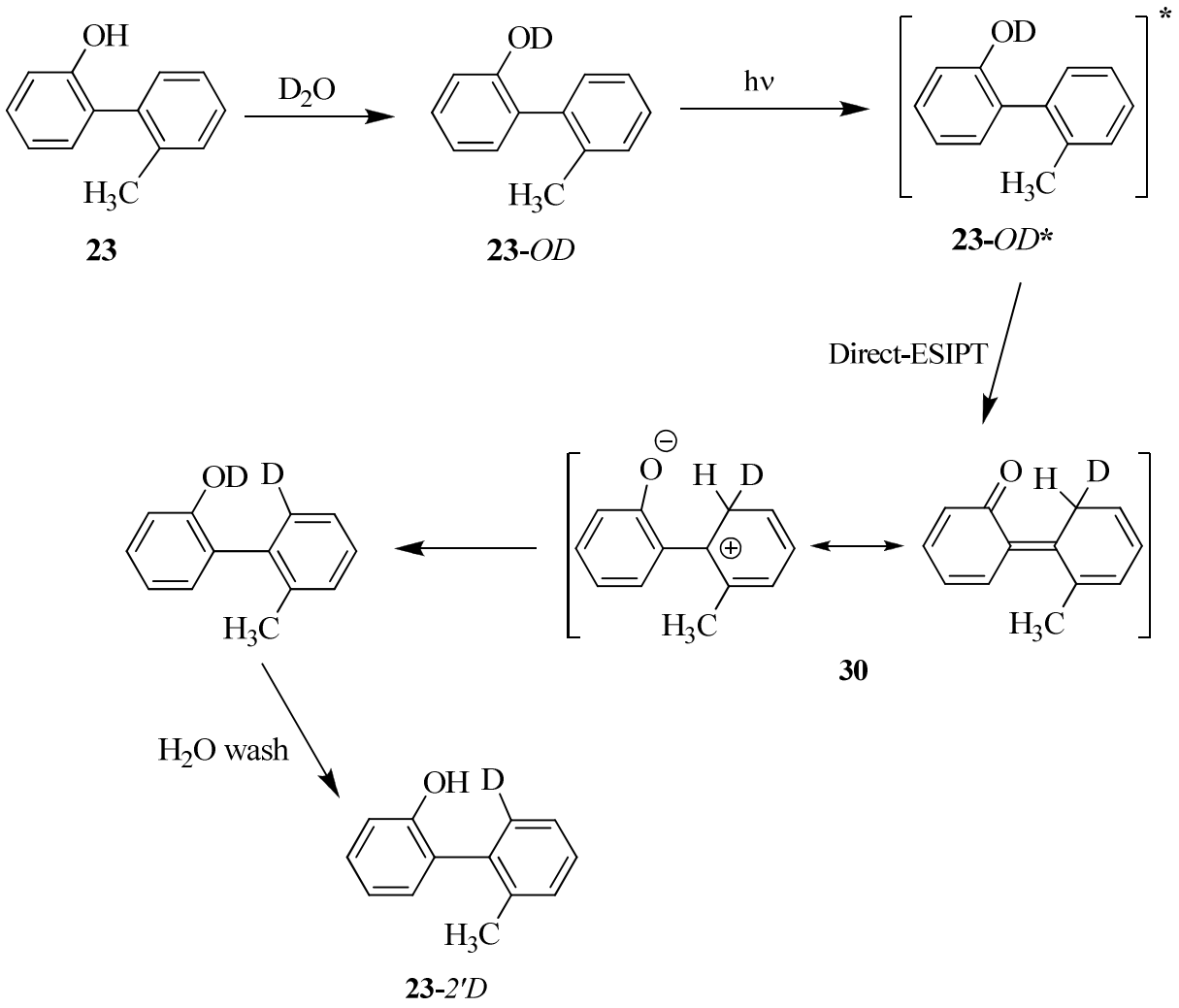

Scheme 2.2 Proposed mechanism of direct ESIPT for **23.**

For illustration purposes, a mechanistic scheme showing the proposed direct ESIPT mechanism responsible for the photochemical deuterium exchange at the 2'-positions of **23** is presented in Scheme 2.2. The deuterium exchange reaction at the 2'-position of **23** appears to proceed *via* this direct ESIPT mechanism. This exchange showed a lack of dependence on the water content.

Compound **23** has a twisted geometry in the ground state (prior to the excitation) (Figure 2.2). This allows some degree of overlap between the s-orbital of the acidic OH

proton of the phenol and the accepting π-system. This overlap apparently facilitates the ESIPT. Photochemical excitation of **23** excites the molecule to S_1, followed by direct proton transfer from OH (OD) to the 2'-position, affording a zwitterionic (quinone methide) intermediate **30** (Scheme 2.2). As mentioned in Section 1.2.2.1, this intermediate can lose either the hydrogen or the deuterium from the site of the deuteration. Loss of hydrogen (which should be kinetically preferred) generates deuterated **23** at the 2'-position (**23-***2'D*).

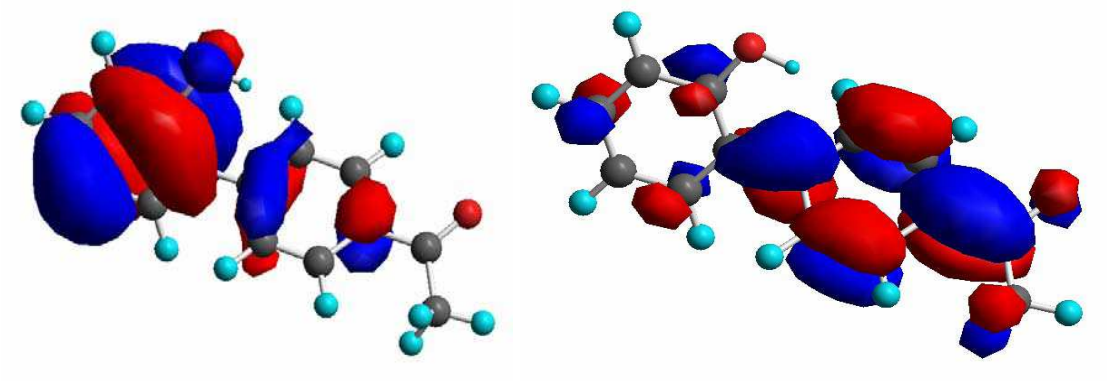

Figure 2.15 Calculated (AM1, Chem 3D/MOPAC) HOMO (left) and LUMO (right) for ketone **27**.

The calculated HOMO and LUMO for the unreactive compound **27** are shown in Figure 2.15. There is migration of charge from the HOMO to the LUMO but it is qualitatively lower at the 2'-position compared to the other biphenyls studied; instead, the charge extends well into the carbonyl group, making the carbonyl oxygen more basic in the excited state. Since proton transfer to heteroatoms will be intrinsically faster than to carbon atoms, ESPT from solvent water to the carbonyl oxygen should be the dominant process for this compound. This offers an explanation for the lack of deuterium exchange for **27**.

2.5.2 Water-Mediated ESPT

The mechanism responsible for the exchange at the 4'-position is a water-mediated ESPT from the phenolic OH to the 4'-position. For instance, when **26** is excited in a solvent containing significant amounts of water, a new photochemical proton transfer process can occur. The water-mediated ESPT from the phenolic OH to the solvent water generates **26**$^-$, which upon protonation at the 4'-position generates the quinone methide **31** (Scheme 2.3).

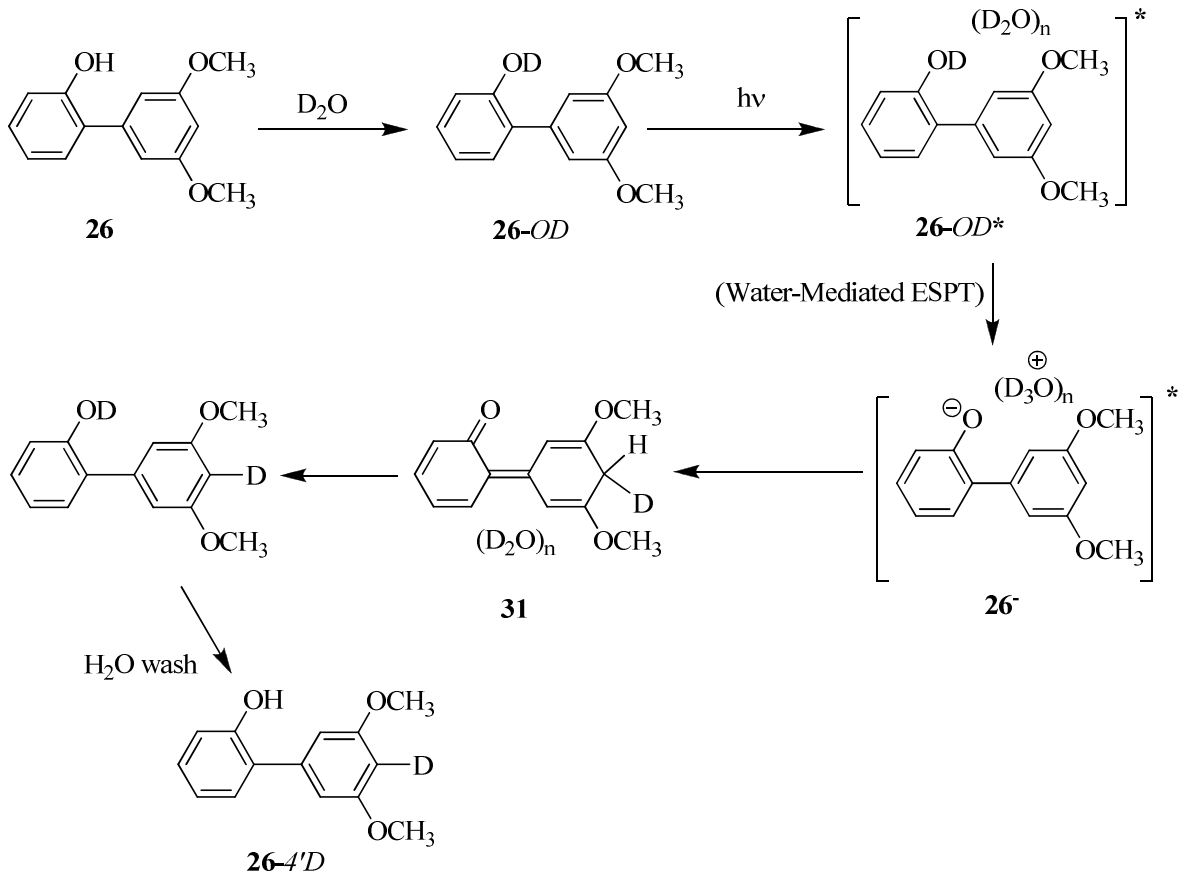

Scheme 2.3 Proposed mechanism of water-mediated ESPT for **26**.

2.5.3 Photosolvolysis

The photosolvolysis of hydroxylbenzyl alcohols has been studied by Wan and co-workers [23] and it has been shown that photolysis of the compound leads to initial the heterolytic cleavage of C-OH bond. In this study, based on its structure, **28** has the potential to undergo both ESIPT and photosolvolysis reactions.

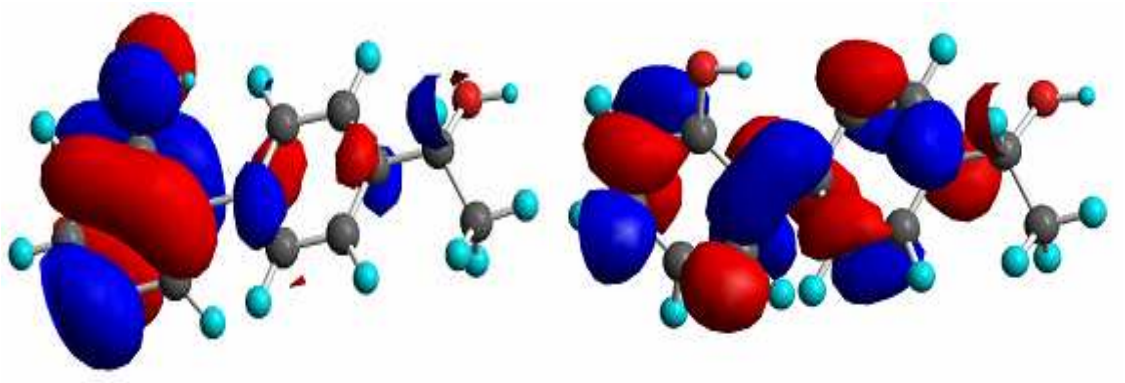

Figure 2.16 Calculated (AM1, Chem 3D/MOPAC) HOMO (left) and LUMO (right) for diol **28**.

The calculated HOMO and LUMO for **28** are shown in Figure 2.16. The migration of charge from the phenol ring to the carbon atoms of the adjacent phenyl ring is apparent. In addition, there is significant new charge density at the 4'-position which is required for subsequent elimination of the benzylic hydroxyl group (as OH^-).

Photolysis of **28** in 1:1 (H_2O-CH_3OH) yielded the corresponding methyl ether **29** as the only product. As shown in Scheme 2.4, water molecules can be trapped easily between the two hydroxyl moieties of **28**, *via* the formation of hydrogen bonds. Upon excitation, the formal loss of water, presumably driven in part by the enhanced acidity of the phenolic OH and enhanced electron density at the 4'-position, will result in the

formation of a zwitterionic (quinone methide) intermediate **32**. The corresponding methyl ether adduct **29** is formed by attack of **32** by CH_3OH (Scheme 2.4).

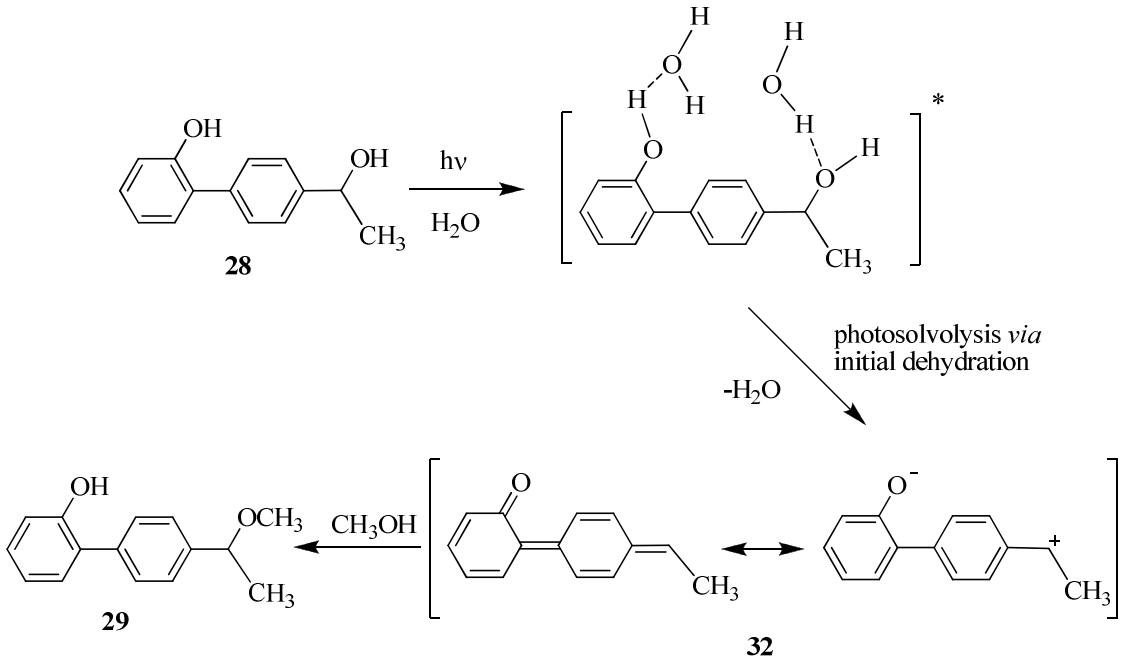

Scheme 2.4 Proposed mechanism of photosolvolysis for **28**.

As shown above, the photosolvolysis of **28** in 1:1 (H_2O-CH_3OH) gave the corresponding methyl ether adduct **29** as the only product. In the presence of D_2O, deuterated **28** and **29** at the 2'-position were the major products, indicating that ESIPT is a competing pathway. The combination of ESIPT and photosolvolysis results in the proposed mechanism of photoreaction of **28** in D_2O-CH_3OH (Scheme 2.5).

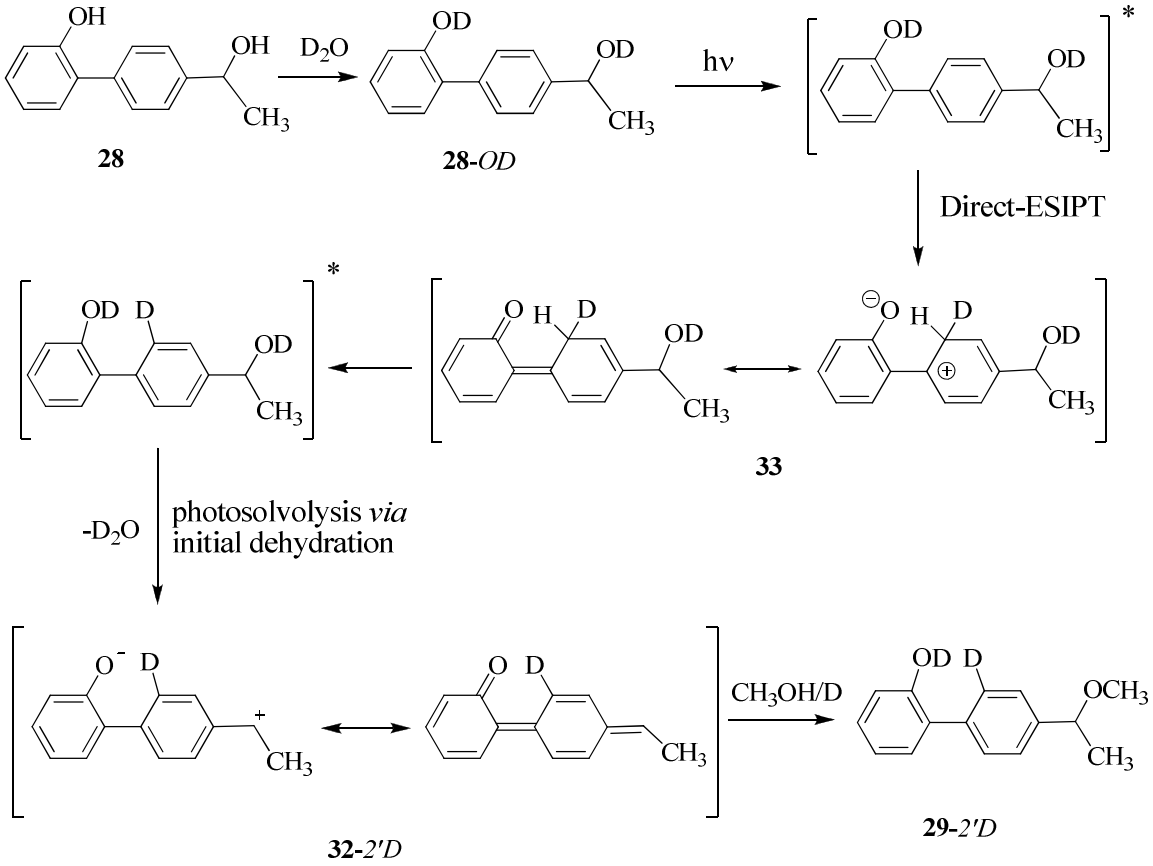

Scheme 2.5 Proposed mechanism of direct ESIPT and photosolvolysis for **28**.

2.6 Conclusions

The results for the successfully synthesized compounds **23-28** presented in this Thesis showed the effect of electron-donating and electron-withdrawing substituents on the adjacent proton accepting phenyl ring with respect to a new type of ESIPT process. The study has provided additional new insights into the details of these types of photochemical reactions. For instance, the addition of a simple methyl group at the 2'-position on the proton accepting ring resulted in a reduction of ESIPT efficiency. This is believed to be due to much larger dihedral angle between the two phenyl rings ($\approx 69.2^{o}$, Figure 2.2) and hence a poorer overlap between the s-orbital of hydroxyl group in the *ortho* position and the accepting π-system of the adjacent ring prior to the ESIPT process.

In general, the addition of an electron donating methoxy substituent on the proton accepting phenyl ring enhanced the quantum yields for deuterium exchange, even when the methoxy group is at the 2'-position. Closer inspection using AM1 calculations indicated the methyl group of the OCH_3 substituent is held farther away from the adjacent phenyl ring due to the length of the C-O ether bond. Hence, the ground state structure of **24** (unlike **23**) satisfies the geometry required for efficient ESIPT from phenol to the adjacent phenyl ring.

The presence of a methoxy group in the *para* position of **25** also increased the quantum yield for deuterium exchange. The results obtained from steady state fluorescence measurements showed that the phenolate emission band was not observed for **25** upon addition of water consistent with the existence of non-radiative pathways for the phenolate **25** in the excited state.Compound **26** with two methoxy groups at *meta* positions had the highest quantum yield for deuterium exchange.

Ketone **27** was the only compound that did not undergo observable photochemical reaction. The calculated HOMO and LUMO for **27** showed the electron density migrated to the carbonyl oxygen upon excitation, which makes it more basic than the benzene ring, thus diverting the ESIPT to the carbonyl oxygen. In addition, the presence of a carbonyl group in the molecule causes the molecule to undergo very fast intersystem crossing to the triplet excited state which is probably unreactive with respect to ESIPT.

Since **28** has a close structural resemblance to the rest of the biphenyls, its photochemical behaviour was expected to be the same. However, unlike the situation in other biphenyls, the presence of a benzyl alcohol chromophore on the molecule allowed photosolvolysis to compete with the ESIPT process.

Chapter 3
Experimental

3.1 General

^{1}H and ^{13}C NMR spectra were recorded on a Bruker Avance 500 instrument. Mass spectra (MS) were recorded on a Kratos Concept H spectrometer (EI). UV-Vis spectra were recorded on a Varian Cary 50 instrument. D_2O and $(CD_3)_2CO$ were purchased from Cambridge Isotope laboratory. Chromatographic separations were carried out by using 200 mL silica gel columns as the stationary phase and hexane/ethyl acetate or dichloromethane/ethyl acetate as mobile phases.

3.2 Materials

The following compounds and reagents were purchased from Aldrich and used as received: 2-bromophenol, 2-methylphenylboronic acid, 4-methylphenylboronic acid, 4-acetylphenylboronicacid, 3,5-dimethylphenylboronic acid, 2,2'-biphenol, $NaBH_4$, Pd $(PPh_3)_4$, CH_3I, polyethylene glycol.

3.2.1 Synthesis

The general procedure for the synthesis of **23** and **25**-**27** employs the well-known Suzuki coupling reaction, adapted from the work of Nam *et al.*[29], and is described as follows. A mixture of 1 equivalent of 2-bromophenol and 1.2-1.3 equivalents of the phenylboronic acid were dissolved in THF in a 100 mL Schlenk flask. To the reaction mixture were added 2 equivalents of aqueous Na_2CO_3, and the solution was purged with

N_2 for 20 min. This was followed by addition of 0.03-0.05 equivalents of Pd $(PPh_3)_4$ and the mixture was refluxed for up 24 h with monitoring of reaction progress by TLC. After reflux, the solution was cooled to room temperature, dried over anhydrous Na_2SO_4 and filtered through Celite. The pure product was obtained by chromatography on silica gel using 10-20% ethyl acetate/n-hexane as eluent.

3.2.1.1 2'-Methylbiphenyl-2-ol (23)

The yield of this light yellow oil[30] was 1.1 g (71%). ^{1}H NMR ($(CD_3)_2CO$, 500 MHz) δ 7.95 (OH, 1H), 7.17-7.23 (m, 4H), 7.13 (d, 1H, *J* = 10 Hz), 7.04 (dd, 1H, *J* = 10 and 2 Hz), 6.94 (dd, 1H, *J* = 10 and 1 Hz), 6.89 (ddd, 1H, *J* = 10, 10 and 1 Hz), 2.21 (s, 3H) (Figure A.1); ^{13}C NMR ($(CD_3)_2CO$, 125 MHz) δ 19.17, 115.46, 119.41, 125.31, 127.07, 127.84, 128.83, 129.47, 129.99, 130.66, 136.63, 138.61, 154.10 (Figure A.2); MS (EI) m/z = 184 for M^+. HRMS calculated for $C_{13}H_{12}O$ 184.0888, observed 184.0888.

3.2.1.2 4'-Methoxybiphenyl-2-ol (25)

The yield of light yellow oil was 0.78 g (45%). ^{1}H NMR ($(CD_3)_2CO$, 500 MHz) δ 8.17(OH, 1H), 7.53 (dd, 2H, *J* = 10 and 5 Hz), 7.25 (dd, 1H, *J* = 10 and 2 Hz), 7.14 (ddd, 1H, *J* = 10, 10 and 1 Hz), 6.97 (m, 3H), 6.90 (ddd, 1H, *J* = 10, 10 and 1 Hz), 3.82 (s, 3H) (Figure A.5); ^{13}C NMR ($(CD_3)_2CO$, 125MHz) δ 55.59, 114.37,116.99, 120.91, 128.92, 129.15, 131.29, 132.07, 155.06, 159.72 (Figure A.6); MS (EI) m/z = 200 for M^+. HRMS calculated for $C_{13}H_{12}O_2$ 200.0837, observed 200.0837.

3.2.1.3 3’, 5’-Dimethoxybiphenyl-2-ol (26)

The yield of light yellow oil[31] was found to be 1.5 g (38 %). ^{1}H NMR ($(CD_3)_2CO$, 500 MHz) δ 8.17 (OH, 1H), 7.31 (dd, 1H, *J* = 10 and 3 Hz), 7.18 (ddd, 1H, *J* = 10, 10 and 1 Hz), 6.97 (dd, 1H, *J* = 10 and 2 Hz), 6.92 (ddd, 1H, *J* = 10, 10 and 1 Hz), 6.73 (d, 2H, *J* = 5 Hz), 6.45 (t, 1H, *J* = 5 Hz), 3.81 (s, 6H) (Figure A.7); ^{13}C NMR ($(CD_3)_2CO$, 125MHz) δ 55.63, 99.69, 108.34, 117.09, 120.82, 129.39, 129.53, 131.35, 141.55, 155.02, 161.63 (Figure A.8); MS (EI) m/z = 230 for M^+. HRMS calculated for $C_{14}H_{14}O_3$ 230.0942, observed 230.0946.

3.2.1.4 4’-Acetylbiphenyl-2-ol (27)

The yield of white solid (mp 142-144 °C)[32] was 4.5 g (50 %). ^{1}H NMR ($(CD_3)_2CO$, 500 MHz) δ 8.54 (OH, 1H), 8.01 (d, 2H, *J* = 10 Hz), 7.73 (d, 2H, *J* = 10 Hz), 7.35 (dd, 1H, *J* = 10 and 3 Hz), 7.22 (ddd, 1H, *J* = 10, 10 and 1 Hz), 7.01 (dd, 1H, *J* = 10 and 3 Hz), 6.95 (ddd, 1H, *J* = 10, 10 and 1 Hz), 2.59 (s, 3H) (Figure A.9); ^{13}C NMR ($(CD_3)_2CO$, 125MHz) δ 25.69, 116.17, 120.04, 127.19, 127.80, 129.22, 129.29,130.41, 135.44, 134.52, 154.23, 196.60 (Figure A.10); MS (EI) m/z = 212 for M^+. HRMS calculated for $C_{14}H_{12}O_2$ 212.0837, observed 212.0840.

3.2.1.5 2’-Methoxybiphenyl-2-ol (24)

This compound was prepared based on a published report[26] but modified by the addition of polyethylene glycol as solvent. A dry 100 mL one-neck round bottom flask

was charged with 30 mL of acetone and 10 mL of polyethylene glycol under N_2. This was followed by the addition of 2, 2'-biphenol (1 eq, 8.15 mmol) and methyl iodide (2 eq, 16.3 mmol). Then K_2CO_3 (0.5 eq, 4.07 mmol) was added and the mixture was stirred at room temperature for 24 h. The resulting solution was extracted with 3 x 50 mL CH_2Cl_2. Upon evaporation of the organic solvent, the crude material was purified by chromatography on silica (2:1 hexane-CH_2Cl_2), to give **24** as a white solid (mp 48-50°C) (1.4 g, 85%). ^{1}H NMR ($(CD_3)_2CO$, 500 MHz) δ 7.55 (OH, 1H), 7.33 (ddd, 1H, *J* = 10, 10 and 1 Hz), 7.23 (dd, 1H, *J* = 10 and 3 Hz), 7.18 (dd, 1H, *J* = 10 and 3 Hz), 7.16 (ddd, 1H, *J* = 10, 10 and 1 Hz), 7.06 (dd, 1H, *J* = 10 and 1 Hz), 7.00 (ddd, 1H, *J* = 10, 10 and 1 Hz), 6.91 (dd, 1H, *J* = 10 and 1 Hz), 6.88 (ddd, 1H, *J* = 10, 10 and 1 Hz), 3.81 (s, 3H) (Figure A.3); ^{13}C NMR ($(CD_3)_2CO$, 125MHz) δ 56.03, 112.27, 117.08, 120.45, 121.57, 127.15, 128.57, 129.40, 129.71, 132.38, 132.63, 155.58, 157.81 (Figure A.4); MS (EI) m/z = 200 for M^+. HRMS calculated for $C_{13}H_{12}O_2$ 200.0837, observed 200.0845.

3.2.1.6 4'-(1''-Hydroxyethyl) biphenyl-2-ol (28)

Alcohol **28** was made *via* standard $NaBH_4$ reduction of ketone **27** in methanol. A dry 250 mL one-neck round bottom flask under N_2 was charged with 20 mL of methanol. This was followed by the addition of **28** (1 equiv, 0.5 gram, and 2.35 mmol) and $NaBH_4$ (6 equiv, 0.54 gram). The reaction mixture was left to stir at room temperature for 20 minutes. Meanwhile, 6mL of 5M H_2SO_4 in100 mL ice was prepared in a 250 mL beaker. The borate ester complex mixture was added slowly to the above ice-acid mixture and was stirred for 20 minutes. The organic phases were extracted with 3x50 mL CH_2Cl_2. The crude white solid was purified by chromatography on silica (5: 95 ethyl acetate-CH_2Cl_2)

and followed by re-crystallization from ethanol, to give 0.46 gram (91%) white solid (mp114-116 °C).^{1}H NMR (CD_3CN, 500 MHz) δ 7.50 (d, 2H, *J* = 12 Hz), 7.40 (d, 2H, *J* = 12 Hz), 7.26 (dd, 1H, *J* = 10 and 3 Hz,), 7.20 (ddd, 1H, *J* = 10, 10 and 1 Hz), 6.94 (m, 2H), 6.80 (OH, 1H), 4.84 (m, 1H), 3.20 (d, OH, 1H, *J* = 5 Hz), 1.41 (d, 3H, *J* = 8 Hz) (Figure A.11); ^{13}C NMR (CD_3CN, 125MHz) δ 26.03, 70.04, 117.03, 121.43, 126.28,129.43, 129.68, 130.19, 131.64, 138.08, 146.77, 154.69 (Figure A.12). MS (EI) m/z = 214.06 for M^+. HRMS calculated for $C_{14}H_{14}O_2$ 214.09938, observed 214.09953.

3.3 Photolysis

3.3.1 General Procedure for Photochemical Exchange of 23-26 in D_2O-CH_3CN.

All the irradiation experiments were performed in a Rayonet photochemical reactor equipped with 16 lamps (254 nm). The solutions were prepared by first dissolving the compound in the organic solvent before being mixed with the aqueous component. The solutions were contained in quartz tubes (100 mL), which were cooled to ≤ 15 ^{o}C with tap water by an internal cold finger. The solutions of 10^{-3} M concentration were prepared and purged with argon 15 min prior to irradiation and continuously during the irradiation. Photolysis times varied from 5 min to 6 h. Workup involved extraction of the photolysed solution with CH_2Cl_2, followed by drying the combined organic layer over anhydrous Na_2SO_4, and removing of the solvent under reduced pressure. The irradiation products were separated (if necessary) by preparative thin-layer chromatography (TLC) and then analyzed by ^{1}H NMR and MS.

3.3.1.1 Photolysis of 23 in 1:9 D_2O-CH_3CN

A 20 mg sample of **23** in 100 mL of 1:9 (v/v) D_2O-CH_3CN was irradiated for 1 h; the photoproduct was analyzed by ^1H NMR, which showed 33% deuterium exchange at the 2'-position and 14% deuterium exchange at the 4'-position. ^1H NMR ($(CD_3)_2CO$, 500 MHz) δ 7.95 (OH, 1H), 7.17-7.23 (m, 3.86H), 7.13 (d, 0.67H, *J* = 10 Hz), 7.04 (dd, 1H, *J* = 10 and 2 Hz), 6.94 (d, 1H, *J* = 10 Hz), 6.89 (ddd, 1H, *J* = 10, 10, 1Hz), 2.21 (s, 3H).

3.3.1.2 Photolysis of 24 in 1:1 D_2O-CH_3CN

A 20 mg sample of **24** in 100 mL of 1:1 (v/v) D_2O-CH_3CN was irradiated for 2 h; the photoproduct was analyzed by ^1H NMR, which showed 96% deuterium exchange at the 2'-position and 71% deuterium exchange at the 4'-position. ^1H NMR ($(CD_3)_2CO$, 500 MHz) δ 7.55 (OH, 1H), 7.32 (t, 0.29H, *J* = 5 Hz), 7.23 (d, 0.04H, *J* = 5 Hz), 7.17 (dd, 1H, *J* = 10 and 3 Hz), 7.14 (ddd, 1H, *J* = 10, 10 and 1 Hz), 7.06 (m, 1H, *J* = 5 Hz), 7.00 (s, 1H), 6.91(dd, 1H, *J* = 10 and 1 Hz), 6.88 (ddd, 1H, *J* = 10, 10 and 1 Hz), 3.79 (s, 3H).

A second sample of 20 mg of **24** in 100 mL of 0.5:99.5 (v/v) D_2O-CH_3CN was irradiated for 5 min and clearly gave **24** with 37% deuterium incorporation at the 2'-position and 0% deuterium incorporation at the 4'-position. MS also indicated extensive deuteration with significant M+1 peak. MS gave **24** (69%) and **24**-D_1 (31%).

3.3.1.3 Photolysis of 25 in 1:1 in D_2O-CH_3CN

A 20 mg sample of **25** in 100 mL of 1:1 (v/v) D_2O-CH_3CN was irradiated for 2 h; the photoproduct was analyzed by ^1H NMR, which showed 100% deuterium incorporation at the 2'-position. ^1H NMR ($(CD_3)_2CO$, 500 MHz) δ 8.18 (OH, 1H), 7.25 (dd, 1H, *J* = 10 and 3 Hz), 7.12 (ddd, 1H, *J* = 10, 10 and 1 Hz), 6.93 (m, 3H), 6.88 (ddd, 1H, *J* = 10, 10 and 1 Hz), 3.81 (s, 3H). MS indicated extensive deuteration with significant M+1 and M+2 peaks. MS gave **25** (5%), **25**-D_1 (25%), **25**-D_2 (62%), and **25**-D_3 (8%).

3.3.1.4 Photolysis of 26 in 1:3 in D_2O-CH_3CN

A 20 mg sample of **26** in 100 mL of 1:3 (v/v) D_2O-CH_3CN was irradiated for 2 h; the photoproduct was analyzed by ^1H NMR, which showed 99% deuterium incorporation at the 2'-position and 22% deuterium incorporation at the 4'-position. ^1H NMR ($(CD_3)_2CO$, 300 MHz) δ 8.17 (OH, 1H), 7.31(dd, 1H, *J* = 6 and 2 Hz), 7.18 (ddd, 1H, *J* = 6, 6 and 1 Hz), 6.97 (dd, 1H, *J*= 6 and 1 Hz), 6.92 (ddd, 1H, *J* = 6, 6 and 1Hz), 6.73 (d, 0.02H, J = 3 Hz), 6.45 (s, 0.78H), 3.81 (s, 6H). MS indicated extensive deuteration with noticeable M+2 and M+3 peaks. MS gave **26** (4%), **26**-D_1 (9%), **26**-D_2 (52%), and **26**-D_3 (36%).

A second sample of 20 mg of **26** in 100 mL of 1:3 (v/v) D_2O-CH_3CN was irradiated for 30 min and clearly gave **26** with 71% deuterium incorporation at the 2'-position and 7% deuterium incorporation at the 4'-position.

3.3.1.5 Photolysis of 28 in 1:3 D_2O-CH_3CN

A 20 mg sample of **28** in 100 mL of 1:3 (v/v) D_2O-CH_3CN was irradiated for 10 min; the photoproduct was analyzed by ^1H NMR, which showed 14% deuterium incorporation at the 2'-position. ^1H NMR (CD_3CN, 300 MHz) δ 7.50 (d, 1.72H, *J* = 8 Hz), 7.40 (m, 2H), 7.27 (dd, 1H, *J* = 6 and 3 Hz,), 7.20 (ddd, 1H, *J* = 10, 10 and 1 Hz), 6.94 (m, 2H), 6.84 (OH, 1H), 4.84 (m, 1H), 3.22 (d, 1H, *J* = 3 Hz), 1.41 (d, 3H, *J*= 6 Hz).

3.3.1.6 Photosolvolysis of 28 in H_2O-CH_3OH

A 20 mg solution of **28** in 100 mL of 1:1 H_2O:CH_3OH was irradiated for 10 minutes; the photoproduct (methyl ether) was analyzed by ^1H NMR, methyl ether **29** (67%); ^1H NMR (CD_3CN, 300 MHz) δ 7.50 (d, 2H, *J* = 8 Hz), 7.35 (d, 2H, *J* = 8 Hz), 7.27 (dd, 1H, *J* = 6 and 2 Hz,), 7.18 (ddd, 1H, *J* = 6, 6 and 1 Hz), 6.94 (m, 2H), 6.87 (OH, 1H), 4.36 (m, 1H), 3.20 (s, 3H, OCH_3), 1.41 (d, 3H, *J* = 6 Hz). MS (EI) m/z = 227.99 for M^+.

3.3.1.7 Photolysis of 28 in 1:1 in D_2O-CH_3OH

A 20 mg solution of **28** in 100 mL of 1:1 (v/v) D_2O-CH_3OH was irradiated for 10 minutes; the photoproduct was analyzed by ^1H NMR, which gave a mixture of deuterated **28** at the 2'-position (**28**-*2'D*) as well as deuterated methyl ether (**29**-*2'D*). The mixture was separated by preparative TLC on silica (1:9 ethyl acetate-CH_2Cl_2), to give **28**-*2'D*

(26% deuterium incorporation) and methyl ether **29**-*2'D* (60% ether yield, 31% sdeuterium incorporation).

3.4 Quantum Yields

Quantum yields for deuterium exchange (Φ_{ex}) for **23**-**26**, and **28** were measured using the deuterium exchange reaction of 2,2'-biphenol[13] as a reference standard. A known amount of compound was dissolved in 1:3 (v/v) D_2O-CH_3CN in a quartz tube and irradiated long enough to give a low amount of conversion. This was followed by preparing an equimolar solution of the reference, which was irradiated under the same conditions. Integration from ^1H NMR spectrum was used to determine the relative conversions of deuterium exchange products**.** Each system was maintained at ~15 °C by means of an internal cold finger and was bubbled with argon for 10 min prior to irradiation. All values are the result of at least three independent irradiations.

3.5 General Procedure for Steady-State and Time-Resolved Fluorescence Measurements

Solutions for steady-state and time-resolved fluorescence measurements were prepared by dissolving the samples in CH_3CN and adjusting the concentrations to have optical densities at the excitation wavelength (273-285 nm) ≤ 0.1. The measurements were performed at 20 °C on a Photon Technology International (PTI) A-1010 Quanta-Master luminescence spectrometer. Solutions were bubbled with argon for 5-10 min prior to irradiation.

Fluorescence quantum yields were determined by comparing the integral of the emission bands to that of Fluorene in CH_3CN ($\Phi_s = 0.68$)[33] , which was used as the

standard. For fluorescence lifetimes using single photon counting, fluorescence decay histograms were obtained on an Edinburgh OB920 instrument equipped with a hydrogen flash lamp, using the time-correlated single photon counting technique in 1023 channels. Histograms of the instrument response functions (using a LUDOX scatterer) and sample decays were recorded until they typically reached 4×10^3 counts in the peak channel.

For the experiments of fluorescence quenching by water, the stock volume solutions (50 mL) of the substrate in CH_3CN and water were prepared to give OD = 0.1 at the excitation wavelength. A volume of 3mL of each solution was added to a 1 cm quartz cuvette. Solutions were bubbled with argon for 5 min prior to excitation.

Appendix

NMR Spectra of Synthesized Compounds

Figure A.1 ^{1}H-NMR spectrum (500 MHz) of **23** in $(CD_3)_2CO$. 66

Figure A.2 ^{13}C-NMR spectrum (125 MHz) of **23** in $(CD_3)_2CO$. 67

Figure A.3 ^{1}H-NMR spectrum (500 MHz) of **24** in $(CD_3)_2CO$. 68

Figure A.4 ^{13}C-NMR spectrum (125 MHz) of **24** in $(CD_3)_2CO$..... 69

Figure A.5 ^{1}H-NMR spectrum (500 MHz) of **25** in $(CD_3)_2CO$. 70

Figure A.6 ^{13}C-NMR spectrum (125 MHz) of **25** in $(CD_3)_2CO$. 71

Figure A.7 ^{1}H-NMR spectrum (500 MHz) of **26** in $(CD_3)_2CO$. 72

Figure A.8 ^{13}C-NMR spectrum (125 MHz) of **26** in $(CD_3)_2CO$. 73

Figure A.9 ^{1}H-NMR spectrum (500 MHz) of **27** in $(CD_3)_2CO$. 74

Figure A.10 ^{13}C-NMR spectrum (125 MHz) of **27** in $(CD_3)_2CO$. 75

Figure A.11 ^{1}H-NMR spectrum (500 MHz) of **28** in CD_3CN. 76

Figure A.12 ^{13}C-NMR spectrum (125 MHz) of **28** in CD_3CN. 77

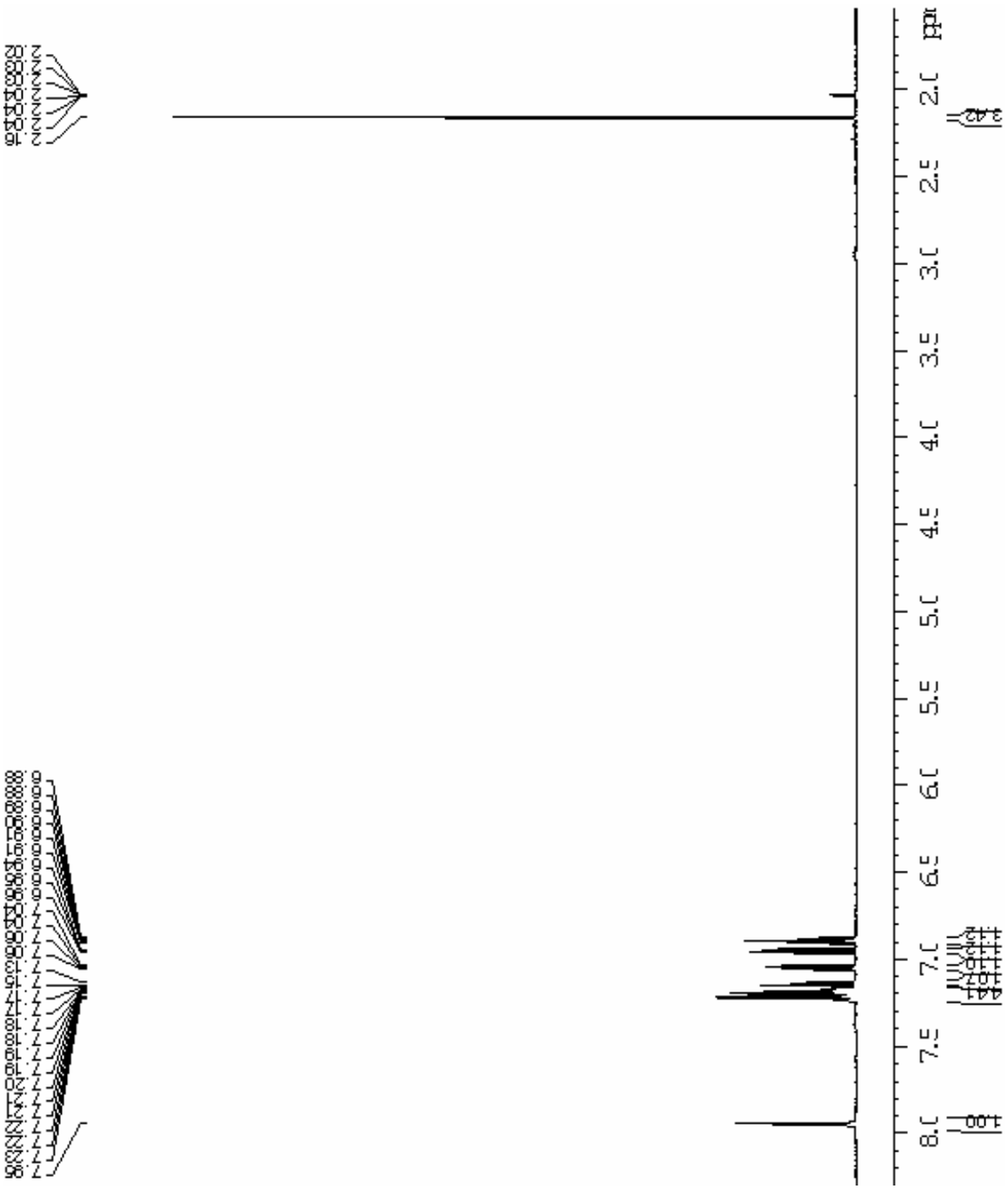

Figure A.1 ^{1}H-NMR spectrum (500 MHz) of **23** in $(CD_3)_2CO$.

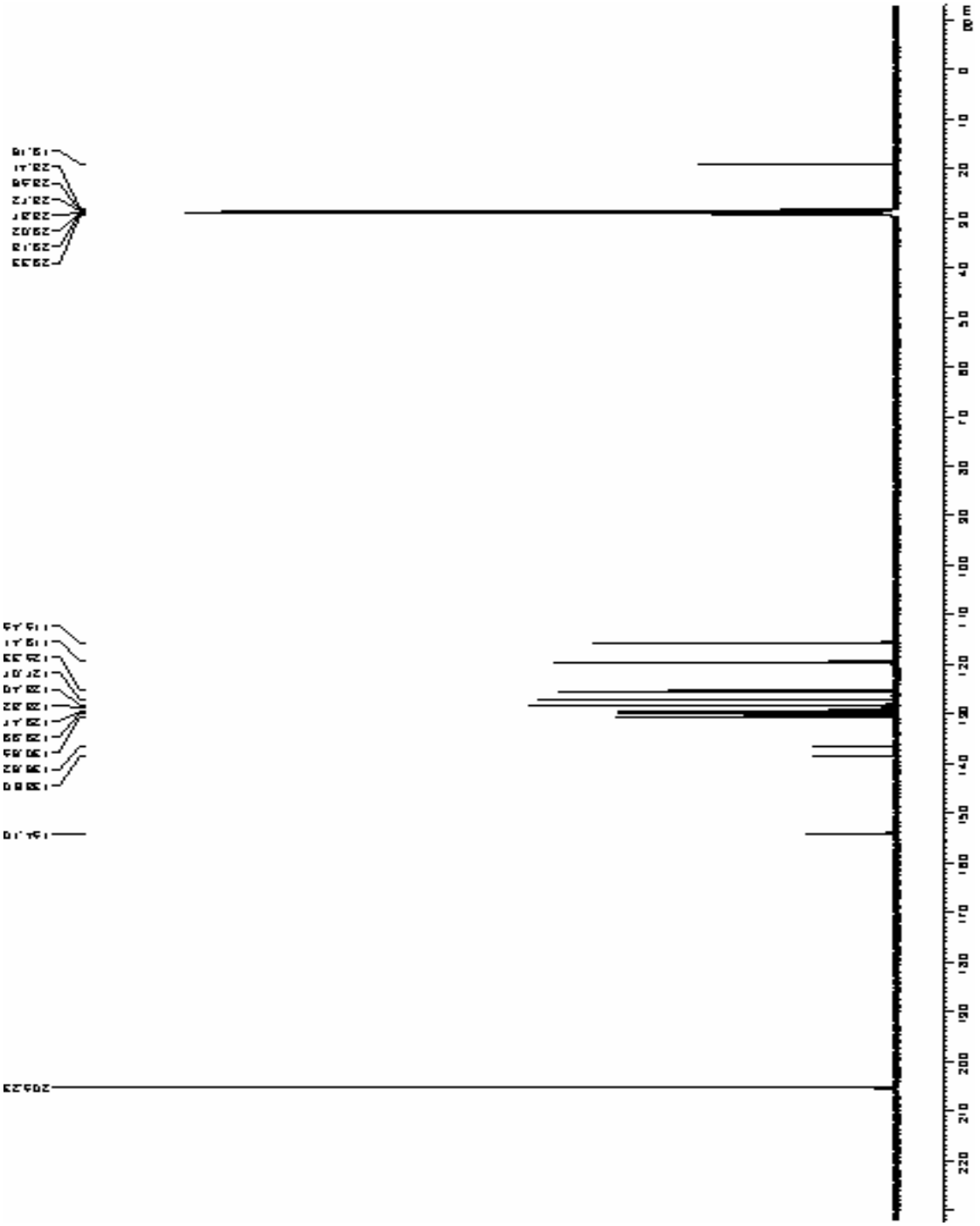

Figure A.2 ^{13}C-NMR spectrum (125 MHz) of **23** in $(CD_3)_2CO$.

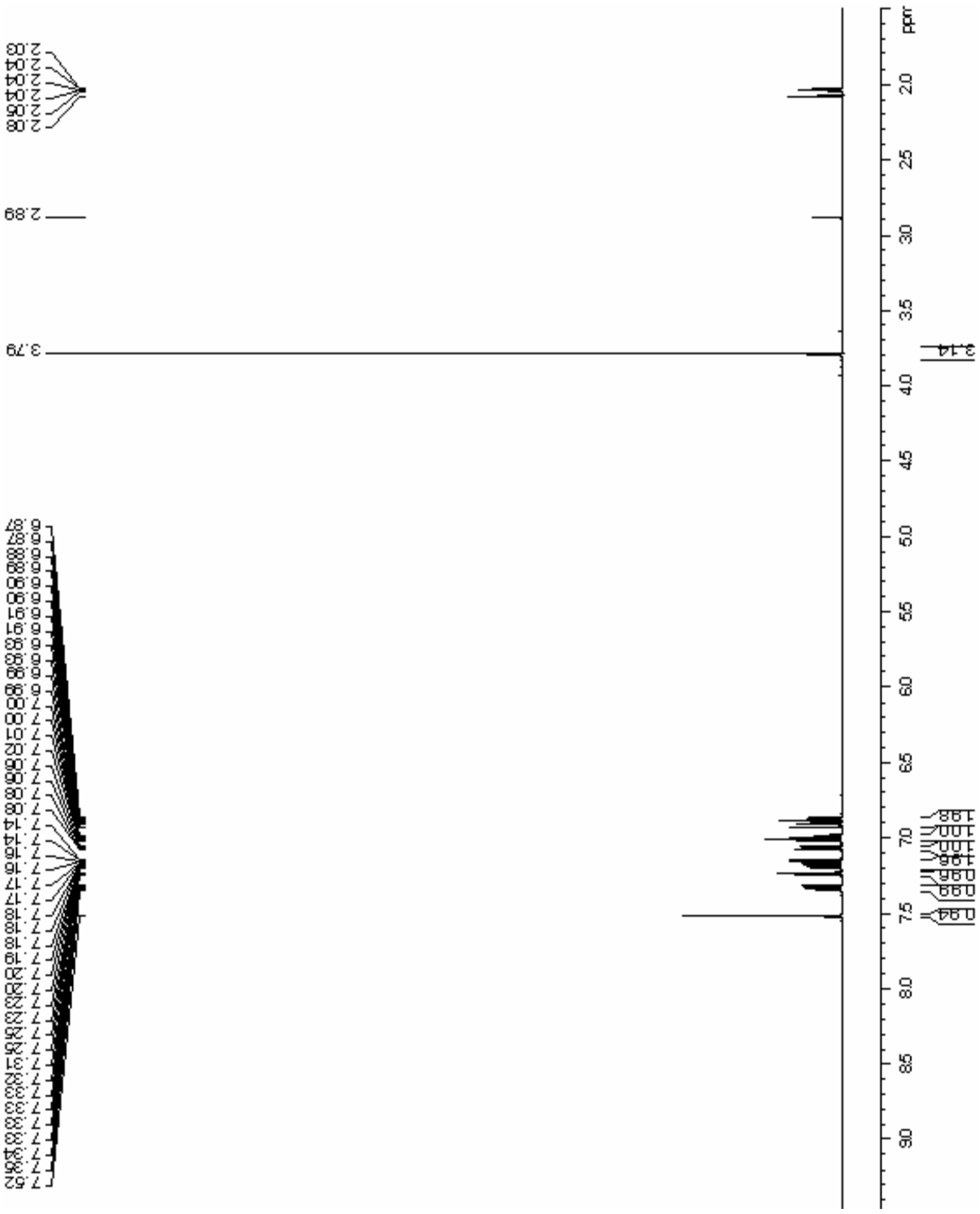

Figure A.3 ^{1}H-NMR spectrum (500 MHz) of **24** in $(CD_3)_2CO$.

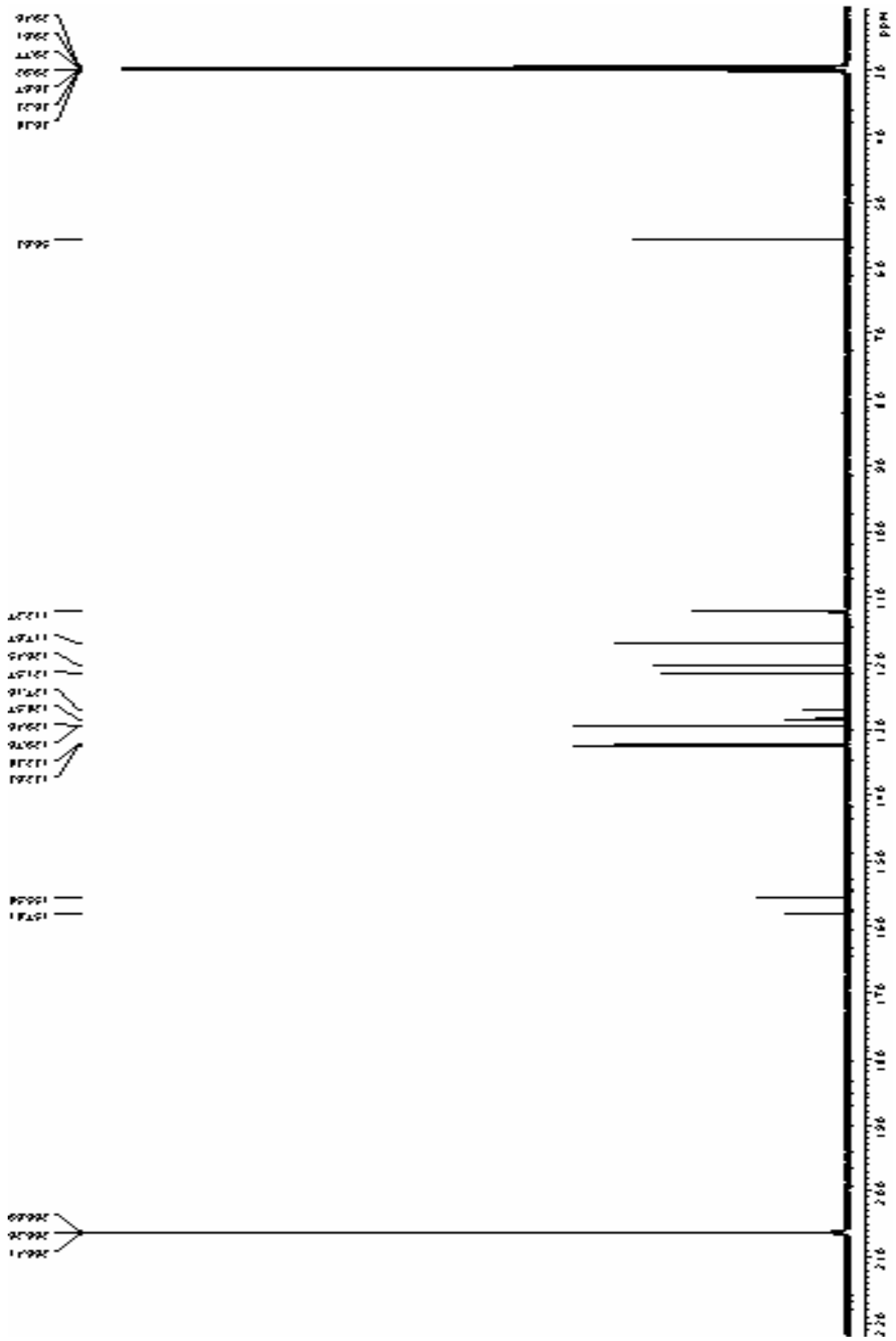

Figure A.4 ^{13}C-NMR spectrum (125 MHz) of **24** in $(CD_3)_2CO$.

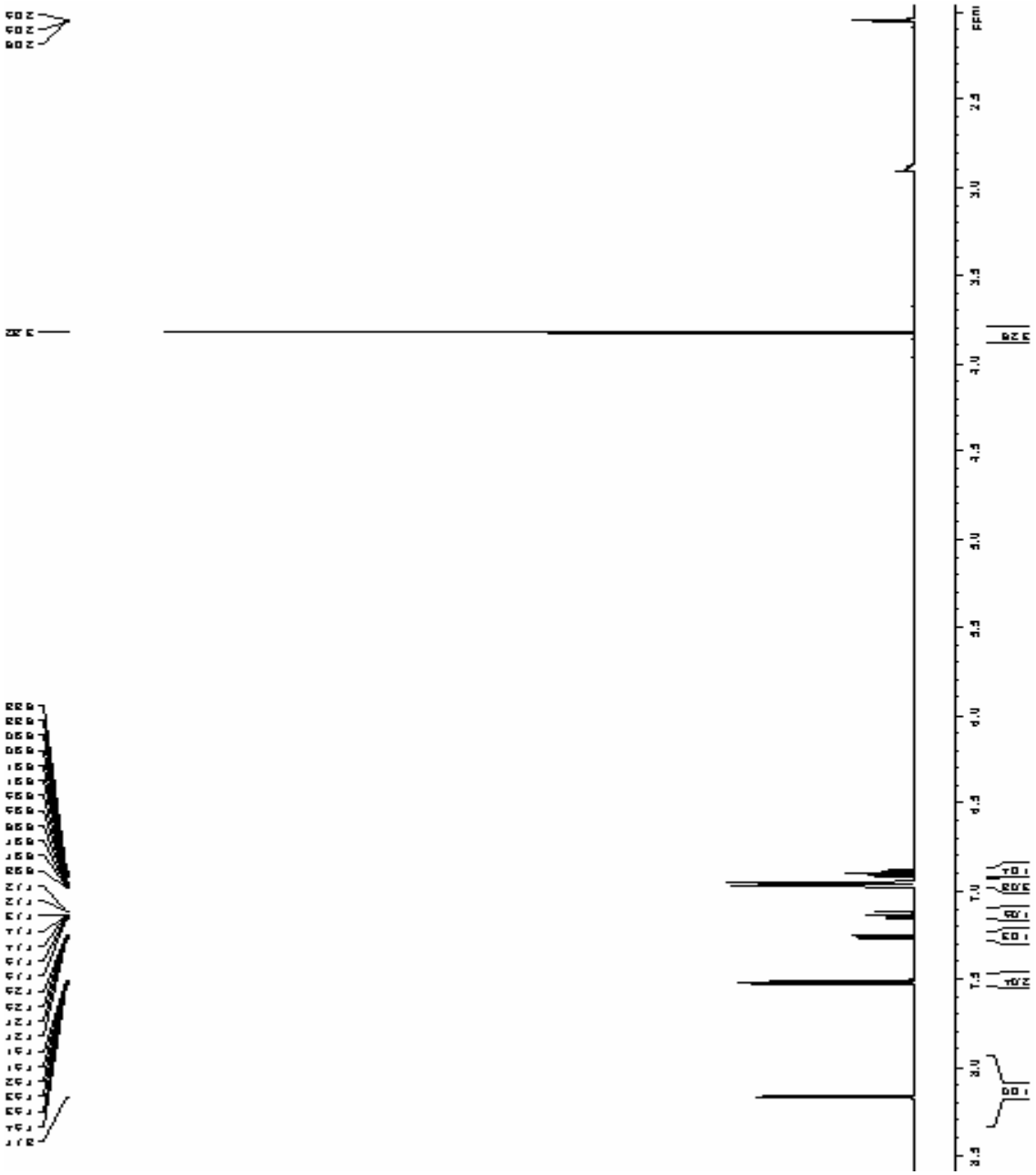

Figure A.5 ^{1}H-NMR spectrum (500 MHz) of **25** in $(CD_3)_2CO$.

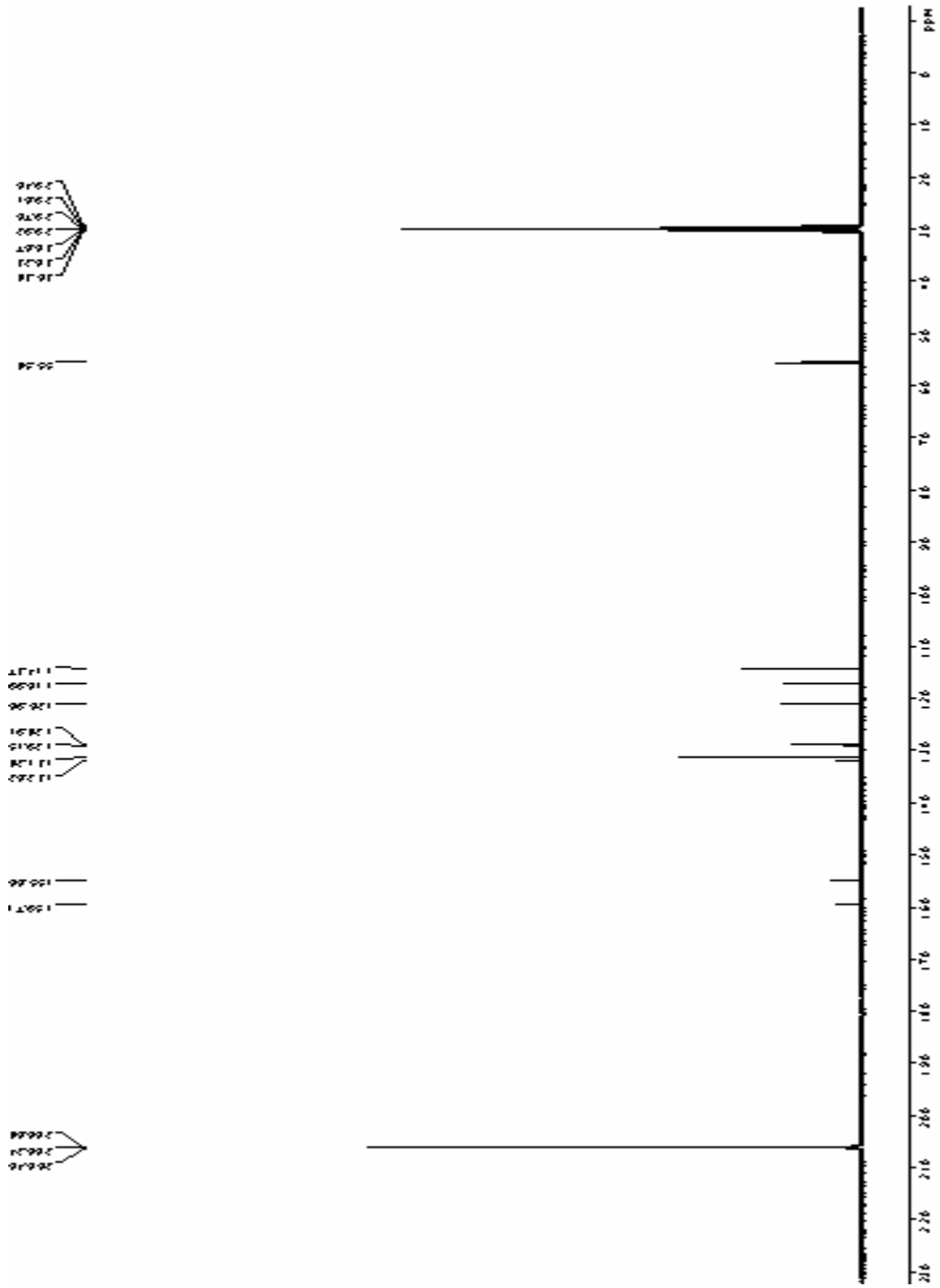

Figure A.6 ^{13}C-NMR spectrum (125 MHz) of **25** in $(CD_3)_2CO$.

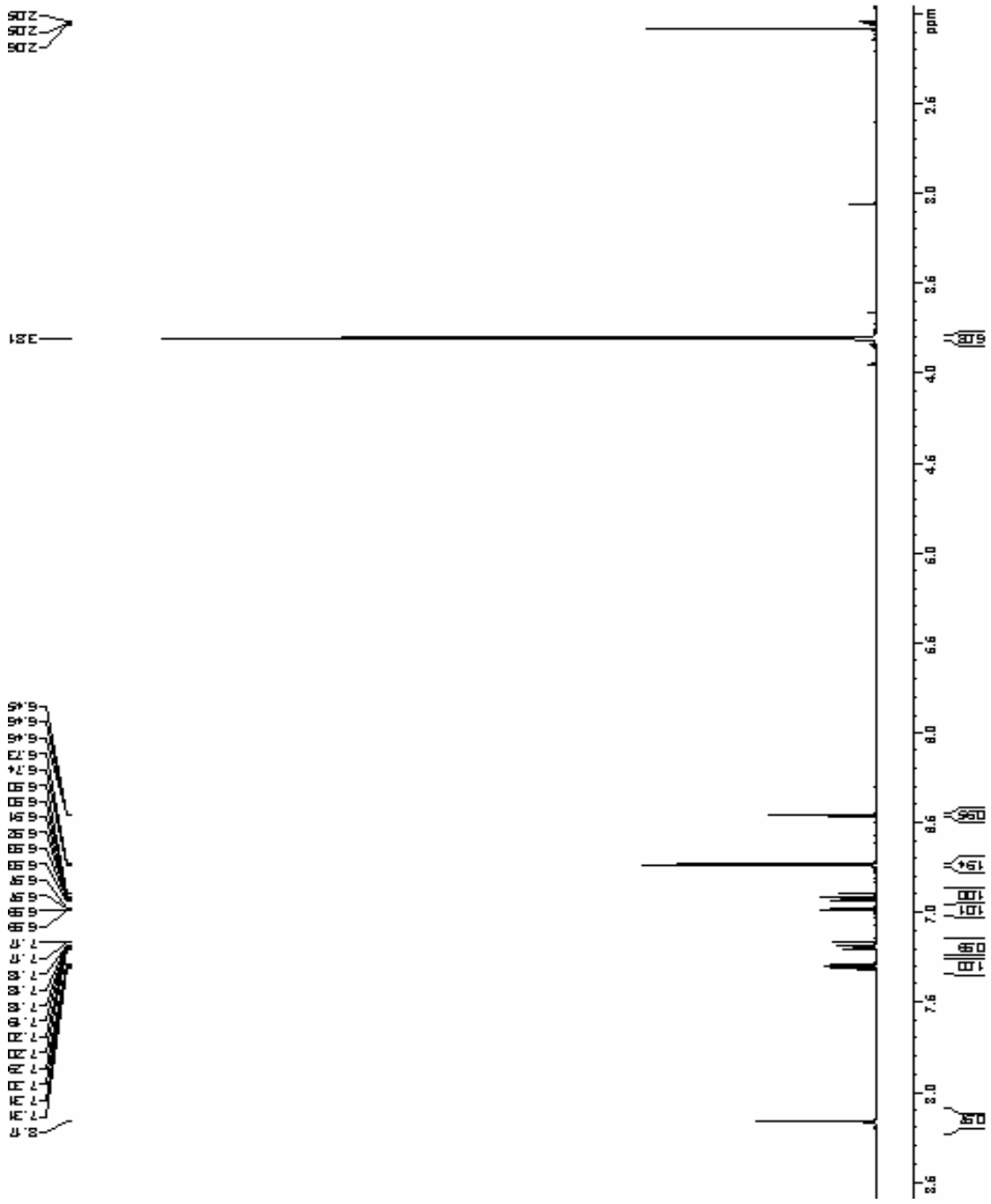

Figure A.7 ^{1}H-NMR spectrum (500 MHz) of **26** in $(CD_3)_2CO$.

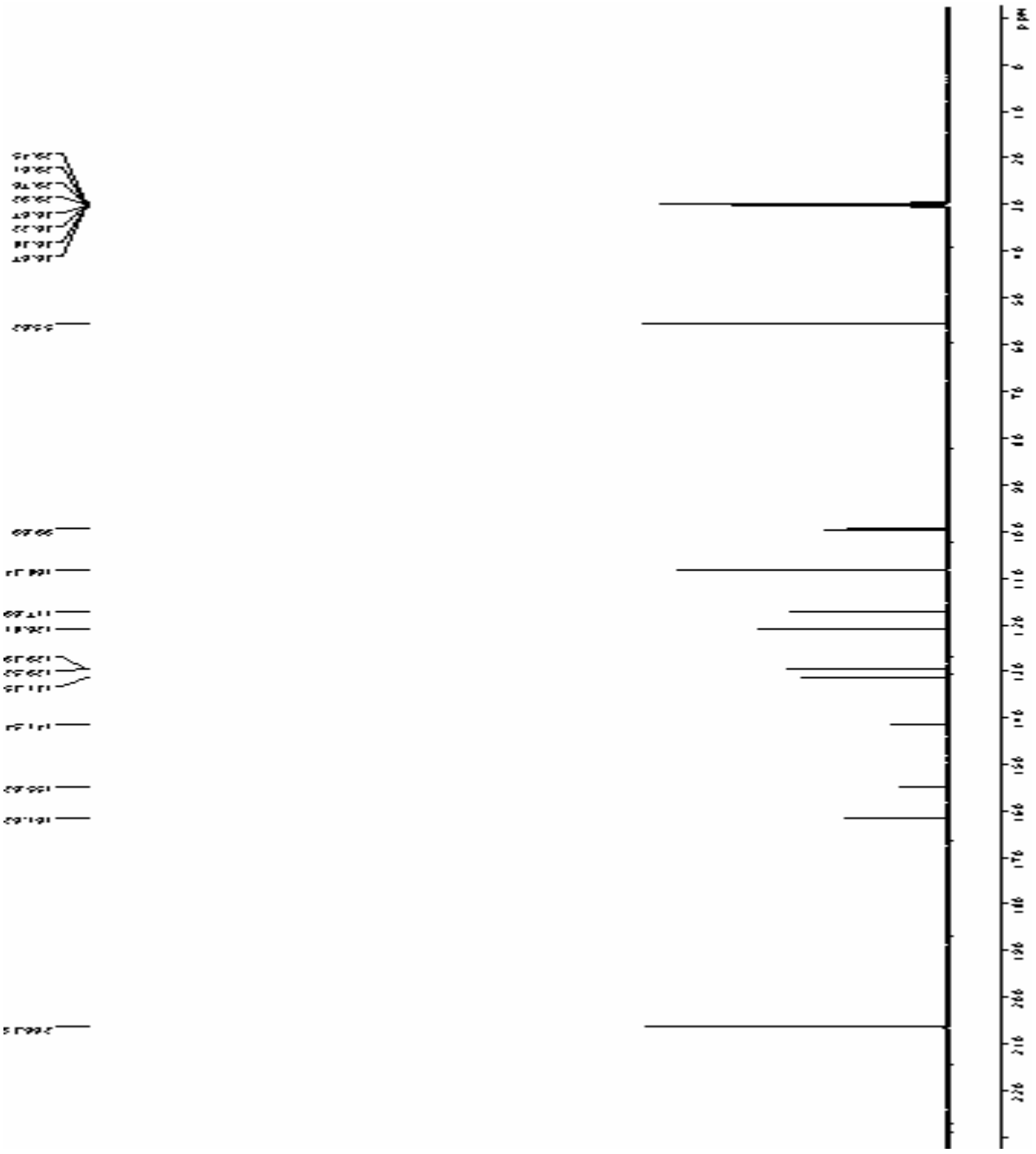

Figure A.8 ^{13}C-NMR spectrum (125 MHz) of **26** in $(CD_3)_2CO$.

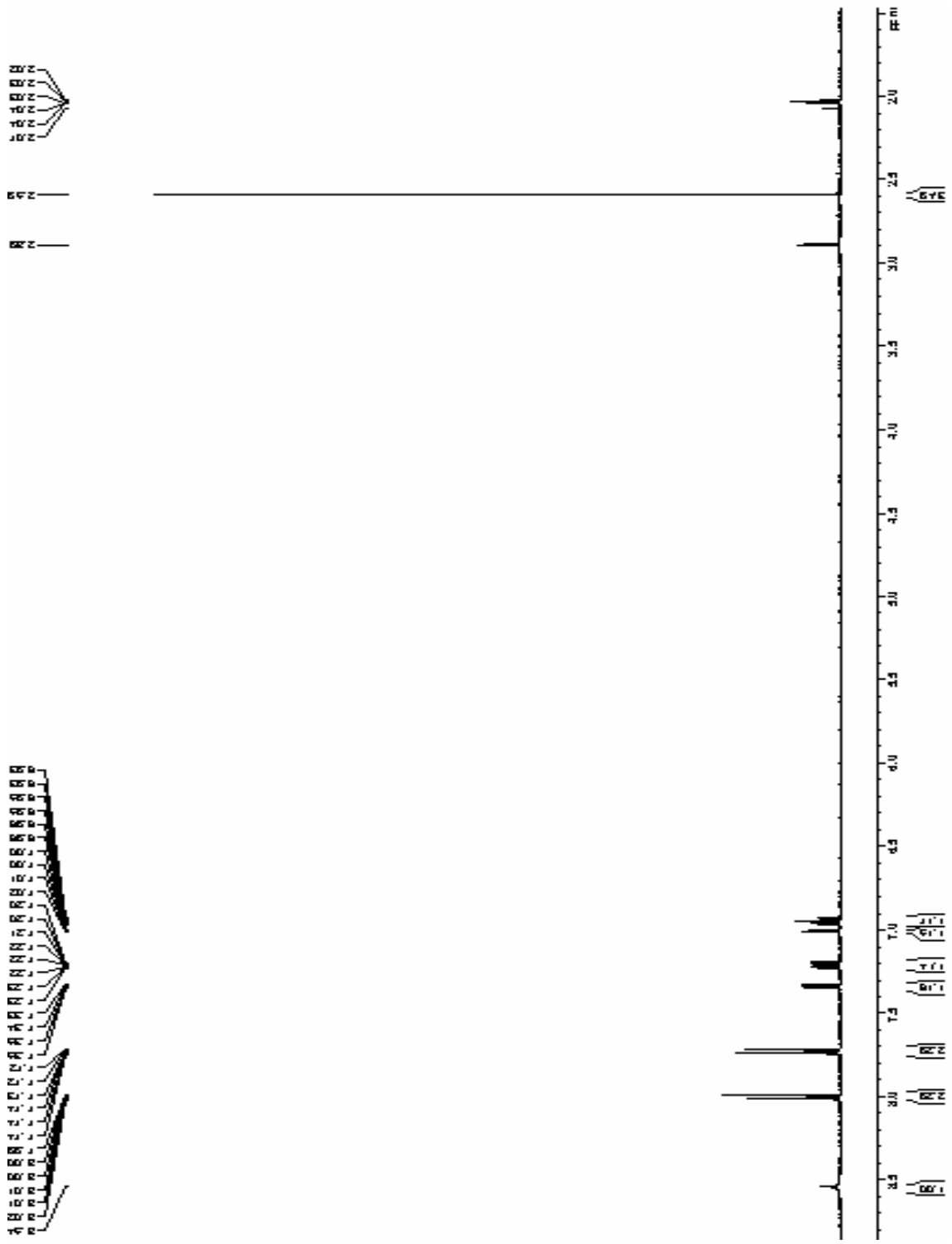

Figure A.9 ^{1}H-NMR spectrum (500 MHz) of **27** in $(CD_3)_2CO$.

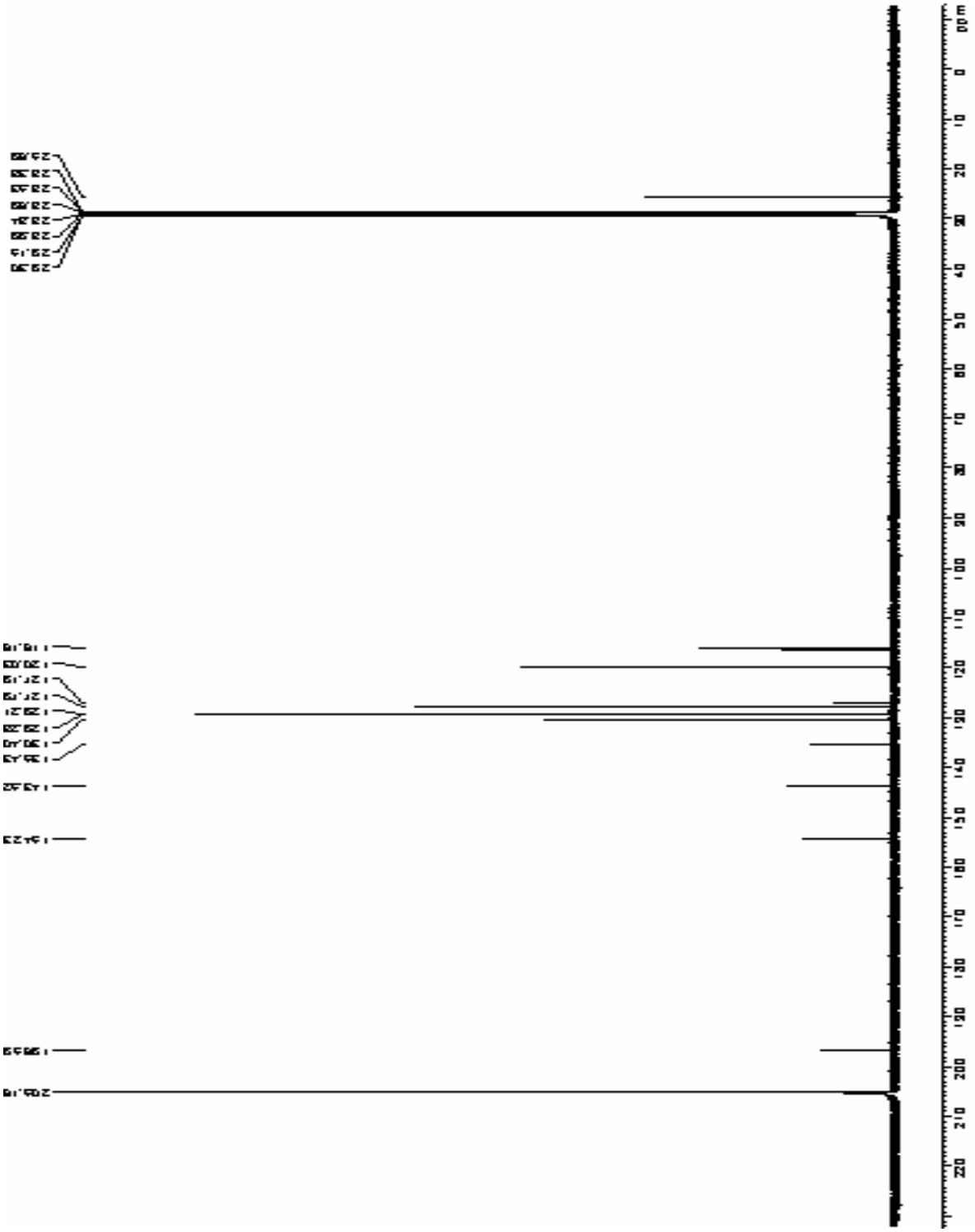

Figure A.10 ^{13}C-NMR spectrum (125 MHz) of **27** in $(CD_3)_2CO$.

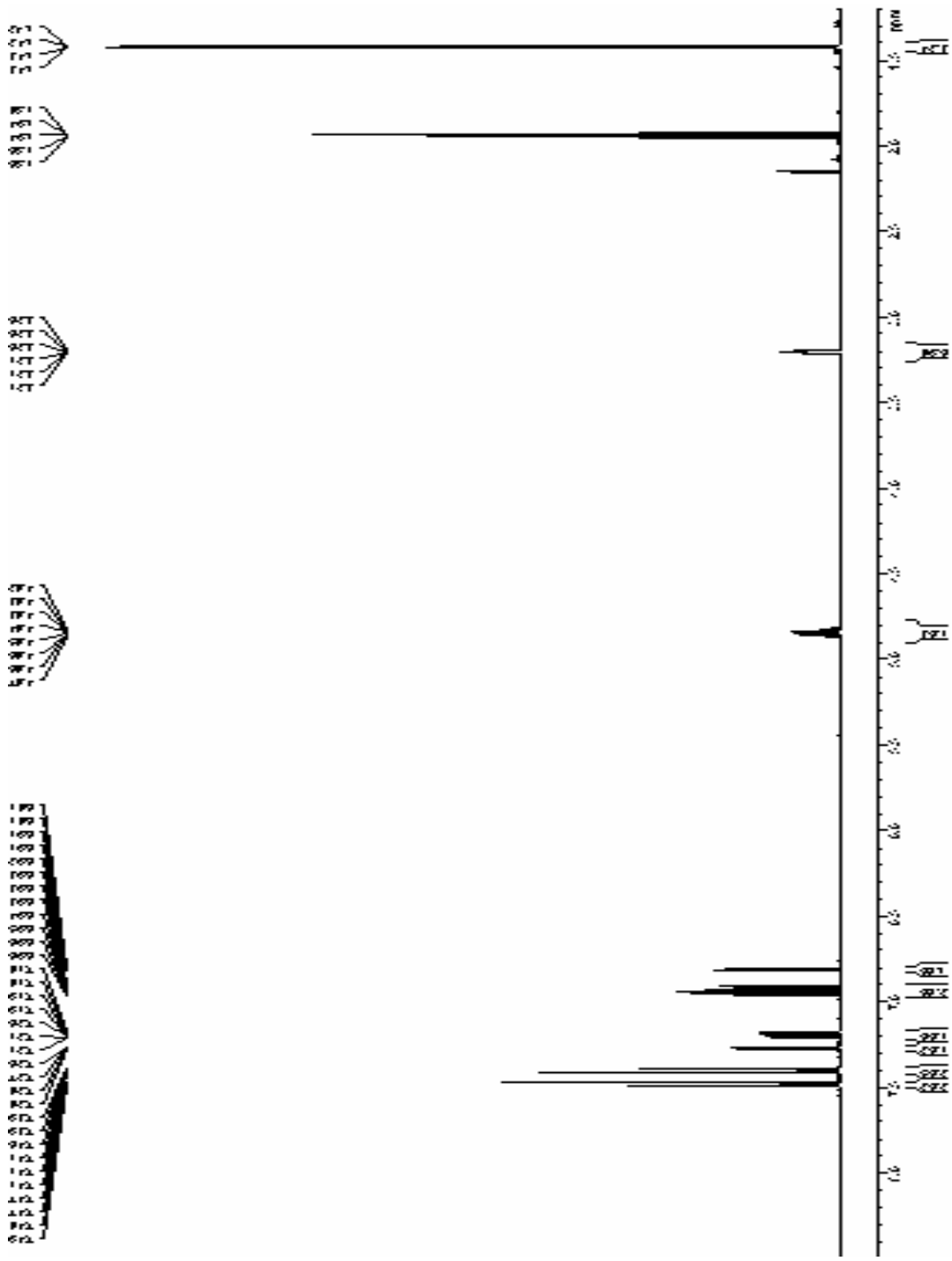

Figure A.11 ^{1}H-NMR spectrum (500 MHz) of **28** in CD_3CN.

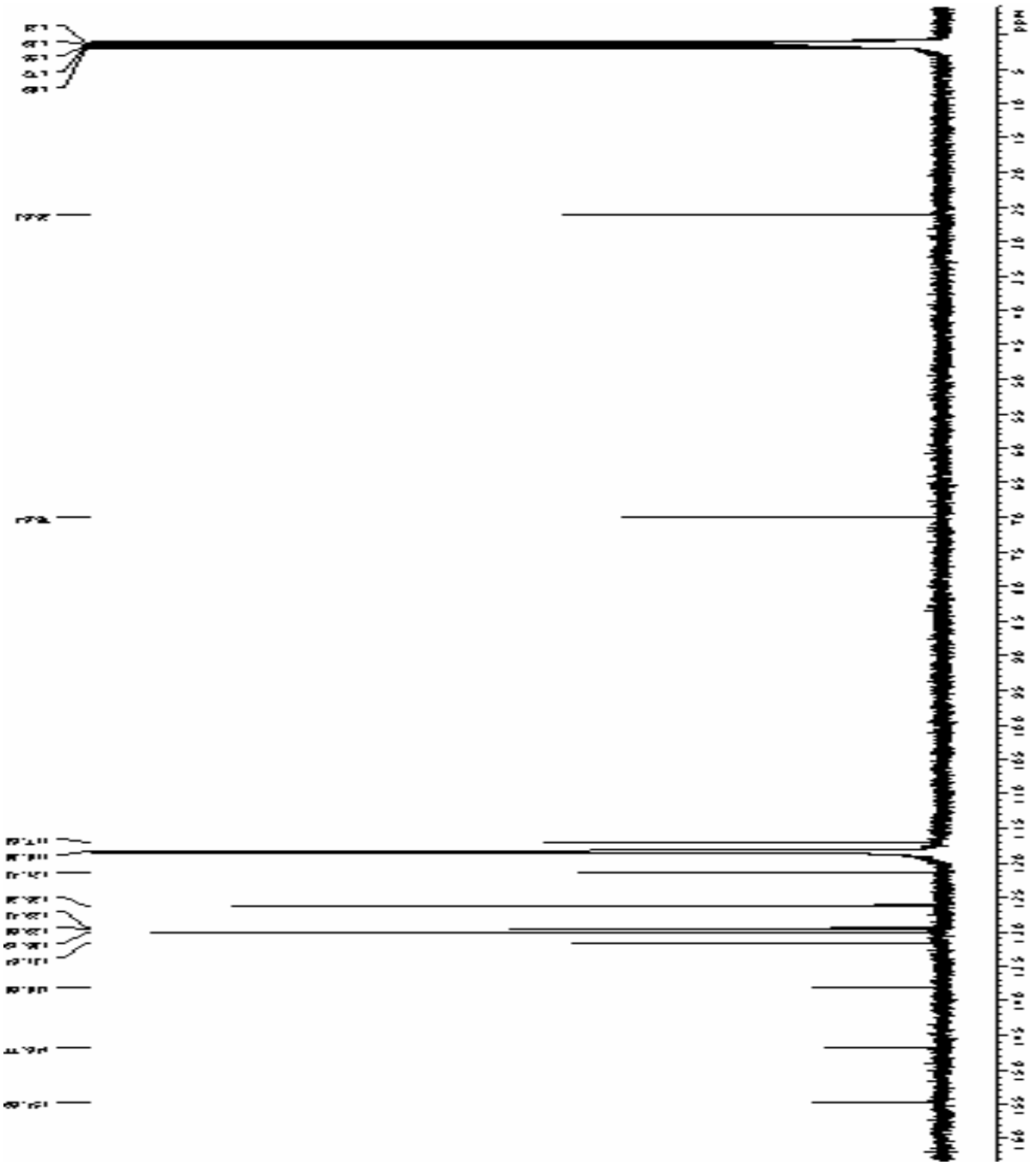

Figure A.12 ^{13}C-NMR spectrum (125 MHz) of **28** in CD_3CN.

References

1. R.P. Bell, The proton in chemistry, Cornell University press: NewYork, 1973.

2. D.Devault, *Q.Rev. Biophys*. **13** (1980) 387.

3. H. Abramczyk, Introduction to Laser Spectroscop, 1st ed.; Elsevier Science: Poland, 2005.

4. D. N. Sathyanarayana, Electronic absorption spectroscopy and related techniques, 1st ed.; University Press (India) limited: Hyderabad, 2001.

5. R. O. Kan, "Organic Photochemistry" McGraw-Hill, New York, 1966.

6. K. Weber, *Z. phys. chem.*, B15 (1931).

7. L. G. Arnaut and S. J. Formosinho, *J. Photochem. Photobiol. A: Chem*., **75** (1993)1.

8. T. Föster, *Naturwiss.*, **36** (1949) 186.

9. N. Agmon, *J. Phys. Chem.*, **109** (2005) 13.

10. P. R. Bangal and S. Chakravorti, *J. Phys. Chem. A* **103** (1999) 8585.

11. A.Weller, *Naturwisss.*, **42** (1955) 175.

12. N.S. Allen, *Polymer Photochemistry*, **3** (1983) 167.

13. M. Lukeman and P. Wan, *J. Chem. Soc., Chem. Commun*. (2001) 1004.

14. M. Lukeman and P.Wan, *J. Am. Chem. Soc*. **124** (2002) 9458.

15. K. Tokumura, M. Natsume, T. Nakagawa, M. Hashimoto, T. Yuzawa. H. Hamaguchi, and M. Itoh, *Chem. Phys. Lett*. **271** (1997) 320.

16. J. Mohanty, A .V. Sapre, R. D. Saini, T. Mukherjee, and H. Pal, *Research on Chemical Intermediates*, **31** (2005) 47.

17. (a) M. T. Htun, A. Suwaiyan, A. Baig, and U. K. A. Klein, *J. Phys. Chem. A.* **102** (1998) 8230. (b) M. T. Htun, A. Suwaiyan and U. K. A. Klein, *Chem. Phys. Lett*. **243** (1995) 71.(c) L. M. Tolbert and J. E. Haubrich, *J. Am. Chem*. Soc. **116** (1994) 10593.(d)

M. L. Tolbert, L. C. Harvey, and R. C. Lum, *J. Phys. Chem*. **97** (1993) 13335.(e) D. Huppert, E. Kolodney, M. Gutman, and E. Nachliel, *J. Am. Chem. Soc*. **104** (1982) 6949.

18. D. A. Malencik and S. R. Anderson, *Biochem. Biophys. Res. Commun*. **178** (1991) 60.

19. (a) M. Isaks, K. Yates, and P. Kalanderopoulis, *J. Am. Chem. Soc*., **106** (1984) 2728; (b) P. Kalanderopoulis and K. Yates, *J. Am. Chem. Soc*., **108** (1986) 6290.

20. (a) M. Isaks, K. Yates, and P. Kalanderopoulis, *J. Am. Chem. Soc.*, **106** (1984) 2728; (b) P. Kalanderopoulis and K. Yates, *J. Am. Chem. Soc*., **108 (**1986) 6290.

21. S. P. Webb, L. A. Philips, S. W. Yeh, L. M. Tolbert and J. H. Clark, *J. Am.Chem.* Soc., **90** (1986) 5154.

22. (a) P.Wan and E. Krogh, *J. Am. Chem. Soc*.**111** (1989) 4887. b) M. Fischer, Y. Shi, B. Zhao, V. Snieckus, and P. Wan, *Can. J. Chem.* **77** (1999) 868.

23. L. Diao, C. Yang, and P. Wan, *J. Am. Chem. Soc*., **117** (1995) 5369.

24. (a) M. K. Nayak and P. Wan, *Photochem. Photobiol. Sci*. **7** (2008) 1544; (b) M. Flegel, M. Lukeman, and P. Wan, *Can. J. Chem*. 86 (2008), 161; (c) N. Basarić and P. Wan, *Photochem.Photobiol. Sci.* **5** (2006) 656; (d) N. Basarić and P. Wan, J. Org. Chem. **71** (2006) 2677; (e) M. Flegel, M. Lukeman, L. Huck, and P. Wan, *J. Am. Chem. Soc*. 126 (2004) 7890; (f) M. Lukeman, P. Wan, *J. Am. Chem. Soc*. **125** (2003) 1164.

25. H. Nam, B. Boury, and S. Y. Park, *Chem. Mater*. **18** (2006) 5716.

26. D. C. Harrowven, T. Woodcock, and P. D. Howes, *Tetrahedron Lett*. **43** (2002) 9327.

27. N. Behin Aein and P.Wan, *Journal of Photochemistry and Photobiology A: Chemistry* **208** (2009) 42.

28. S. L. Murov, I. Carmichael, and G. L. Hug, Handbook of Photochemistry, 2nd ed.; Marcel Dekker: New York, 1993.

29. H. Nam, B. Boury, and S. Y. Park, *Chem. Mater*. **18** (2006) 5716.

30. M. Solinas, R. E. Meadows, C. Wilson, A. J. Blake, and S. Woodward, *Eur. J. Org. Chem.* (2007) 1613.

31. R. Lebeuf, F. Robert, and Y. Landais, Org. Lett. **7** (2005) 4557.

32. T. Drapala, *Roczniki Chemii.*, **42** (1968) 1287.